Many Phases of Accelerating Black Holes in 2+1 Dimensions

ARENAS-HENRIQUEZ, GABRIEL

Many Phases of Accelerating Black Holes in 2+1 Dimensions

Gabriel Darío Arenas Henríquez

A thesis presented for the degree of
Doctor of Philosophy

Centre for Particle Theory
Department of Mathematical Sciences
The University of Durham
United Kingdom
August 2, 2023

Many Phases of Accelerating Black Holes in 2+1 Dimensions

Gabriel Darío Arenas Henríquez

Abstract

This thesis focuses on the study of accelerating solutions within the context of Einstein-AdS gravity in 2+1 dimensions, exploring both classical and holographic perspectives. These solutions exhibit a diverse range of phases that bear similarities to the C-metric in 3+1 dimensions while displaying certain peculiarities and novelties.

We start by describing the different classes of geometries that can be obtained from analysing the three-dimensional C-metric. After including a domain wall that acts as the external force driving the acceleration, we construct accelerating point particles and accelerating Bañados–Teitelboim–Zanelli (BTZ) black holes exhibiting distinct accelerated phases depending on the energy density of the domain wall. Furthermore, we present a novel accelerating black hole that is not continuously connected with the BTZ black hole. A detailed description of the spacetimes and their embedding into AdS_3 is presented.

From there, we investigate the boundary description of such geometries with particular emphasis on the accelerating BTZ black holes. We find that the Fefferman–Graham prescription developed for accelerating black holes in four–dimensions leads to a holographic stress tensor that depends on the conformal freedom of the boundary metric. While this behaviour is natural, computing holographic quantities requires choosing a particular conformal representative. As an alternative, we propose that using an Arnowitt–Deser–Misner (ADM) "radial" decomposition offers a more suitable identification of the boundary data. Our findings reveal that the dual conformal field theory lies in a curved background being characterised by the stress tensor of a perfect fluid.

The Euclidean action is also obtained ensuring a well-posed variational principle. This requires including contributions from the internal boundaries generated when including a domain wall to the spacetime. We show that these boundary terms can be expressed in terms of the Nambu–Goto action of the domain wall which is added on top of the standard renormalised Einstein–Hilbert action for AdS_3.

Finally, we compute the entanglement entropy by using the fact that the solution can be mapped to Rindler-AdS where the Ryu–Takayanagi surface is easily identifiable. As the acceleration increases the accessible region of the conformal boundary decreases and therefore the entanglement entropy also decreases. This is interpreted as a process in which the dual theory loses information due to the acceleration.

Supervisors: Aristomenis Donos and Ruth Gregory

Declaration

The work in this thesis is based on research carried out at the Centre for Particle Theory, Department of Mathematical Sciences, University of Durham, England and it has been funded by Agencia Nacional de Investigación y Desarrollo (ANID), Chile, Scholarship No. 72200271.

No part of this thesis has been submitted elsewhere for any other degree or qualification, and it is the sole work of the author unless referenced to the contrary in the text.

Publications

This thesis is based in the following publications

[1] Gabriel Arenas-Henriquez, Ruth Gregory, and Andrew Scoins. "On acceleration in three dimensions". In: *JHEP* 05 (2022), p. 063. arXiv: 2202.08823 [hep-th]

[2] Gabriel Arenas-Henriquez, Adolfo Cisterna, Felipe Diaz, and Ruth Gregory. "Accelerating Black Holes in $2+1$ dimensions: Holography revisited". In: (2023). arXiv: 2308.00613 [hep-th]

While this thesis was being prepared, the following collaborative works were also published by the author, results from which have not been included in this thesis:

[3] Gabriel Arenas-Henriquez, Felipe Diaz, and Per Sundell. "Logarithmic corrections, entanglement entropy, and UV cutoffs in de Sitter spacetime". In: *JHEP* 08 (2022), p. 261. arXiv: 2206.10427 [hep-th]

[4] Gabriel Arenas-Henriquez, Felipe Diaz, and Yerko Novoa. "Thermal fluctuations of black holes with non-linear electrodynamics and charged Renyi entropy". In: *JHEP* 05 (2023), p. 072. arXiv: 2211.06355 [hep-th]

Acknowledgements

First and foremost, I would like to express my deepest gratitude to my supervisor, Aristomenis Donos. Working under his guidance for the past two years has been an incredible privilege. His encouragement and belief in my abilities never wavered, even when I doubted myself. I am truly fortunate to have had a supervisor who not only guided me academically but also cared about my well-being as a person.

I would also like to extend my heartfelt thanks to my second supervisor, Ruth Gregory. From the moment I joined Durham University, Ruth graciously took me under her wing and provided me with invaluable guidance and encouragement. Her insightful feedback, academic rigor, and constant motivation have been pivotal in the development of my research and my growth as a physicist. I am truly grateful for the opportunity of working with her.

My sincere gratitude goes to my collaborators, Adolfo Cisterna, Felipe Diaz, Andy Scoins, and Per Sundell, whose contributions have significantly enriched the work presented in this thesis. I want to give a special thanks to Felipe, not only for being my main collaborator but also for being an incredible friend from whom I have learned so much. I hope our collaboration continues for years to come.

I would also like to express my gratitude to the faculty members, postdocs, and students of the CPT group in the Department of Mathematical Sciences at Durham University. I want to specifically thank Andreas Braun, Nabil Iqbal, and Simon Ross for their insightful discussions and valuable comments on my work and related topics.

During my PhD journey, I have had the pleasure of engaging with amazing individuals in the department, with whom I have shared ideas, discussions, and plenty of food. I want to express my sincere thanks to Moh Al Attar, Fede Albertini, Connor Armstrong, Jose Cerqueira-Sa, Mauricio Che, Arpit Das, Gabriele Dian, Dario Domingo, Luigi Guerrini, Sophie Hosseini, Lim Zheng Liang, Viktor Matyas, Leonie Papon and Scott Stirling, for tolerating me during the last four years. I

am deeply grateful for the laughter, support, and intellectual exchanges we have shared over the years.

I would like to give a heartfelt thank you to my dear friends Viktor and Sophie, with a special mention to Alavya. Your support and friendship have been invaluable, and I greatly appreciate each one of you. Without your presence, my time in Durham wouldn't have been as special. I wish you all the best in your endeavors, a life filled with happiness, and a lot of running. A lot.

I also want to thank some people scattered around the world that has contributed to my growth both as a human being and a researcher. Thanks to David Rivera-Betancour, Mairym Busnego-Barrientos, Olivera Miskovic, Rodrigo Olea, Damian Galante, Kevin Nguyen, Tomas Frias, Veronica Gaete, Diego Vargas, Shi-Qian Hu, Jacek Rzemieniecki, Carolina Girones, Martins Kandeh and Nam Nguyen.

Most importantly, I want to thank to all my family. None of this would have been possible without their unwavering support. To my grandpa who is a great inspiration for me. To my dad and mom, who I deeply admire, I am forever grateful. I am who I am because of you, and I hope to live up to your expectations. Wherever I go, you will both be with me in my heart.

I'll be here fading away.
No, I never cared about moving. No, I never cared about now.
None of the notes I'm playing.
Is there room in the dark, in between the changes?
I'm like a light that is drifting, in reverse I'm moving.

Adam Granduciel.

Contents

List of Figures

List of Tables

Dedicado a mi familia,
Mario, Adela y Juana

Chapter 1

Introduction

Black holes are one of the most fascinating and, at the same time, "obscure" objects in nature. Predicted by Einstein's theory of general relativity, black holes are regions in the spacetime where matter has collapsed under its own gravitational attraction into an incredibly dense point which is surrounded by an event horizon. Beyond this horizon, our intuition about laws of nature breakdown into nothing. The study of black holes has forced us to expand our comprehension of gravity, leading to incredible developments in our understanding of the universe.

One of the most significant breakthroughs in black hole physics was the discovery of thermodynamic properties of black holes initiated by Bekenstein in 1973 [5] by noting a relation between the area of the event horizon and entropy. Building upon Bekenstein's insights – Bardeen, Carter, and Hawking – extended the understanding of black hole thermodynamics by formulating a set of laws analogous to the laws of classical thermodynamics [6]. These laws, known as the black hole mechanical laws, provided intriguing parallels between the behaviour of black holes and the laws that govern thermal objects. Despite being purely classical observations, these laws hinted at a deeper connection between black holes and thermodynamics.

However, in a seminal work in 1974 [7], Stephen Hawking proved that in fact, black holes can be viewed as thermodynamical systems. Considering asymptotically flat space and using semiclassical techniques, Hawking studied quantum effects near a black hole horizon showing that virtual particle-antiparticle pairs are produced in the vicinity of it. Once these pairs are created, one can fall into the black hole while the other one escapes seen in the form of radiation. As the black hole radiates, its energy decreases and the horizon shrinks, a process in which eventually the black hole fully evaporates. The existence of this radiation, today known as Hawking radiation, implies that the black hole has a temperature, given by the inverse of its mass, and therefore the black hole thermodynamics laws are not simply analogues but rather physically correct [8]. This groundbreaking discovery revealed the quantum nature of black holes opening a new era in the quest for a

consistent theory of quantum gravity [9, 10].

In that regard, string theory provided a framework in which, for the first time, all laws of nature can be derived from the same source. In the context of black hole thermodynamics, string theory offers a microscopic description of the underlying degrees of freedom responsible for the entropy of black holes [11]. According to the holographic principle [12, 13], the information within a black hole is fully encoded on its event horizon. This remarkable property suggests that the behaviour of a black hole can be fully described by a lower-dimensional field theory.

This idea finds a concrete manifestation by means of the AdS/CFT correspondence, also known as the gauge/gravity duality [14, 15] establishing an equivalence between certain gravitational theories in Anti-de Sitter (AdS) spacetime and conformal field theories (CFTs) living at their boundary. The AdS/CFT correspondence provides a powerful tool to study strongly coupled systems, such as black holes, by mapping them to weakly coupled field theories.

In this context, three-dimensional gravity plays an important role as a testing ground for understanding the broader AdS/CFT correspondence and its implications for quantum gravity. Compared to higher-dimensional gravity, it is much simpler and completely solvable [16]. The lack of propagating degrees of freedom [17–19] hinted some triviality in the theory but regained attention after Bañados, Teitelboim and Zanelli found that the theory admits "black hole" solutions in the presence of negative cosmological constant [20]. The idea was later refined by the same authors in collaboration with Henneaux [21] showing that these spacetimes arise as isometric identifications of AdS space. The "physical" singularity is then replaced by a conical singularity introduced by the orbifold procedure and acts only locally in the spacetime. The absence of a physical singularity in the Bañados–Teitelboim–Zanelli (BTZ) black hole does not imply the lack of physical interest: these still possess an event horizon exhibiting thermodynamical features as higher-dimensional black holes [22, 23].

This thesis is devoted to accelerating spacetimes in 2+1 dimensions. It involves describing the three-dimensional C-metric from a classical and holographic perspective. Classically, we investigate various classes of solutions derived from the three-dimensional C-metric. These solutions exhibit distinct phases depending on the interplay between their physical parameters, and in particular, their "acceleration". By exploring holographic properties, we aim to deepen our understanding of acceleration and its effect in the dual quantum field theory.

The content is organised as follows:

Chapter 2 provides a comprehensive overview of some of the concepts utilised throughout this thesis. We begin by introducing the notion of asymptotically AdS spaces to delve into the distinctive properties of three dimensions. We study the

BTZ black hole in detail; from its construction by orbifolding the spacetime to its thermodynamic properties. Briefly, we state the correspondence between the gravity partition function and the generating functional of a quantum field theory defined at the boundary of the spacetime which allows to obtain correlators by means of a classical on-shell gravitational action. The holographic renormalisation method and holographic stress tensor are also presented in detail, with a particular emphasis on their application in the 2+1-dimensional bulk setting.

In Chapter 3, we present the four-dimensional C-metric and analyse its properties in detail. We explore the meaning of "acceleration" within this context, further implications and we demonstrate that, in a particular approximation, the spacetime can be seen as an off-centre perspective of AdS_4. Furthermore, we review the recent efforts and developments in understanding the thermodynamic aspects of these black holes along with their holographic characteristics.

Then, in Chapter 4, we turn our attention to the three-dimensional C-metric and the different classes of accelerating solutions obtained from the analysis of the metric functions. We introduce a domain wall into the spacetime by cutting and gluing along a hypersurface with non-trivial tension. From there, we construct single-wall or single-strut solutions that produce either accelerating particles or accelerating black holes. Each of these solutions is meticulously analysed, highlighting their novel features and elucidating the differences which set them apart from their higher-dimensional analogues.

We describe the boundary of the 2+1 C-metric in Chapter 5. Building upon techniques introduced for four-dimensional accelerating black holes, we obtain the holographic data associated with both, accelerating black holes and particles. Our analysis reveals that when evaluating the renormalised action on-shell, a new divergence appears due to the presence of the domain wall. To address this issue, we introduce boundary terms associated to the internal boundaries of the space. These are reexpressed as the Nambu-Goto action of the wall effectively regulating the divergence. Furthermore, we compute the entanglement entropy, shedding light on the effect of the acceleration in the boundary field theory which plays a significant role in the subleading behaviour.

Finally, Chapter 6 serves as a comprehensive summary of our findings, engaging some discussion and providing possible future directions for research.

Chapter 2

Asymptotically AdS spaces, black holes in 2+1 dimensions and gauge/gravity duality

For the last 25 years, Maldacena's conjecture [14] has been a central pillar in the quest to understand the mysteries of quantum gravity and black holes. It has proven to be a handy tool in connecting seemingly disparate fields, facilitating the translation of problems in quantum gravity to well-understood concepts in field theory.

Moreover, the insights gained from the AdS/CFT correspondence have extended beyond gravitational settings. The correspondence has found applications in condensed matter physics, hydrodynamics, nuclear physics, and even in quantum information theory, demonstrating its versatility and broad impact, see for example some remarkable results [24–40] and reference therein.

In this chapter, we will introduce some of the basic concepts of the duality which are of relevance for the analysis done in this thesis.

We begin by describing asymptotically AdS spaces to then move to the particular case of three dimensions. We will see that a black hole solution can be constructed via reparametrisation of AdS_3 or as a quotient space. Exploring the asymptotic symmetries of AdS_3 spaces, we make an explicit connection between gravity and conformal symmetry: the asymptotic symmetry algebra generated by the global charges corresponds to a direct sum of two copies of a Virasoro algebra. This works as a perfect preamble for the AdS/CFT correspondence introduced in a brief manner. As final ingredients, we review the prescription for dealing with infrared divergences which allow computing finite correlation functions and boundary stress tensor.

2.1 Asymptotically Anti-de Sitter spaces

General relativity in $d+1$ dimensions is essentially described by the Einstein–Hilbert action *

$$I_{\rm EH} = \frac{1}{16\pi G}\int_{\mathcal{M}} \sqrt{-g}\,(R-2\Lambda)\,, \tag{2.1}$$

where Λ is the cosmological constant. Without the presence of matter, an arbitrary variation of the action with respect to the metric $g_{\mu\nu}$ produces the Einstein field equations

$$R_{\mu\nu} - \frac{1}{2}Rg_{\mu\nu} + \Lambda g_{\mu\nu} = 0. \tag{2.2}$$

Although solving these equations can be extremely convoluted, the simplest way of finding a solution is to look at their trace

$$R = 2\frac{d+1}{d-1}\Lambda\,, \tag{2.3}$$

suggesting that, locally, the equation is satisfied for a space of constant curvature. In fact, the solution can be expressed in terms of the Riemann tensor as

$$R_{\mu\nu\alpha\beta} = \frac{2\Lambda}{d(d-1)}\left(g_{\nu\beta}g_{\mu\alpha} - g_{\nu\alpha}g_{\mu\beta}\right)\,, \tag{2.4}$$

which describes a maximally symmetric spacetime. These spacetimes are characterised by possessing the maximum number of isometries. The simplest example is to consider $\Lambda = 0$, corresponding to Minkowski space. In $d+1$ dimensions, the Poincaré group contains $d+1$ translational isometries and $(d+1)d/2$ rotations including boosts. This implies that there are $(d+1)(d+2)/2$ total isometries meaning that Minkowski space has $(d+1)(d+2)/2$ linearly independent Killing vectors. For Lorentzian manifolds, apart from flat space, there are two spaces that satisfy this condition. The positive curvature case ($\Lambda > 0$) corresponds to de Sitter (dS) space while negative curvature ($\Lambda < 0$) defines anti-de Sitter (AdS) space. We focus on the latter as it is of a central role in the next chapters.

The $d+1$-dimensional AdS space can be seen as the following Lobachesvki-like embedding in $d+2$-dimensional Minkowski space with signature $(-,+,\cdots,+,-)$ and isometry group $O(d,2)$ with the following line element and constraint, respectively,

$$\begin{aligned} ds^2 =& -(dX^0)^2 + \sum_{i=1}^{d}(dX^i)^2 - (dX^{d+1})^2, \\ -(X^0)^2 &+ \sum_{i=1}^{d}(X^i)^2 - (X^{d+1})^2 = -\ell^2\,. \end{aligned} \tag{2.5}$$

where ℓ is the characteristic radius of curvature of AdS. It is important to note that in this form is evident that the isometry group of AdS_{d+1} is $O(d,2)$, which

*We will work with the mostly positive signature for Lorentzian metrics, i.e., $(-+++\cdots)$.

have indeed $(d+1)(d+2)/2$ generators as we anticipated for maximally symmetric spaces.

The metric of AdS can be written in different coordinate systems which may serve distinct purposes. An useful example is the Poincaré patch defined a parametrisation of the hyperboloid (2.5) using the coordinates $t \in \mathbb{R}^{d+2}$, $x^i = (x^1, \cdots, x^{d-1}) \in \mathbb{R}^{d+2}$ and $r \in \mathbb{R}_+$,

$$\begin{aligned} X^0 &= \frac{\ell^2}{2r}\left(1 + \frac{r^2}{\ell^4}(x^2 - t^2 + \ell^2)\right), \\ X^i &= r\frac{x^i}{\ell}, \\ X^d &= \frac{\ell^2}{2r}\left(1 + \frac{r^2}{\ell^4}(x^2 - t^2 - \ell^2)\right), \\ X^{d+1} &= \frac{rt}{\ell}, \end{aligned} \tag{2.6}$$

with $i = 1, \ldots, d-1$ and $x^2 = \eta_{ij}x^i x^j$ where $\eta_{ij} = \text{diag}[-1, +1, \cdots, +1]$. Note that restricting r to be positive only allows access to one-half of the spacetime. Substituting (2.6) into (2.5) leads to the induced metric

$$ds^2 = \frac{\ell^2}{r^2}dr^2 + \frac{r^2}{\ell^2}\eta_{ij}dx^i dx^j\,. \tag{2.7}$$

A straightforward computation reveals that the Ricci scalar of this solution is $R = -\frac{d(d+1)}{\ell^2}$. Compared with (2.3), it is evident then that the cosmological constant is defined in terms of the AdS radius as

$$\Lambda = -\frac{d(d-1)}{2\ell^2}\,. \tag{2.8}$$

In these coordinates, AdS space can be seen as flat space but with an extra dimension that also serves as a warping factor of the flat directions. This warped factor is in fact induced by the gravitational potential, i.e., the intrinsic pressure of the spacetime. There is a degenerate Killing horizon when $r \to 0$ is known as the Poincaré horizon. This is only a coordinate singularity as can be observed from the Kretschmann scalar

$$\mathcal{K} = R_{\mu\nu\alpha\beta}R^{\mu\nu\alpha\beta} = \frac{24}{\ell^2}\,, \tag{2.9}$$

showing that the spacetime is devoid of curvature singularities. Nevertheless, note that a quadratic pole exists when $r \to \infty$. This divergence in (2.7) is a defining feature of asymptotically AdS spaces [41–43]. As we do not have access to the "physical" boundary – in the same sense of a compact space – notice that it is possible to achieve finiteness at $r \to \infty$ by considering the defining function $\Omega = \frac{\ell^2\omega(t,x^i)}{r^2}$ such that the boundary of the spacetime is then realised as

$$g_{(0)} = \lim_{r\to\infty}\Omega^2 g = \omega\left(-dt^2 + (dx^i)^2\right)\,. \tag{2.10}$$

The last expression implies that the boundary – which from now on we refer to as *conformal boundary* – of asymptotically anti-de Sitter spaces is not unique: it is defined by an equivalence class of metrics related by conformal transformations. We refer to ω as the *conformal representative* as distinct choices render to different boundary metrics. The existence of this particular conformal structure will be crucial when treating the divergences of gravitational actions in AdS.

It is convenient to introduce the inverse of the radial coordinate $z = \ell^2/r$. Evidently, the conformal boundary $r \to \infty$ corresponds now to $z = 0$ whereas $r \to 0$ is now replaced by $z \to \infty$. Then, AdS space in Poincaré coordinates is cast as

$$ds^2 = \frac{\ell^2}{z^2}\left(dz^2 + \eta_{ij}dx^i dx^j\right) . \tag{2.11}$$

Another useful parametrisation of AdS is

$$\begin{aligned} X^0 &= \ell\cos(\tau)\cosh(\rho) \\ X^{d+1} &= -\ell\sin(\tau)\cosh(\rho) \\ X^i &= \ell\sinh(\rho)\Omega^i , \end{aligned} \tag{2.12}$$

where Ω^i with $i = 1, \ldots, d$ is the unit S^{d-1}, $\tau \in [0, 2\pi[$ and $\rho \in \mathbb{R}_+$. This chart is usually referred to as *global coordinates* of AdS since it contains all the accessible regions of the hyperboloid 2.5. The metric in these coordinates is then

$$ds^2 = \ell^2\left(-\cosh^2(\rho)d\tau^2 + d\rho^2 + \sinh^2(\rho)d\Omega^2_{d-1}\right) . \tag{2.13}$$

Let us pause a bit to analyse some manifest features of this metric. First, it is straightforward that there is a global timelike Killing vector ∂_τ. The coordinate τ is usually known as *global time*. The second important observation comes from the isometries of 2.13. Note that $SO(2)$ generates translations in τ, while $SO(d)$ generates rotations over the rest of the coordinates. This implies that only the maximal compact subgroup of $SO(2, d)$ is manifest, namely, $SO(2) \times SO(d)$. The third observation comes from the boundary. In fact, the properties discussed above for the Poincaré observer are not clear here at first sight. Instead, we can introduce the compact coordinate $\theta \in [0, \frac{\pi}{2}]$ by using $\tan(\theta) = \sinh(\rho)$. This leads to the Einstein static universe

$$ds^2 = \frac{\ell^2}{\cos^2(\theta)}\left(-d\tau^2 + d\theta^2 + \sin^2(\theta)d\Omega^2_{d-1}\right) . \tag{2.14}$$

The choice of θ to be compact limits an observer to only have access to one half of $\mathbb{R} \times S^d$. In this way, the conformal boundary is located at $\theta = \pi/2$. Additionally, note that the timelike coordinate τ is compact. This implies that global AdS has closed timelike curves that can be avoided in the universal cover obtained by unwrapping the time coordinate, i.e., taking $\tau \to t \in \mathbb{R}$.

Finally, it is important to introduce the Euclidean version of AdS_{d+1}. Let us consider a Wick rotation of the X^0 coordinate in 2.5. The isometry group is now $SO(d+1,1)$. In global coordinates, Euclidean AdS is described by

$$ds^2 = \ell^2 \left(\cosh^2(\rho) d\tau_{\mathrm{E}}^2 + d\rho^2 + \sinh^2(\rho) d\Omega_{d-1}^2 \right) , \tag{2.15}$$

where we have introduced the Euclidean time $\tau_{\mathrm{E}} \equiv i\tau$. In Poincaré coordinates

$$ds^2 = \frac{\ell^2}{z^2} \left(dz^2 + \delta_{ij} dx^i dx^j \right) . \tag{2.16}$$

2.2 Einstein-AdS gravity in 2+1 dimensions and BTZ black hole

General Relativity in $2+1$ dimensions with $\Lambda = -1/\ell^2$ can be understood as a Chern-Simons (CS) theory whose gauge connection is identified with the gauge field of the $\mathrm{SO}(2,2)$ group [44, 45] (see Appendix A). It is known that the theory is in fact topological [16]. A simple way of observing this is by counting the propagating degrees of freedom of the theory in $d+1$ dimensions: the metric tensor has $(d+1)(d+2)/2$ components from which $d+1$ of them can be removed by using diffeomorphism invariance. Additionally, there are $d+1$ components in the Lagrangian that are Lagrange multipliers. Then, the bulk degrees of freedom are

$$\mathrm{dof} = \frac{(\mathrm{d}+1)(\mathrm{d}+2)}{2} - (\mathrm{d}+1) - (\mathrm{d}+1). \tag{2.17}$$

For $2+1$ dimensions, we get that the last expression vanishes. In fact, the Weyl tensor also cancels identically in 2+1 dimensions. This means that all solutions of the theory are, locally, nothing else than AdS_3 space being characterised by a constant Riemann tensor

$$R_{\mu\nu\alpha\beta} = -\frac{1}{\ell^2} \left(g_{\nu\beta} g_{\mu\alpha} - g_{\nu\alpha} g_{\mu\beta} \right) . \tag{2.18}$$

In global coordinates, *vacuum* AdS space is given as

$$ds^2 = -\left(1 + \frac{r^2}{\ell^2} \right) dt^2 + \left(1 + \frac{r^2}{\ell^2} \right)^{-1} dr^2 + r^2 d\phi \, , \tag{2.19}$$

where we are employing the universal cover time coordinate $t \in \mathbb{R}$ and we have introduced $r = \ell \sinh(\rho)$. Although the theory is topological, it is possible to find "excitations" by choosing different reparametrisations of the spacetime. Let us consider the case of a conical deficit induced by a parameter $\kappa \in [1, 0]$. Using the

following coordinates

$$\begin{aligned} X^0 &= \frac{ir}{\kappa}\cos(\kappa\phi)\,, \\ X^1 &= \sqrt{\frac{r^2}{\kappa^2}+\ell^2}\sin(\kappa t/\ell)\,, \\ X^2 &= \frac{r}{\kappa}\sin(\kappa\phi)\,, \\ X^3 &= i\sqrt{\frac{r^2}{\kappa^2}+\ell^2}\cos(\kappa t/\ell)\,. \end{aligned} \tag{2.20}$$

renders the hyperbolic metric into

$$ds^2 = -\left(\kappa^2+\frac{r^2}{\ell^2}\right)dt^2 + \left(\kappa^2+\frac{r^2}{\ell^2}\right)^{-1}dr^2 + r^2 d\phi\,. \tag{2.21}$$

Note that in principle $\phi \in [0, 2\pi[$. We can rescale the coordinates with the parameter κ as $t' = t\kappa$, $r' = r/\kappa$ and $\phi' = \phi\kappa$ such that we bring back the metric to global coordinates

$$ds^2 = -\left(1+\frac{r'^2}{\ell^2}\right)dt'^2 + \left(1+\frac{r'^2}{\ell^2}\right)^{-1}dr'^2 + r^2 d\phi'\,. \tag{2.22}$$

Note that range of t and r has not changed, however, there is now a deficit angle as $\phi \in [0, 2\pi\kappa]$. The size of this deficit is

$$\delta = 2\pi(1-\kappa)\,, \tag{2.23}$$

and can be visualised as cutting out a slice of the angular coordinate from the spacetime. If we identify the edges of the piece that has been removed from the boundary, the spacetime becomes a cone. It is important to notice that, locally, the spacetime is still AdS_3, and therefore the Ricci scalar remains constant. Nevertheless, close to the deficit, one can check that the Ricci scalar behaves as a delta function localised at the tip of the cone producing a naked singularity. This particular type of singularity is usually referred to as *conical singularity*. In fact, conical singularities can be thought of as "point particles" [18] with mass

$$m = \frac{\delta}{8\pi G} = \frac{1-\kappa}{4G}\,. \tag{2.24}$$

Additionally, we can explore the case where $k \to i\sqrt{M}$. The metric in this case takes the form of the static Bañados–Teitelboim–Zanelli (BTZ) black hole [20, 21]

$$ds^2 = -\left(-M+\frac{r^2}{\ell^2}\right)dt^2 + \left(-M+\frac{r^2}{\ell^2}\right)^{-1}dr^2 + r^2 d\phi\,. \tag{2.25}$$

This black hole is not a "black hole" in the strict sense of general relativity. It possesses a Killing horizon at $r_h = \sqrt{M}\ell$ but the singularity behind the event

horizon has been replaced by a conical defect at the origin. As we mentioned previously for the particle, the mass of the black hole produces no gravitational effect and therefore the Ricci scalar is the same everywhere. The massless limit $M \to 0$ brings the metric into the Poincaré patch or massless BTZ. In fact, to obtain global AdS, we need to go to $M = -1$. This is understood as the *mass gap* of AdS_3 as it is separated from the massless limit of the BTZ.

It is also possible to unwrap the S^1 in the transverse section mapping ϕ to a non-compact coordinate $\xi \in \mathbb{R}$ giving the "planar" BTZ space.

The rotating version of the BTZ black hole, now parametrised by M and J, is described by the line element

$$ds^2 = -N^{\perp}dt^2 + \frac{1}{f(r)^2}dr^2 + r^2(N^{\phi}dt + d\phi)^2, \tag{2.26}$$

where $N^{\perp}$ and N^{ϕ} are the lapse and shift functions respectively

$$N^{\perp} = f(r)^2 = -M + \frac{r^2}{\ell^2} + \frac{J^2}{4r^2}, \quad N^{\phi} = -\frac{4GJ}{r^2}. \tag{2.27}$$

It is straightforward to see that the metric (2.26) has two Killing vectors, ξ_t and ξ_ϕ. The parameters M and J can be identified as the conserved quantities associated with the corresponding temporal and angular isometries. There are two coordinate singularities when $f(r_\pm) = 0$,

$$r_\pm^2 = 4GM\ell^2\left(1 \pm \left[1 - \left(\frac{J}{M\ell}\right)^2\right]^{1/2}\right). \tag{2.28}$$

There is an event horizon located at r_+ and an inner Cauchy horizon (when $J \neq 0$) at r_-. The mass and angular momentum can be expressed in terms of the horizons* as

$$M = \frac{r_+^2 + r_-^2}{8G\ell^2}, \quad J = \frac{r_+ r_-}{4G\ell}. \tag{2.29}$$

When $J = M\ell$, the horizons coincide $r_+ = r_-$ defining the so-called *extremal BTZ*. The angular momentum is bounded by cosmic censorship

$$J \leq M\ell\,. \tag{2.30}$$

For J sufficiently large (or $M < 0$), the event horizon disappears and there is a naked singularity at $r = 0$.

Additionally, the BTZ black hole exhibits interesting non-trivial thermodynamics. The Hawking temperature is

$$T_{\mathrm{BTZ}} = \frac{(r_+^2 - r_-^2)}{2\pi\ell^2 r_+}, \tag{2.31}$$

*See [46, 47] for a detailed discussion of the thermodynamics of asymptotically AdS space in $2+1$ dimensions.

and its entropy

$$S_{\text{BTZ}} = \frac{A}{4G} \tag{2.32}$$

with $A = 2\pi r_+$ the area of the horizon. The stability of the solution is given by the sign of its heat capacity

$$C_V = T\frac{\partial S}{\partial T}\Big|_V . \tag{2.33}$$

A thermodynamic system with negative heat capacity $C_V < 0$ is said to be *unstable*. In the case of a Schwarszchild black hole, the heat capacity is negative indicating that, due to the Hawking radiation, the black hole can lose mass until fully evaporates. Nevertheless, this is different for the BTZ as $C_V > 0$. One can interpret this stability as the black hole being inside a box. When its radiation reaches the boundary, this acts as a well reflecting the radiation into the black hole all over again leaving the system in thermal equilibrium. The first law of black hole thermodynamics is satisfied. We can see by varying the mass (2.29) and using (2.31) and (2.32),

$$dM = T_{\text{BTZ}} dS_{\text{BTZ}} + \Omega dJ, \tag{2.34}$$

with $\Omega = r_-/r_+\ell$ as the angular velocity of the black hole horizon. When the extended phase space is considered [48], the cosmological constant becomes a canonical variable [42] giving rise to a pressure term in (2.34). The presence of the pressure in black hole thermodynamics allows for the study of various interesting phenomena, such as phase transitions and critical behavior, analogous to those seen in ordinary thermodynamics [49, 50]. From the point of view of AdS/CFT correspondence, including this term can have profound consequences. The cosmological constant in the bulk gravity theory is related to the central charge of the dual CFT. Therefore, changing the value of Λ can lead to a different CFT with distinct central charge.

2.2.1 Euclidean BTZ

An interesting exercise is to consider the Euclidean version of the BTZ black hole which allows us to see its geometry as a quotient space in a straightforward manner [22]. We can Wick rotate the time coordinate $t \to i\tau_{\text{E}}$, where now τ_{E} is the Euclidean time, to obtain the Euclidean BTZ black hole

$$ds^2 = \left(-M + \frac{r^2}{\ell^2}\right) d\tau_{\text{E}}^2 + \left(-M + \frac{r^2}{\ell^2}\right)^{-1} dr^2 + r^2 d\phi\,. \tag{2.35}$$

Let us introduce the following coordinates

$$\begin{aligned} x &= \left(1-\frac{M\ell^2}{r^2}\right)^{1/2}\cos\left(\frac{\sqrt{M}\tau_{\rm E}}{\ell}\right)e^{\sqrt{M}\phi}\,, \\ y &= \left(1-\frac{M\ell^2}{r^2}\right)^{1/2}\sin\left(\frac{\sqrt{M}\tau_{\rm E}}{\ell}\right)e^{\sqrt{M}\phi}\,, \\ z &= \frac{\sqrt{M}\ell}{r}e^{\sqrt{M}\phi}, \quad z>0\,, \end{aligned} \tag{2.36}$$

which renders the metric to

$$ds^2=\frac{\ell^2}{z^2}(dx^2+dy^2+dz^2)\,. \tag{2.37}$$

The above line element describes the upper half-space of the hyperboloid $\mathbb{H}^3$. The periodicity of the coordinate ϕ demands the following isometric identifications

$$(x,y,z)\sim\left(e^{2\pi\sqrt{M}}x, e^{2\pi\sqrt{M}}y, e^{2\pi\sqrt{M}}z\right)\,. \tag{2.38}$$

Therefore, the Euclidean BTZ black hole can be understood as the quotient of the hyperbolic space $\mathbb{H}^3$ by the isometries written above.

2.2.2 Brown-Henneaux conformal symmetry

Even before gauge/gravity correspondence, there was evidence suggesting the possible connection between gravity in AdS spaces with conformal field theories in one spatial dimension lower. A remarkable result obtained by Brown and Henneaux in 1986 [51] hinted a deeper connection between the asymptotic region of the spacetime and conformal symmetry. In fact, we mentioned that gravity in 2+1 dimensions has no propagating degrees of freedom. As we will see, AdS_3 has boundary degrees of freedom that are related by an underlying boundary theory.

Let us review this observation by considering light-cone coordinates $x^{\pm}\equiv t\pm\phi$. The derivative in this coordinates $\partial_{\pm}=\frac{1}{2}(\partial_t\pm\partial_\phi)$. Let us consider a radial foliation of the spacetime

$$ds^2=\frac{\ell^2}{r^2}dr^2+h_{ij}(r,x^k)dx^idx^j\,, \tag{2.39}$$

where h_{ij} is the induced metric at the boundary ($r\to\infty$). Expanding the induced metric in power series until leading order $h_{ij}=r^2g_{(0)ij}+\mathcal{O}(1)$. We defined asymptotically AdS spaces to be described by a line element of the form (2.39) and whose boundary metric is expressed as

$$g_{(0)ij}dx^idx^j=-dx^+dx^-, \tag{2.40}$$

where $g_{(0)}$ corresponds to the "conformal" boundary metric as defined in (2.10). The most general solution of Einstein's equations with negative cosmological constant that satisfies the Brown-Henneaux boundary conditions (2.39) and (2.40) was

found in [52]

$$ds^2 = \frac{\ell^2}{r^2}dr^2 - \left(rdx^+ - \frac{\ell^2}{r}L_-(x^-)dx^-\right)\left(rdx^- - \frac{\ell^2}{r}L_+(x^+)dx^+\right). \tag{2.41}$$

Here $L_-(x^-)$ and $L_+(x^+)$ are arbitrary functions of x^- and x^+. In fact, two different physical configurations have different values for L and $\bar{L}$. We can see that Poincaré space (2.7) is recovered when $L_- = L_+ = -1/4$. The massless BTZ corresponds to $L_- = L_+ = 0$. For constant values of $L_- = L_0$ and $L_+ = \bar{L}_0$, a massive spinning state is characterised by

$$M = \frac{L_0 + \bar{L}_0}{4G}, \quad J = \ell\frac{L - \bar{L}_0}{4G}. \tag{2.42}$$

In fact, Cangemi and collaborators [53] proved that the ADM invariants (2.42) correspond to gauge invariant quantities of the SO(2,2) group giving a beautiful geometric interpretation for the mass and angular momentum of the BTZ black hole.

The asymptotic symmetries are produced by the Killing vectors ξ^μ that preserve the Brown-Henneaux boundary conditions, i.e., the metric (2.41).

For a set of gauge parameters λ and $\bar{\lambda}$, we can construct the global Noether charges associated with the asymptotic symmetries as

$$Q_\lambda = -\frac{\ell}{8\pi G}\int_0^{2\pi}\frac{\ell\lambda}{\sqrt{2}}L_-d\phi, \quad Q_{\bar{\lambda}} = -\frac{\ell}{8\pi G}\int_0^{2\pi}\frac{\ell\bar{\lambda}}{\sqrt{2}}L_+d\phi, \tag{2.43}$$

that fulfill the Poisson brackets* $\delta_{\lambda_1}Q_{\lambda_2} = \{Q_{\lambda_2}, Q_{\lambda_1}\}$. We can Fourier expand L_+ and L_- where each mode is given as

$$L_m^{(-)} = \frac{\ell}{8\pi G}\int_0^{2\pi}e^{imx^-}L_-(x^-)d\phi, \quad L_m^{(+)} = \frac{\ell}{8\pi G}\int_0^{2\pi}e^{imx^+}L_+(x^+)d\phi. \tag{2.44}$$

Knowing that the components of the stress tensor transform as

$$\begin{aligned}\delta_+L_+ &= V\partial_+L_+ + 2L_+\partial_+V_+ - \frac{1}{2}\partial_+^3V_+\,,\\ \delta_+L_- &= 0\,,\end{aligned} \tag{2.45}$$

we can compute the Poisson brackets by evaluating the modes explicitly

$$\begin{aligned}i\{L_m^{(+)}, L_n^{(+)}\} &= \frac{i\ell}{8\pi G}\int_0^{2\pi}d\phi e^{imx^+}\left(e^{inx^+}\partial_+L_+ + 2L_+\partial_+e^{inx^+} - \frac{1}{2}\partial_+^3e^{inx^+}\right)\\ &= \frac{\ell(m-n)}{8\pi G}\left(\int_0^{2\pi}d\phi e^{i(m+n)x^+}L_+\right) + \frac{c}{12}m^3\delta_{m+n,0}\\ &= (m-n)L_{m+n}^{(+)} + \frac{c}{12}m^3\delta_{m+n,0}\,.\end{aligned} \tag{2.46}$$

*We define the Poisson brackets as $\{F_\xi, G_\eta\} = \mathcal{L}_\eta F_\xi$ where $\mathcal{L}_\eta$ is the Lie derivative in the direction η.

Analogously, we compute

$$\begin{aligned} i\{L_m^{(-)}, L_n^{(-)}\} &= (m-n)L_{m+n}^{(-)} + \frac{\bar{c}}{12}m^3\delta_{m+n,0}, \\ i\{L_m^{(+)}, L_n^{(-)}\} &= 0. \end{aligned} \tag{2.47}$$

We identify $c = \bar{c} = 3\ell/2G$ as the Brown-Henneaux central charge. This last expression (2.47) defines a centrally extended Witt algebra known also as Virasoro algebra. The Virasoro modes $L_m^{(\pm)}$ define the components of the stress tensor of a two–dimensional CFT as can be seen from [54, 55] hinting an intrinsic relation between AdS_3 space and a two-dimensional CFT. In fact, the presence of a non-trivial central extension in even-dimensional CFTs diagnoses a conformal symmetry breaking at the quantum level giving rise to the Weyl anomaly. The result by Brown and Henneaux is quite remarkable considering that is based on purely classical considerations. Although the bulk theory is trivial – in the sense of local degrees of freedom – the asymptotic symmetries suggest that the boundary has similar dynamics to the one of a conformal field theory. As we will see later, the Brown-Hennaux central charge can be also obtained through the AdS/CFT duality.

2.3 AdS/CFT in a nutshell

The holographic principle [12, 13] states that the information of gravity theory is fully contained in a lower dimensional quantum theory without gravity. Maldacena in 1997 [14] came out with a concrete example of this idea by considering branes in Type IIB string theory. In the low energy limit, he observed that there is a correspondence between the supergravity solution on $AdS_5 \times S^5$ and a quantum field theory, $\mathcal{N} = 4$ super Yang–Mills (YM) with gauge group $SU(N)$ in four-dimensions in the large N limit [56]. This "correspondence" implies that the two theories – string theory in AdS and the CFT – provide equivalent descriptions of the same underlying physics. In fact, the defining free parameters of the field theory, the coupling constant $g_{\rm YM}$ and the rank of the group N, are mapped to the parameters of the string theory, the string length $\ell_s = \sqrt{\alpha'}$ and coupling g_s, in the following way

$$g_{\rm YM}^2 = 2\pi g_s \quad , \quad 2g_{\rm YM}^2 N = \frac{\ell^4}{\alpha'^2}\,. \tag{2.48}$$

In principle, the conjecture relates both theories at all levels. From the point of view of the energy, it is clear from (2.48) that the duality relates the *strong* regime on one side with a *weak* regime on the other side. For large N limit – or 't Hooft limit – we are left only with one free parameter at each side, the 't Hooft parameter $\lambda = g_{\rm YM}^2 N$ and the ratio of the AdS curvature and string length $\ell/\sqrt{\alpha'}$. As we approach the large 't Hooft limit $\lambda \to \infty$ on the field theory side, the string length $\sqrt{\alpha'}$ becomes very small compared to the AdS radius ℓ such that $\sqrt{\alpha'}/\ell \to 0$. In

this limit, string theory becomes purely classical gravity, or in order words, type IIB string theory is reduced to type IIB supergravity. Alternatively, one could look at the perturbative limit of Yang–Mills theory (λ small) which would correspond to the non-perturbative regime of string theory. This leads to the notion of a *strong/weak duality* as the weakly coupled string theory is mapped to a strongly coupled field theory and vice versa.

A concrete map between two theories requires a well-defined dictionary in which one could identify quantities from one side with quantities on the other side. In this regard, Gubser, Klebanov and Polyakov [57] followed by Witten [15] provided a very clear manner in which the correspondence is realised. The prescription dispenses a one-to-one relation between operators on the CFT and fields propagating in the gravity theory by relating the generating functions of both theories. A field φ propagating in the bulk of AdS takes a value $\varphi_{(0)}$ near the boundary. This boundary field now sources an operator $\mathcal{O}$ in the dual theory. In Euclidean signature, the generating functional $W[\varphi_{(0)}]$ of connected graphs, defined as

$$W[\varphi_{(0)}] = -\log(Z[\varphi_{(0)}])\,, \tag{2.49}$$

with $Z[\varphi_{(0)}]$ the quantum partition function

$$Z[\varphi_{(0)}] = \left\langle \exp\left(\int d^d x \varphi_{(0)}(x)\mathcal{O}(x)\right)\right\rangle_{\text{CFT}}\,, \tag{2.50}$$

is mapped to the supergravity action by means of

$$W[\varphi_{(0)}] = -I_{\text{sugra}}\left[\varphi \to \varphi_{(0)}\right]\,. \tag{2.51}$$

This, usually referred to as the *weak conjecture* or *saddle-point approximation*, relates the generating functional of the d-dimensional field theory to the classical gravitational action on $d+1$-dimensional AdS space, upon the boundary condition that $\varphi \to \varphi_{(0)}$. It provides a precise identification between the information contained in both sides of the duality allowing us to obtain correlation functions of gauge invariant operators $\mathcal{O}$ in terms of functional variations of the classical gravity action

$$\langle \mathcal{O}(x_1)\cdots\mathcal{O}(x_n)\rangle = -\frac{\delta^n I_{\text{sugra}}(\varphi_{(0)})}{\delta\varphi_{(0)}(x_1)\cdots\delta\varphi_{(0)}(x_n)}\bigg|_{\varphi_{(0)}=0}\,. \tag{2.52}$$

2.3.1 Holographic renomalisation

Despite Witten's prescription for extracting correlation functions is straightforward, in practice, the process can be quite involved due to infrared divergences in the gravity sector. These divergences, associated with the boundary behaviour of fields in AdS, require to implement a renormalisation scheme to obtain finite holographic data. Luckily, there is a consistent and systematic procedure for dealing

with them. The method, first introduced by Henningson and Skenderis [58] and then formalised and extended in [59–61], utilises the conformal structure of AdS to make a covariant derivation of the series of counterterm that needs to be included in the gravity action in order to cancel the divergences. We will illustrate the procedure for the metric field as it is of major relevance for the upcoming chapters.

Let us start with the Einstein–Hilbert action in $d+1$ dimensions supplemented with the Gibbons–Hawking–York boundary term [62, 63],

$$I_{\text{dirichlet}} = \frac{1}{16\pi G}\int_{\mathcal{M}} d^3x\sqrt{-g}\,(R-2\Lambda) + \frac{1}{8\pi G}\int_{\partial\mathcal{M}} d^2x\sqrt{-h}K \tag{2.53}$$

ensuring a well-posed variational principle under Dirichlet boundary conditions. Let us also consider that any asymptotically AdS space can be written as

$$ds^2 = \frac{\ell^2}{z^2}\left(dz^2 + h_{ij}(z,x)dx^i dx^j\right)\,, \tag{2.54}$$

where h_{ij} is the induced metric at $z=$ const hypersurface *. Remember that in principle, at the boundary $z=0$, the metric has a double pole. This can be bypassed by considering the conformal representative $g_{(0)}$ as defined in (2.10). In fact, the Fefferman–Graham [64] theorem states that it is always possible to find a coordinate transformation for a conformally compact Einstein manifold that renders its metric into (2.54) with an expansion near the boundary of the form

$$h_{ij}(z,x) = g_{(0)ij}(x) + z g_{(1)ij}(x) + z^2 g_{(2)ij}(x) + \cdots\,. \tag{2.55}$$

Note that each coefficient $g_{(n)ij}(x)$ is independent of the radial direction z. For simplicity, we omit the coordinate dependence from now on. The holographic reconstruction prescription [59] uses Einstein's equations to determine all the functions $g_{(n)ij}$ order by order in z, in terms of $g_{(0)ij}$ whereas $g_{(0)ij}$ is in principle arbitrary, defined up the conformal representative ω (2.10). This implies that given a bulk metric, there is a family of conformally equivalent boundary metrics $[g_{(0)ij}]$ that reconstruct the same bulk information. When pure gravity is considered, it is possible to show that all coefficients with odd powers of z do not contribute up to order d. For even-dimensional boundary, i.e., $d=2n$ there is an extra logarithmic contribution at order z^d,

$$h_{ij}(z,x) = g_{(0)ij} + z^2 g_{(2)ij} + \cdots + z^d(g_{(d)ij}(x) + \tilde{h}_{(d)ij}\log(z^2)) + \cdots\,. \tag{2.56}$$

The term $h_{(d)ij}$ that accompanies the logarithm contains information about the conformal anomaly, as we will see later. The last term of the expansion, $g_{(d)}ij$ cannot be determined except for its trace and covariant derivative. The holographic renormalisation method consists in evaluating the gravity action (2.53) using the

*This is the same radial foliation employed by Brown and Henneaux (2.39) but we have replaced $r \to z$ as it encapsulates a more general "radial" direction.

Fefferman–Graham metric (2.54) with the expansion near the boundary explicitly. Thus, the action takes the form

$$I = \frac{1}{16\pi G}\int d^{d+1}x\sqrt{g_{(0)}}\left(\epsilon^{-d}a_{(0)} + \epsilon^{-d+2}a_{(2)} + \cdots - \log\epsilon^2 a_{(d)}\right) + I_{\text{finite}}\,, \quad (2.57)$$

where we introduced the infrared cutoff $z = \epsilon$. The term I_{finite} contains the finite contributions to the action. The problem is reduced to determining the coefficients $a_{(n)}$ in terms of the leading order of the Fefferman–Graham expansion $g_{(0)ij}$, its covariant derivatives, which can be expressed in terms of the intrinsic curvature of the conformal boundary $\mathcal{R}_{ij}$, and further contractions. For instance, the first few coefficients are

$$\begin{aligned} a_{(0)} &= \frac{2(d-1)}{\ell}, \\ a_{(2)} &= \frac{\ell}{2(d-1)}\mathcal{R}, \\ a_{(4)} &= \frac{\ell^3}{2(d-2)^2}\left(\mathcal{R}^{ij}\mathcal{R}_{ij} - \frac{1}{d-1}\mathcal{R}^2\right). \end{aligned} \quad (2.58)$$

Putting together all the coefficients, we construct the counterterm action that should be added on top of the on-shell action (2.57) to cancel the bulk divergences. Thus, the renormalised action reads

$$I_{\text{ren}}[g_{(0)}] = \lim_{\epsilon\to 0}\frac{1}{16\pi G}\left[I - \int d^{d+1}x\sqrt{g_{(0)}}\left(\epsilon^{-d}a_{(0)} + \epsilon^{-d+2}a_{(2)} + \cdots +\right)\right], \quad (2.59)$$

where remove the regulator ϵ by approaching the conformal boundary. The resulting action contains only the finite pieces of the on-shell action (2.57). It is possible to write the counterterms as a surface term by expressing them in terms of the boundary metric h_{ij}. In three-dimensional gravity, the only divergent coefficient is $a_{(0)}$, and therefore the renormalised action is

$$I_{2+1} = I_{\text{dirichlet}} - \frac{1}{8\pi\ell}\int_{\partial\mathcal{M}} d^2x\sqrt{-h}. \quad (2.60)$$

In 3+1 dimensions, we need to include up to $a_{(2)}$ for which the action takes the form

$$I_{3+1} = I_{\text{dirichlet}} - \frac{1}{8\pi G}\int_{\partial\mathcal{M}} d^2x\sqrt{-h}\left[\frac{2}{\ell} + \frac{\ell}{2}\mathcal{R}\right]. \quad (2.61)$$

2.3.2 Quasilocal energy and holographic stress tensor

Quasilocal energy provides a way to characterise the energy within a finite region by considering the energy-momentum flow across the boundary of that region. In this regard, Brown and York [65] gave a definition of quasilocal energy by constructing

a gravitational stress tensor as functional variations of the Dirichlet action (2.53) with respect to the boundary metric h_{ij}, namely

$$T_{ij}[h] = -\frac{2}{\sqrt{-h}}\frac{\delta I_{\text{dirichlet}}}{\delta h^{ij}}. \tag{2.62}$$

However, this definition of energy for asymptotically AdS spacetimes suffers from the same bulk divergences described in 2.3.1. Instead, Balasubramanian and Kraus [55] realised that one can replace the Dirichlet action for the renormalised action (2.59) and consider variations with respect to the conformal boundary metric $g_{(0)ij}$,

$$\langle T_{ij}\rangle = -\frac{2}{\sqrt{-g_{(0)}}}\frac{\delta I_{\text{ren}}}{\delta g^{ij}_{(0)}} = \lim_{\epsilon\to 0}\left(\frac{1}{\epsilon^{d-2}}T_{ij}[h]\right). \tag{2.63}$$

For Einstein-AdS gravity in 3+1 dimensions, evaluating the renormalised action (2.61), we get the holographic stress tensor

$$\langle T_{ij}\rangle_{2+1} = \lim_{z\to 0}\frac{-1}{z}\frac{1}{8\pi G}\left(K_{ij} - Kh_{ij} - \frac{2}{\ell}h_{ij} - \ell\mathcal{G}_{ij}\right) \tag{2.64}$$

with $\mathcal{G}_{ij}$ being the Einstein tensor of the boundary metric h_{ij}. In the case of 2+1 dimensions, the evaluation of (2.60) yields

$$\langle T_{ij}\rangle_{2+1} = \lim_{z\to 0}\frac{-1}{8\pi G}\left(K_{ij} - Kh_{ij} - \frac{1}{\ell}h_{ij}\right), \tag{2.65}$$

which can be also expressed in terms of the Fefferman–Graham coefficients $g_{(0)}$ and $g_{(2)}$ as

$$\langle T_{ij}(g_{(0)})\rangle_{2+1} = \frac{-1}{8\pi G}\left(g_{(2)ij} - g_{(0)ij}\text{Tr}\left[g^{-1}_{(0)}g_{(2)}\right]\right). \tag{2.66}$$

The energy density of the spacetime ρ_{E} is contained in the $tt-$component of the energy-momentum tensor. From the holographic point of view, the Balasubramanian–Kraus stress tensor contains information about the energy of the dual field theory. Moreover, from Witten's prescription, the energy-momentum tensor (2.63) is interpreted as the boundary operator generated by the fluctuations of the bulk metric. It is, in this way, sourced by the boundary metric $g_{(0)}$ and therefore corresponds to a one-point function in the CFT. The holographic Ward identities associated with diffeomorphism invariance guarantee that the boundary stress tensor is conserved

$$\nabla^i\langle T_{ij}[g_{(0)}]\rangle = 0\,, \tag{2.67}$$

where ∇^i is the covariant derivative constructed with the CFT background metric $g_{(0)ij}$.

2.3.3 Holographic Weyl Anomaly for AdS_3

In a classical field theory invariant under conformal transformations, the trace of the energy-momentum tensor vanishes

$$\langle T^i_i\rangle = 0\,. \tag{2.68}$$

At the quantum level, this is not always true. In CFTs with non-vanishing central charge, the stress tensor is not a primary operator and therefore transforms under conformal transformations. Moreover, instead of being traceless, its trace is proportional to the conformal anomaly which accounts for the breaking of conformal symmetry at the quantum level. This is the case of even-dimensional CFTs as the one observed in Section 2.2.2. Henningson and Skenderis [58] computed the Weyl anomaly by studying how the renormalised action transforms under Weyl rescaling. Alternatively, one can use the already defined Balasubramanian–Kraus stress tensor [55] evaluated on-shell to diagnose the conformal anomaly. We will use this last approach to show the explicit computation for 2+1 dimensional gravity.

Let us consider an asymptotically AdS_3 space written in Gauss-normal coordinates,

$$ds^2 = N(r)^2 dr^2 + h_{ij}(r, x^k) dx^i dx^j \,, \tag{2.69}$$

where N is the radial lapse function. Comparing with (2.39), we identify $N = \ell/r$. The extrinsic curvature $K_{ij} = \frac{1}{2}\mathcal{L}_n h_{ij}$ is

$$K_{ij} = -\frac{1}{2N}\partial_r h_{ij} = -\frac{r}{2\ell}\partial_r h_{ij} \,. \tag{2.70}$$

Evaluating the trace of the stress tensor (2.65) in these coordinates, we get

$$\langle T_i^i \rangle = \lim_{r\to\infty} -\frac{1}{8\pi G}\left(-\frac{r}{2\ell}h^{ij}\partial_r h_{ij} + \frac{2}{\ell}\right) , \tag{2.71}$$

which we can actually expand using the Fefferman-Graham coefficients (2.56). Therefore, we get

$$\langle T_i^i[g_{(0)}] \rangle = \lim_{r\to\infty} -\frac{1}{8\pi G\ell r^2}\mathrm{Tr}\left[g_{(0)}^{-1}g_{(2)}\right] = -\frac{\ell}{16\pi G}\mathcal{R}[g_{(0)}] \,, \tag{2.72}$$

where we have already identified the Ricci scalar of the boundary metric $g_{(0)ij}$ when taking the limit $r \to \infty$, viz.

$$\mathcal{R}[g_{(0)}] = \lim_{r\to\infty} \frac{2}{\ell^2 r^2}\mathrm{Tr}\left[g_{(0)}^{-1}g_{(2)}\right] \,. \tag{2.73}$$

In a two-dimensional conformal field theory that has Weyl anomaly, the trace of the stress tensor is

$$\langle T_i^i \rangle = \mathcal{A} = -\frac{c}{24\pi}\mathcal{R} \,, \tag{2.74}$$

where $\mathcal{R}$ is the Ricci scalar of the background metric. After comparing both expressions (2.72) and (2.74), we identify the Brown–Henneaux central charge $c = 3\ell/3G$.

Chapter 3

Accelerating Black Holes in 3+1–dimensions

An accelerating black hole is described by what is usually known as the C–metric. Originally found by Levi-Civita [66] and subsequently by Weyl [67], the C–metric was first analysed in detail by Kinnersley and Walker [68], and Bonnor [69]. The authors interpreted the solution as a pair of black holes uniformly accelerating in opposite directions. The force responsible for the acceleration is due to the presence of one or two antipodal conical deficits in the transverse section. One can think of these defects as coming from a string that extends from infinity and pushes both black holes in opposite directions. This was later extended to Einstein–Maxwell theory in four dimensions by Plebanski and Demianski [70] to include mass, angular momentum, acceleration, NUT parameter, electric and magnetic charges and the cosmological constant Λ. Since then, the C–metric has been extensively studied [71–77] and extended to diverse scenarios such as Einstein–Maxwell–Dilaton gravity [78], braneworld models [79], quantum black holes [80–82] and supergravity [83]. More recently supersymmetric extensions were constructed in $D = 4$ gauged supergravity [84–86]. These solutions can be uplifted using a Sasaki-Einstein manifold SE_7 to supergravity in $D = 11$ resulting in a smooth geometry with properly quantised fluxes.

For negative cosmological constant $\Lambda < 0$, the C-metric exhibit a "slowly accelerating" phase [87] in which there is neither an acceleration horizon nor a second black hole. This is interpreted as a black hole in equilibrium suspended at a fixed distance from the centre of AdS – a locally accelerating frame. The drastic simplification which occurs in this phase has led to significant advances understanding the role of acceleration.

Throughout this chapter, we are going to focus in the classical description of a sub-class of the C-metric parametrised by only two quantities, its mass m and acceleration A. Starting from the most general form of the Plebánski–Demiański

metric within its full parameter space, we will study the physical properties of the four-dimensional accelerating black hole in different coordinate patches. This would allow to explore different aspects of the structure of the spacetime. In specific, addressing the question of what it means for these black holes to be "accelerating".

3.1 C–metric in four-dimensions

As aforementioned, the most general analytic solution to Einstein–Maxwell theory with negative cosmological constant $\Lambda = -3/\ell^2$ is given by the Plebánski-Demiański metric

$$ds^2 = \frac{1}{A^2(x-y)^2}\Bigg[-\frac{P(y)}{1+(aAxy)^2}\Big(d\tau + aAx^2 d\sigma\Big)^2 + \frac{1+(aAxy)^2}{P(y)}dy^2 + \frac{1+(aAxy)^2}{Q(x)}dx^2 + \frac{Q(x)}{1+(aAxy)^2}\Big(d\sigma - aAy^2 d\tau\Big)^2\Bigg], \quad (3.1)$$

with

$$P(y) = \left(\frac{1}{A^2\ell^2} - \kappa\right) + \frac{2n}{A}y + \varepsilon y^2 + 2mAy^3 + A^2(\kappa a^2 + e^2 + g^2)y^4,$$
$$Q(x) = \kappa - \frac{2n}{A}x - \varepsilon x^2 - 2mAx^3 + \left(\frac{a^2}{\ell^2} - A^2(\kappa a^2 + e^2 + g^2)\right)x^4, \quad (3.2)$$

and gauge field

$$\mathcal{A} = -\frac{ey}{1+(aAxy)^2}\Big(d\tau + aAx^2 d\sigma\Big) + \mathcal{A}_\tau d\tau + \mathcal{A}_\sigma d\sigma + \frac{gx}{1+(aAxy)^2}\Big(d\sigma - aAy^2 d\tau\Big). \quad (3.3)$$

It is important to notice that the equations of motion are satisfied for any value of $\mathcal{A}_\tau$ and $\mathcal{A}_\sigma$. We also see that there are seven physical quantities namely the mass m, angular momentum a, acceleration A, NUT parameter n, electric and magnetic charge e, g respectively and AdS radius ℓ. There is also two extra parameters κ and ε that correspond to gauge freedoms. We will take the gauge parameters to be $\kappa = \varepsilon = 1$. The NUT parameter n is induced by the presence of Misner strings [88–90] at $x = \pm 1$. Setting $n = 0$ removes the Misner strings leading the rotating charged C-metric [76]. In order to isolate the effect of the acceleration we will turn off these parameters leaving just m, A and ℓ leading to

$$ds^2 = \frac{1}{A^2(x-y)^2}\left(-P(y)d\tau^2 + \frac{1}{P(y)}dy^2 + \frac{1}{Q(x)}dx^2 + Q(x)d\sigma^2\right) \quad (3.4)$$

where

$$P(y) = \left(\frac{1}{\ell^2 A^2} - 1\right) + y^2 - 2mAy^3,$$
$$Q(x) = 1 - x^2 - 2mAx^3. \quad (3.5)$$

A simple inspection shows that the boundary of the spacetime is located at $x = y$. There are also curvature singularities at $y = \pm\infty$ and $x = \pm\infty$ which can be seen from the Kretschmann scalar

$$\mathcal{K} = R_{\mu\nu\alpha\beta}R^{\mu\nu\alpha\beta} = \frac{24}{\ell^4} + 48A^6m^2(x-y)^6 + \cdots . \tag{3.6}$$

Although this coordinate system is not physically intuitive, gives interesting information about the structure of the spacetime and more specifically, the range of the variables in which the Lorentzian signature is preserved. This is provided for $Q(x) \geq 0$ that imposes $2mA \leq 1$ which can be seen as a bound for the acceleration. It also restricts the range of the coordinate x between $x_1 < x < x_2$. In general, $Q(x)$ has three roots for which at least one is real. For $0 < mA < 1/3\sqrt{3}$, there are 3 real roots $x_0 < x_1 < 0 < x_2$. The location of the boundary $x \neq y$ allow us to restrict the coordinate y to lie in the range $-\infty < y < x$ or $x < y < \infty$. If we choose $-\infty < y < x$, there is a black hole horizon at $y_h = -1/2mA$ and a second degenerate horizon $y = 0$ with zero Hawking temperature. The coordinate σ can be chosen to be compact and since $Q(x)$ vanishes at x_1 and x_2, there might be conical singularities. As we will see later, these points correspond to antipodal defects induced by the tension of a cosmic string and they cannot be regularised both at the same time by a choice of parameters.

To make this issue evident and get a better understanding of the black hole structure is convenient to perform the following metric functions factorisation introduced by Hong and Teo in [91], viz.

$$P(y) = \frac{1}{A^2\ell^2} + (y^2-1)(1-2mAy), \quad Q(x) = (1-x^2)(1+2mAx). \tag{3.7}$$

Note that includes an extra linear term in y. This does not alter the dynamics as it corresponds to a purely kinematic term. We then introduce the Boyer-Lindquist coordinates (t, r, θ, ϕ) by taking

$$y = -\frac{1}{Ar}, \quad x = \cos\theta, \quad \sigma = \frac{\phi}{K}. \tag{3.8}$$

where we have introduced a new parameter K such that range of the new angular coordinate ϕ is $\phi \in [0, 2\pi]$. The time coordinate can be rescaled as $\tau \to At/\alpha$ leading to

$$ds^2 = \frac{1}{\Omega^2}\left[-f(r)\frac{dt^2}{\alpha^2} + \frac{1}{f(r)}dr^2 + r^2\left(\frac{d\theta^2}{g(\theta)} + g(\theta)\sin^2\theta\frac{d\phi^2}{K^2}\right)\right], \tag{3.9}$$

where

$$\begin{aligned} \Omega &= 1 + Ar\cos\theta, \\ f(r) &= (1-A^2r^2)\left(1-\frac{2m}{r}\right) + \frac{r^2}{\ell^2}, \\ g(\theta) &= 1 + 2mA\cos\theta. \end{aligned} \tag{3.10}$$

In principle, the radial coordinate ranges from $0 \leq r \leq \infty$. There is a coordinate singularity at $r = 0$, and the conformal boundary is located at $r = -1/A\cos\theta$ meaning that the only point where the radial coordinate reaches the infinity is at $\theta = \pi/2$. For $\theta < \pi/2$, the conformal boundary is located beyond the radial infinity suggesting that these coordinates do not capture the conformal structure correctly. There is a smooth limit for when $A \to 0$ where the solution becomes Schwarzschild AdS and the flat space limit is obtained for $\ell \to \infty$ recovering [92]. As was noted in the canonical coordinates, the horizons are given by the roots of $f(r) = 0$ that in this case depends on the interplay between m, A and ℓ. The largest root corresponds to the black hole horizon r_h and there is an additional accelerating horizon due to A. For $A\ell < 1$, there is only one Killing horizon at $r_h \sim 2m$. We will refer to this limit as the *slowly accelerating* phase. This phase will allow us to study the thermodynamic properties of the solution with the standard methods as the black hole is in thermal equilibrium.

Next, we turn our attention to the massless limit of the solution. The purpose of this exercise is to examine the physical implications of the parameter A and its relation with K.

3.1.0.1 Acceleration and conical deficits

We can use the slow accelerating phase to reveal the effect of A in the spacetime. In fact, the effect of the acceleration can be observed more clearly when the massless limit is under consideration. If we take the $m \to 0$ limit in (3.9), we get AdS_4 in Rindler coordinates,

$$ds^2 = \frac{1}{\Omega^2}\left[-\left(1 - A^2r^2 + \frac{r^2}{\ell^2}\right)\frac{dt^2}{\alpha^2} + \frac{1}{\left(1 - A^2r^2 + \frac{r^2}{\ell^2}\right)}dr^2 + r^2\left(d\theta^2 + \sin^2\theta\frac{d\phi^2}{K^2}\right)\right]. \tag{3.11}$$

Setting $K = 1$, we can apply a simple coordinate transformation

$$1 + \frac{R^2}{\ell^2} = \frac{1 + (1 - A^2\ell^2)r^2/\ell^2}{(1 - A^2\ell^2)\Omega^2}, \quad R\sin\Theta = \frac{r\sin\theta}{\Omega}, \tag{3.12}$$

which leads to global AdS spacetime

$$ds^2 = -\left(1 + \frac{R^2}{\ell^2}\right)dT^2 + \frac{1}{\left(1 + \frac{R^2}{\ell^2}\right)}dR^2 + R^2\left(d\Theta^2 + \sin\Theta d\phi^2\right), \tag{3.13}$$

where $T = \alpha t$ with $\alpha = \sqrt{1 - A^2\ell^2}$ is the rescaled time. This normalisation is chosen to be the time of an asymptotic observer. We can see that $R = r$ and $T = t$ when the acceleration vanishes. Otherwise, the acceleration counterbalance the effect of the cosmological constant in the new radial and temporal directions

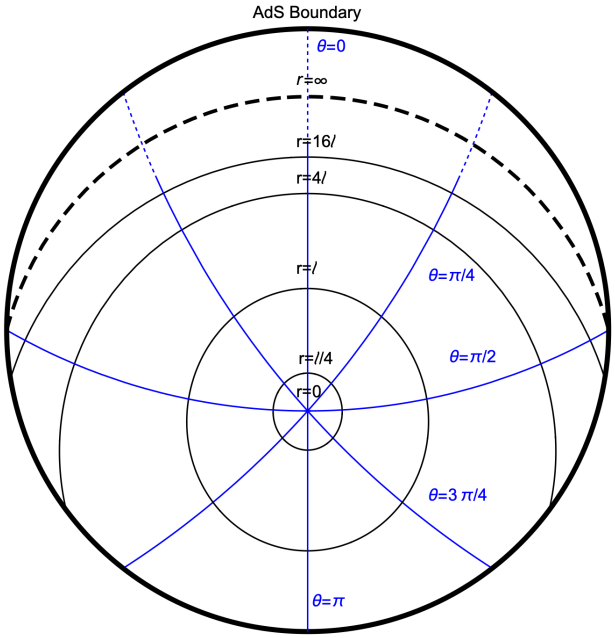

Figure 3.1: The slow accelerating black hole mapped to AdS space with $A = 0.5\ell$. Lines of constant angle θ are shown in solid blue lines. Lines of constant radius r are shown in solid black lines. The $r \to \infty$ surface is shown in dotted black line.

giving a *deformed* perspective of the AdS space as seen from Figure 3.1. In this frame, a particle located at $r = r_0$ follows a worldline with four-velocity

$$u^\mu = \left(\frac{\alpha\Omega}{\sqrt{f(r)}}, 0, 0, 0 \right)^\mu \Big|_{r=r_0} \tag{3.14}$$

and therefore, the four-acceleration defined as $a^\mu = u^\nu \nabla_\nu u^\mu$ at $r = r_0$ has a magnitude $|a| = A$ [73]. This reassures that the interpretation of the parameter A as the acceleration is correct.

Let us now examine the parameter K. This parameter is associated with a conical deficit along the polar direction. A straightforward revision of the regularity of the axes of symmetry of the C-metric line element reveals the existence of conical singularities measured by the conicity

$$\delta = 2\pi \left(1 - \frac{1}{K} \right) = 8\pi\mu \,, \tag{3.15}$$

that can be thought of as produced by the presence of a cosmic string with tension μ. In the literature, the introduction of a cosmic string through the polar axis of a Schwarzschild black hole to produce a conical deficit was first demonstrated by Aryal, Ford, and Vilenkin [93]. However, for accelerating solutions, it is important to note that the conicity at each pole can be different. This is due to an imbalance in the cosmic string tension, which results in a net force on the black hole along

the ϕ axis. Close to the poles in (3.9), the tension (or conicity) is

$$\mu_{\pm} = \frac{\delta_{\pm}}{8\pi} = \frac{1}{4}\left(1 - \frac{g(\theta_{\pm})}{K}\right) = \frac{1}{4}\left(1 - \frac{1 \pm 2mA}{K}\right), \tag{3.16}$$

where $\theta_+ = 0$ denotes the North pole and $\theta_- = \pi$ South pole. An angular excess is also possible being sourced by a negative tension string or *strut*. In four–dimension, we will only be considering angular deficits. Mathematically, the angular section of the metric is still topologically S^2 but with the cosmic string deforming the poles producing what is usually known as a Spindle [84]. From (3.16), we can see that for $A \neq 0$ it is not possible to make both poles regular at the same time. In fact, it is possible to remove –at most– one of them by properly selecting the period of the azimuthal coordinate and therefore translating the whole conicity to one of the poles, usually an angle deficit at the north one. From the point of view of the cosmic string, this is translated as removing half of the string [94]. We choose $K = 1 + 2mA$ that regularises the North pole and leaves the South pole subject to a tension

$$\mu_S = \frac{mA}{K}\,. \tag{3.17}$$

If we identify $M = m/K$ to be the "physical" mass of the black hole, we can see that $\mu = MA$ which satisfies Newton's law. Together with the slow acceleration condition, the force produced by the cosmic string in the South pole cancels out with the intrinsic force of AdS space leaving the black hole suspended off-centre as in (3.13).

3.2 Thermodynamics with Conical Deficit and Acceleration

As we anticipated, the slow accelerating black hole in 3+1-dimensions has a unique horizon at $r = r_h$ with temperature

$$T = \frac{f'(r_h)}{4\pi\alpha} = \frac{1 + 3\frac{r_h^2}{\ell^2} - A^2 r_h^2\left(2 + \frac{r_h^2}{\ell^2} - A^2 r_h^2\right)}{4\pi\alpha r_h(1 - A^2 r_h^2)}\,. \tag{3.18}$$

Requiring the Euclidean time to be periodic, $\tau_{\rm E} \in [0, \beta]$, with $\beta = T^{-1}$, the temperature acquires a contribution from α. The entropy of the black hole is nothing else than the Bekenstein–Hawking entropy, viz.

$$S_{\rm BH} = \frac{A}{4} = \frac{\pi r_h^2}{(1 - A^2 r_h^2)K}. \tag{3.19}$$

Apart from these two quantities, it is important to identify the total energy of the black hole. In this regard, there are several ways for obtaining black hole mass. Among those, the most popular methods are the ADM formalism [95], quasilocal

energy [65] and Noether–Wald formula [96] *. Although these definitions are quite simple, in practice the applicability of the formulas depends on the asymptotics of the black hole under consideration. In particular, the metric (3.9) has a non-standard asymptotic structure which makes the computation of the energy through these methods more involved. An alternative definition was given by Ashtekar, Magnon and Das (AMD) [41, 98]. The AMD formula is constructed in such a way that we remove the divergence appearing at the boundary by considering an unphysical metric $\bar{g}_{\mu\nu} = \bar{\Omega}^2 g_{\mu\nu}$. Then, it is possible to construct a conserved current proportional to the Weyl tensor of the conformally transformed metric, $\bar{W}^{\nu}_{\alpha\mu\beta}$. The conserved charge is obtained by the integration of the current as

$$Q(\xi) = \frac{\ell}{8\pi} \lim_{\bar{\Omega}\to 0} \oint \frac{\ell^2}{\bar{\Omega}} n^{\alpha} n^{\beta} \bar{W}^{\nu}_{\alpha\mu\beta} \xi_{\nu} d\Sigma^{\mu}, \tag{3.20}$$

where $n_\mu = \partial_\mu \bar{\Omega}$ and ξ_μ is the corresponding Killing vector. It has been shown that this formula can be obtained through the traditional Noether-Wald procedure [99, 100] upon a proper renormalisation of the gravity action. We take $\bar{\Omega} = \ell \Omega r^{-1}$ and the surface element tangent to the horizon

$$dS_\mu = \delta^t_\mu \frac{\ell^2 (d\cos\theta) d\phi}{\alpha K}. \tag{3.21}$$

For a timelike Killing vector $\xi_t = \partial_t$, we obtain [101]

$$M = Q(\partial t) = \alpha \frac{m}{K}, \tag{3.22}$$

where α is the time rescaling constant. One can replace the timelike Killing vector $\xi_t \to \frac{\xi_t}{\alpha}$ corresponding to the Killing vector of an asymptotic observer leading to $M = \frac{m}{K}$ as proposed in the previous section by looking at the tension of the cosmic string. Once again, we recover Schwarzschild black hole by taking $A \to 0$ and $K = 1$. The limitation of the AMD formula is the dimensionality of the spacetime. For dimensions lower than four, the Weyl tensor is identically zero making this method inapplicable. Instead, one could make use of the Barnich–Brandt formalism [102] which is usually employed to extract the energy of three–dimensional black holes, Noether-Wald method or standard holographic techniques which seem to be more suitable options to face the problem upon a well-posed action principle [55, 90, 103, 104].

With the aforementioned considerations in mind, it is natural to consider verifying the first law of thermodynamics. To this end, let us assume that the metric function $f = f(r_h, m, \ell, A)$ where r_h denotes the black hole horizon defined by $f(r_h) = 0$. We want to examine small changes δr_h in the black hole horizon which translates into

$$f(r_h + \delta r_h) = f'(r_h)\delta r_h + \frac{\partial f}{\partial m}\delta m + \frac{\partial f}{\partial \ell}\delta \ell + \frac{\partial f}{\partial A}\delta A = 0\,. \tag{3.23}$$

*See [97] for a more detailed comparison between different definitions of energy in asymptotically AdS spaces

In principle, a black hole should be described, thermodynamically, by its entropy $S_{\rm BH}$, temperature T, and total energy M. Additionally, when incorporating the cosmological constant as a thermodynamic variable [50], new quantities come into play. Specifically, we introduce the pressure P, given by

$$P = -\frac{\Lambda}{8\pi} = \frac{3}{8\pi\ell^2} \,, \tag{3.24}$$

and its conjugate variable, the thermodynamic volume [48],

$$V = \frac{4\pi r_h^3}{3K} \,. \tag{3.25}$$

It should be noted that the quantities $S_{\rm BH} = S_{\rm BH}(r_h, K, A)$ and $M = M(m, K, A, \ell)$ can potentially depend on the conical deficit K. Furthermore, we allow for variations in the tension $\mu_\pm$ (as expressed in (3.16)). This implies that variations with respect to μ can be translated into variations of A, K and m, and vice versa. Then, replacing the variations of each quantity and turning variations of K and A into μ, we arrive at the extended form of the first law [105–107]

$$\delta M = T\delta S_{\rm BH} + V\delta P - \lambda_+\delta\mu_+ - \lambda_-\delta\mu_- \tag{3.26}$$

where $\lambda_\pm$ is the conjugate variable to the tensions referred to as the thermodynamic length

$$\lambda_\pm = \frac{r_h}{1 \pm Ar} \,, \tag{3.27}$$

associated with the string attached at each pole. The black hole also follows the standard Smarr relation

$$M = 2TS_{\rm BH} - 2PV \,. \tag{3.28}$$

3.3 Holographic Stress Tensor

As we have seen, these black holes seem to follow slightly different thermodynamic relations, being the tension of the cosmic string, an important factor to consider. Another interesting way of examining the properties of the spacetime is to consider the holographic data. The standard recipe when treating with asymptotically AdS spacetimes is to consider a Fefferman–Graham near the boundary by identifying the holographic coordinate that defines the (conformal) boundary of the spacetime as shown in 2.3.1.

However, the asymptotic structure of the C-metric (3.9) possesses a challenge in this regard as the conformal boundary is not given by a constant value of the radial coordinate and as we saw previously the conformal boundary is located at a surface $r = \frac{-1}{A\cos\theta}$ which implies that $r \to \infty$ is just a single point of the boundary. Intuitively, one could make a coordinate transformation such that we introduce

a coordinate z which leaves the boundary at $z = 0$. This coordinate should be related to both r and θ and it should be perpendicular to the boundary. This has been explored in [85, 108] by rewriting the metric (3.1) into ADM coordinates allowing to identify of the boundary metric in a straightforward manner but with a non-diagonal line element.

Alternatively, one could try to force the accelerating black hole into the Fefferman-Graham gauge. Using an asymptotic expansion for both the radial and angular coordinates in terms of the Fefferman–Graham coordinates, the authors [101] identified the boundary metric up to a conformal representative ω. In four–dimensions, this is not a problem due to the conformal invariance of the renormalised action [59, 109, 110] meaning that the observables at the boundary are also independent of the conformal representative. In three dimensions, the story is slightly different. We will come back to this discussion later.

Below, we will review each of the methods to construct the boundary metric and holographic stress tensor.

3.3.1 Fefferman-Graham Gauge and Holographic Mass

Following [111], the metric (3.9) can be cast into Fefferman–Graham coordinates

$$ds^2 = \frac{\ell^2}{z^2}dz^2 + \frac{\ell^2}{z^2}\left(g_{(0)ij} + z^2 g_{(2)ij} + z^4 g_{(4)ij} + \cdots\right)dx^i dx^j, \tag{3.29}$$

by introducing a new coordinate system which puts the conformal boundary $r = -1/A\cos\theta$ at $z = 0$. The appropriate transformation near the boundary

$$\begin{aligned} y &= -\tfrac{1}{Ar} = \xi + \sum_{m=1}^{\infty} F_m(\xi) z^m \\ x &= \cos\theta = \xi + \sum_{m=1}^{\infty} G_m(\xi) z^m, \end{aligned} \tag{3.30}$$

where $F_m(\xi)$ and $G_m(\xi)$ are unknown functions that can be determined by requiring the metric (3.9) to behave as (3.29). Note that this transformation is allowed only for the slow accelerating phase. Then, one can solve Einstein's equations order by order in the expansion requiring $g_{zz} \equiv \ell^2/z^2$ and enforcing the lack of crossed terms $g_{z\xi}$ at each order. The procedure allows to determine the unknown functions except F_1 which remains arbitrary defining a family of conformally equivalent boundary metrics $g_{(0)}$. For simplicity, we chose

$$F_1(\xi) = -\frac{(1 - A^2\ell^2 X)^{3/2}}{A\omega(\xi)\alpha}, \tag{3.31}$$

where ω now carries the conformal freedom of the boundary metric and $X = (1 - \xi^2)(1 + 2mA\xi)$. At order $\mathcal{O}(z^{-2})$ we find

$$G_1(\xi) = -\frac{A\ell^2 F_1(\xi) X}{1 - A^2\ell^2 X}, \tag{3.32}$$

which is enough to determine (up to the conformal representative) the boundary metric $g_{(0)}$,

$$ds^2_{(0)} = \omega^2(\xi)\left[-d\tau^2 + \frac{\alpha^2\ell^2 d\xi^2}{X(1-A^2\ell^2X)^2} + \frac{X\alpha^2\ell^2 d\phi^2}{K^2(1-A^2\ell^2X)}\right]. \tag{3.33}$$

In four-dimensions, the Fefferman-Graham expansion terminates at order $\mathcal{O}(z^2)$ for which it is enough to construct the asymptotic expansion up to $m = 4$. With this, it is possible to evaluate the boundary stress tensor (2.64)

$$\langle T_{ij}\rangle = -\frac{X'''(\xi)(1-A^2\ell^2X)^{3/2}}{96\pi A\alpha^3\omega^3}\text{diag}\left[(-(2-3A^2\ell^2X), 1, (1-3A^2\ell^2X)\right]. \tag{3.34}$$

The stress tensor is traceless as expected and covariantly conserved with respect to the boundary metric $g_{(0)}$. We identify the energy density of the boundary CFT as the $\tau\tau$-component, viz.

$$\rho_E = \frac{m}{8\pi\ell^2\alpha^3\omega^3}(1-A^2\ell^2X)^{3/2}(2-3A^2\ell^2X), \tag{3.35}$$

which can be integrated to obtain the holographic mass

$$M = \int d\xi d\phi\sqrt{-g_{(0)}}\rho_E = \frac{\alpha m}{K}. \tag{3.36}$$

This result is consistent with the total mass found using AMD formula (3.22) [101, 111]. Although ρ_E depends on the conformal representative of the boundary metric ω, which has an order of $\mathcal{O}(\omega^{-3})$), the contribution of the metric determinant $g_{(0)}$ is of order $\mathcal{O}(\omega^6)$. Consequently, the integrand of (3.35) is independent of ω. Notably, this is radically different to the three-dimensional case, where the energy of the two–dimensional CFT remains indeterminate unless a specific value of ω is chosen.

Additionally, the dual stress tensor can be written in the fluid/gravity language [112] as

$$\langle T_{ij}\rangle = \Delta(x)\left(\frac{3}{2}u_iu_j + \frac{1}{2}g_{(0)ij}\right) + \xi(C_{ijk}u^k + C_{jik}u^k), \tag{3.37}$$

where $C_{ijk} = \nabla_{[k}R_{j]i} - \frac{1}{4}g_{a[j}\nabla_{k]}R$ is the Cotton tensor of the boundary, $\xi = \frac{\ell^2}{8\pi\sqrt{3}}$ is an universal coefficient, u is the four-velocity

$$u = \sqrt{\frac{3-2A^2\ell^2X}{3\omega(1-A^2\ell^2X)}}\partial_\tau - \frac{AX}{\sqrt{3\omega}\alpha}\sqrt{1-A^2\ell^2X}\partial_\xi, \tag{3.38}$$

and

$$\Delta(x) = \frac{m\sqrt{(1-A^2\ell^2X)^5}}{4\pi\ell^2\omega^3\alpha^3}, \tag{3.39}$$

represents a non-hydrodynamic correction arising from the fact that the boundary is non-conformally flat [101]. In fact, for $\omega = \sqrt{1-A^2\ell^2X}/\alpha$, the boundary metric (3.33) is turned into the one analysed in [108]. In this case, the dual CFT lies in a black hole background. Nevertheless, it remains unclear a proper hydrodynamic description of the boundary theory in which the associated transport coefficients can be identified.

3.3.2 ADM-like coordinates

An alternative to using the Fefferman-Graham gauge is to consider ADM coordinates to foliate the spacetime and identify the boundary metric. That is, we want the bulk metric to behave as

$$ds^2 = N^2 dz^2 + h_{ij}(z, x^i)(dx^i + N^i dz)(dx^j + N^j dz) \,, \tag{3.40}$$

where N is the Lapse function, N^i the shift vector, and the induced metric h_{ij} in the $z = \text{const}$ hypersurface. In this approach, we have replaced the time evolution of the usual ADM formalism for a radial coordinate in agreement with the standard holographic techniques [113]. To cast the accelerating black hole into this frame, we take the following coordinate transformation

$$-\frac{1}{Ar} = \cos\theta + z \,. \tag{3.41}$$

The coordinate z is the new "radial direction" and the boundary defined by the metric h_{ij} is located at $z = 0$. The boundary is now coordinatised with $x^i = (t, \theta, \phi)$. It is now straightforward to identify the lapse function N, N^i and boundary metric h_{ij} by writing (3.9) in this frame and comparing to (5.18) leading to

$$N^2 = \Omega^{-2}(f(z + A\cos\theta)^2 + A^2 g \sin^2\theta)^{-1} \,, \tag{3.42}$$

$$N^i = -\frac{Ag\sin\theta}{f(z + A\cos\theta)^2 + A^2 g\sin^2\theta}\delta^i_\theta \,, \tag{3.43}$$

$$h_{ij} = \text{diag}\left(-\frac{f}{\Omega^2}, \frac{f(z + A\cos\theta)^2 + A^2 g\sin^2\theta}{\Omega^2 f g (z + A\cos\theta)^4}, \frac{g\sin^2\theta}{\Omega^2(z + A\cos\theta)^2}\right) \,. \tag{3.44}$$

Note that now $f = f(z, \theta)$ and $\Omega = Az$. We also defined the outward-pointing normal vector to the hypersurface $z = \text{const}$ as

$$n = \frac{1}{N}(N^i \partial_i - \partial_z) \,, \tag{3.45}$$

and the extrinsic curvature of the boundary h_{ij} as

$$K_{ij} = \frac{1}{2}\mathcal{L}_n g_{ij} = -\frac{1}{2N}\left(\partial_z - \nabla_i N_j - \nabla_j N_i\right) \,, \tag{3.46}$$

with ∇_i the covariant derivative respect to h_{ij} . Let us introduce an infrared cutoff at $z = \delta$ where $\delta \geq 0$. In this way, we can compute regular holographic quantities close but not at the conformal boundary, and then we can take the limit $\delta \to 0$ as the standard dictionary prescribes. The conformal boundary metric is given as

$$\begin{aligned} ds^2_{(0)} &= g_{(0)ij} dx^i dx^j = \lim_{\delta\to 0} \delta^2 h_{ij} dx^i dx^j \\ &= -\frac{A^2 f \cos^2\theta}{\alpha} dt^2 + \frac{f + g\tan^2\theta}{fg} d\theta^2 + g\sin^2\theta d\phi^2 \,. \end{aligned} \tag{3.47}$$

We compute the holographic stress tensor as done in the previous section, leading to

$$\langle T_{ij}\rangle = \frac{\ell m}{8\pi G\Sigma(\theta)}\text{diag}\Bigg[\left(\frac{-2+3\ell^2A^2\sin^2\theta(-1+2mA\cos\theta)}{\alpha}\right),1, \\ \Big(-1-3\ell^2A^2\sin^2\theta(-1+2mA\cos\theta)\Big)\Bigg], \tag{3.48}$$

where we have introduce $\Sigma(\theta) = 1 + 2Am\cos\theta$ for simplicity. Once again, the integration of the tt- component leads the holographic mass obtained in (3.35) [85].

Although, the form of the stress tensor using the FG gauge or ADM differs, both lead to the same energy of the dual theory. In principle, to compare both stress tensors we would need to identify the particular ω in which the metric (3.33) becomes (3.47). For 3+1 dimensions, this is not necessarily a disadvantage for the FG gauge as we saw that the mass does not depend on ω.

3.4 Euclidean Action

In thermodynamics, an important quantity is the Gibbs free energy of a system, given by

$$\mathcal{F} = E - TS\,, \tag{3.49}$$

where E is the total energy, T temperature, and S the entropy. The free energy plays a crucial role in determining the thermodynamics and stability of the gravitational configuration. The free energy can be related to the partition function through the following expression

$$\log Z(\beta) = -\beta\mathcal{F}\,, \tag{3.50}$$

with $\beta = 1/T$ the Euclidean period. In the Euclidean quantum gravity picture, the partition function is obtained by evaluating the classical gravitational action $I[g,\varphi]$ and summing over all smooth geometries g,

$$Z(\beta) = \int \mathcal{D}[g]\exp^{-I_{\rm E}[g]}\,, \tag{3.51}$$

which in the saddle-point approximation becomes

$$-\log Z(\beta) \simeq I_{\rm E}[g]\,. \tag{3.52}$$

In this way, we can relate the Euclidean action $I_{\rm E}$ with the free energy through the quantum statistical relation

$$I_{\rm E} = -\beta\mathcal{F}\,. \tag{3.53}$$

In order to obtain the free energy of the accelerating black hole, it is necessary to evaluate the euclidean renormalised action (2.61) on-shell. For this, we proceed as follows: First, we perform a Wick rotation $t \to -i\tau_E$ and $I_{\mathrm{E}} = -iI_{3+1}$ with the Euclidean period identified as the inverse of the temperature $\beta = T^{-1}$ (3.18).Then we evaluate the Einstein–Hilbert term using the bulk metric (3.9) and the Gibbons–Hawking term and counterterm using the boundary metric (3.47) as done in [85]. This ensures that the action is well-defined and finite. Finally, we integrate over the correct range of coordinates for z, θ and ϕ, leading to

$$I_{\mathrm{E}} = \frac{\beta}{2\alpha GK}\left[m(1-2A^2\ell^2) - \frac{r_h^3}{\ell^2(1-A^2r_h^2)^2}\right]. \tag{3.54}$$

After identifying the correct physical parameters of the black hole, we recover the quantum statistical relation as expected [85, 101]

$$I_{\mathrm{E}} = -S_{\mathrm{BH}} + \beta M = \beta\mathcal{F}\,. \tag{3.55}$$

This demonstrates that the accelerating black hole follows the standard thermodynamic relation between the Euclidean action, free energy, and entropy, indicating its consistency within the thermodynamic framework.

The behaviour of the free energy indicates that there is no Hawking–Page phase transition [101]. However, it remains an open question whether other types of phase transitions may occur in this context. Further investigations are needed to explore the possibility of different phase transitions and to understand the full thermodynamic landscape of accelerating black holes. It is essential to emphasise that the normalisation of the timelike Killing vector is crucial for properly defining the thermodynamics of accelerating black holes, similar to the case of rotating black holes [113]. This normalisation plays a fundamental role in determining the correct thermodynamic quantities and properties of the black hole. Failure to properly normalise the Killing vector could lead to incorrect thermodynamic interpretations and results.

Chapter 4

Accelerating Black Holes in 2+1–dimensions

Overview

Despite the simplicity of lower-dimensional gravity, it still exhibits many of the interesting features shared by its higher-dimensional sibling, including the admission of black holes [20, 21]. However, from the perspective of the path integral, the lack of dynamics renders the theory radically simpler [16]. In fact, for asymptotically AdS solutions (without defect singularities) the path integral may be evaluated explicitly [114]. By constructing three-dimensional solutions analogous to the C-metric, one may be able to apply similar technology to gain insight into the nature of acceleration. For this, we will consider a generic ansatz that resembles the C-metric in four–dimensions. After analysing the coordinate range in which the Lorentzian signature is preserved, one can construct three different classes of geometries which we interpret physically by studying their physical properties.

We find that these classes describe either accelerating conical deficits or point particles [115], or solutions analogous to the C-metric describing a BTZ black hole [20] with a codimension-one defect emerging from its horizon. This defect is under compression so is commonly referred to as a "strut" as it possesses a negative energy density. We show that not only can a more physical solution be constructed, describing a BTZ black hole accelerated by a positive tension wall, but the solution with a strut exhibits a richer phase structure than previously noticed in the literature, possessing a "rapid phase" in which an accelerating horizon forms. This phase transition is directly analogous to the formation of an acceleration horizon in the four-dimensional theory. We also construct a solution analogous to the C-metric describing a black hole that is not continuously connected to the BTZ black hole living only in a specific region of the parameter space. We briefly comment on Class III solutions which have not been analysed in detail yet.

4.1 Constructing a three-dimensional C-metric

As we saw in the previous chapter, the C-metric is usually described by the Plebanski–Demianski metric (3.4) in the canonical coordinates t, y, x, ϕ. A natural ansatz in three-dimensions is to consider a truncation of the PD metric with the following form

$$ds^2 = \frac{1}{\bar{\Omega}^2}\Big[- \bar{P}(y)d\tau^2 + \frac{dy^2}{\bar{P}(y)} + \frac{dx^2}{\bar{Q}(x)}\Big]\,, \tag{4.1}$$

where the conformal factor

$$\bar{\Omega} = \bar{A}(x-y)\,. \tag{4.2}$$

Here, $\bar{A}$ is a parameter with dimensions of inverse length and the conformal boundary is located at $x = y$. The metric polynomials are easily found from the trace of Einstein's field equations with negative cosmological constant $\Lambda = -\ell^{-2}$[70], which yields two quadratic polynomials $P(y)$ and $Q(x)$ of the corresponding coordinates of which, in principle, all polynomial coefficients are arbitrary constants

$$\bar{Q}(x) = c + bx + ax^2\,, \qquad \bar{P}(y) = \frac{1}{\bar{A}^2\ell^2} - \bar{Q}(y)\,. \tag{4.3}$$

The coefficients a, b and c are real numbers as long as the Lorenzian signature of the metric is retained. Nonetheless, there are gauge redundancies that enable us to remove two out of the three parameters.
First, note that the metric is invariant under translation

$$x \to x + s\,, \qquad y \to y + s\,. \tag{4.4}$$

which permits setting $b = 0$. The line element is also invariant under dilatation, viz.

$$x \to sx, \quad y \to sy, \quad \tau \to s\tau. \tag{4.5}$$

for which the metric functions (4.3) transforms as

$$\begin{aligned} \bar{P}(y) &= \frac{1}{\bar{A}^2\ell^2} - a - cs^2y^2, \\ \bar{Q}(x) &= c + as^2x^2, \end{aligned} \tag{4.6}$$

that gives the freedom to set $|a| = |c|$. By absorbing the parameter s into a and c, the polynomials can be expressed in terms of just one coefficient c as

$$\begin{aligned} \bar{P}(y) &= \frac{1}{A^2\ell^2} - c(1 \mp y^2), \\ \bar{Q}(x) &= c(1 \mp x^2). \end{aligned} \tag{4.7}$$

There is an additional gauge freedom that allows to eliminate the remaining coefficient up to a sign. Consider the rescaling of the constant $A \to sA$ and the

coordinate $\tau \to s\tau$. The last transformation does not modify x and y, and leads to

$$\begin{aligned} \bar{P}(y) &= \frac{1}{A^2\ell^2} - s^2 c(1 \mp y^2), \\ \bar{Q}(x) &= s^2 c(1 \mp x^2), \end{aligned} \tag{4.8}$$

where c can be set to be ± 1. This discussion can be summarised by stating that the parameter space consists of 3 possible classes of geometry* distinguished by the sign of c and that of the discriminant $\Delta_{\bar{Q}} = b^2 - 4ac$. The three distinct class and their coordinate range can be seen in table 4.1.

Class	Sgn $\Delta_{\bar{Q}}$	Sgn c
I	+	+
II	+	−
III	−	+

Table 4.1: Three classes of solutions and their defining characteristics.

There is also a symmetry under parity

$$x \to -x\,, \qquad y \to -y\,, \tag{4.9}$$

that allows us to take $x > y$. Finally, a simple redefinition $A = \sqrt{|c|}\bar{A}$ swaps all of the dependence on c into the timelike component of the metric which, since the geometry is static, we are free to absorb by a rescaling $\tau \to \tau/|c|$. This leads us to a set of *canonical gauges* in which all dependencies on a, b, and c have been eliminated, leaving only one remaining free parameter, A. The metric takes the form

$$ds^2 = \frac{1}{\Omega^2}\Big[- P(y)d\tau^2 + \frac{dy^2}{P(y)} + \frac{dx^2}{Q(x)}\Big]\,, \tag{4.10}$$

with the conformal factor given by

$$\Omega = A(x - y) \tag{4.11}$$

and the metric functions in table 4.2. Also given in table 4.2 are the maximal ranges of x for which $Q(x)$ is positive, thus yielding a Lorentzian metric.

Class	$Q(x)$	$P(y)$	Maximal range of x
I	$1 - x^2$	$\frac{1}{A^2\ell^2} + (y^2 - 1)$	$\lvert x\rvert < 1$
II	$x^2 - 1$	$\frac{1}{A^2\ell^2} + (1 - y^2)$	$x > 1$ or $x < -1$
III	$1 + x^2$	$\frac{1}{A^2\ell^2} - (1 + y^2)$	$\mathbb{R}$

Table 4.2: The metric functions in canonical gauge, together with the largest available range of x.

*In fact, there is a fourth possible class, with both $c < 0$ and $\Delta_{\bar{Q}} < 0$, for which no range of x gives a Lorentzian signature. We disregard this case.

It is worth pausing for a bit and analyse the family of solutions found here. First, Class I solutions are very reminiscent of the 4D Rindler metric (3.11) when identifying $x = \cos\theta$. This gives rise a polar system of coordinates with an origin if $y \to -\infty$. We will see later that this corresponds to a spacetime describing accelerating particles in AdS_3 showing similar behaviour as the C-metric in four–dimensions with slow and rapid accelerating phases, but with the peculiarity that also admits an accelerating black hole for a very specific parameter space. On the other hand, Classes II and III look somewhat different, as y is now bounded, and x is non-compact. Class II contains accelerating black holes solutions that can be considered as one-parameter extension of the BTZ black hole, while Class III is reminiscent of braneworld scenarios.

We can also subdivide these classes further by their causal or horizon structure, directly related to the value of $A\ell$. Just as with the 4D C-metric, Class I solutions fall into three possible categories: those which satisfy $A^2\ell^2 < 1$ lack event horizons, those with $A^2\ell^2 > 1$ possess two distinct event horizons and solutions with $A\ell = 1$ possess a single event horizon at $y = 0$. We label these subclasses as *slow*, *rapid*, and *saturated* respectively. Solutions of Class II have a persistent horizon structure over all values of A and ℓ. However, they may be instead categorised by the choice to take x to live in a particular connected component, with either $x < -1$ or $x > 1$. We label these as *left* and *right* subclasses of II respectively. Metrics of Class III attain P positive only if $A^2\ell^2 < 1$. There are then two event horizons, with the valid range of y between them.

Apart from the categorisation of the solutions, an important issue seems to be the fact that none of these solutions appear to have a mass parameter. A simple explanation for this is that gravity in three–dimensions lack propagating degrees of freedom as seen in Chapter 2. As in the BTZ black hole, the "energy" is generated by some sort of identification of three-dimensional AdS space: either one creates a conical deficit in the spacetime, from which we can interpret the deficit as a point mass, or one orbifolds the spacetime with some discrete group, producing the BTZ black hole. As gravity does not work as an attractive force, the local spacetime is always anti-de Sitter space, thus all these three classes are simply different patches of AdS coordinatised in different ways. We derive the coordinate transformations in Appendix C, but for now, note that all of these metrics with x taking its maximal range are just patches of AdS, and do not have the same interpretation of an accelerating black hole as in four–dimensions.

In order to have the interpretation of a point mass or black hole, we must perform the relevant identifications on the geometry. In each case, this involves cutting the spacetime along a curve of $x = \text{const}$, and identifying with another equivalent $x = \text{const}$ curve. Because of the off-centre coordinates, this will turn out to introduce a domain wall into the geometry – a codimension-1 defect that provides the necessary

force for acceleration.

4.2 Introducing a domain wall

In four–dimensions, black holes can be accelerated by inserting a cosmic string along their polar axis as we saw in 3.1.0.1. The cosmic string will produce a conical deficit or excess depending on the sign of its tension [93] that is proportional to the force that drives the acceleration. Due to the dimensionality, in three–dimensions, we are allowed to introduce a codimension-1 object with some nontrivial tension that will play the same role as the cosmic string in the standard four–dimensional accelerating black hole. In particular, we will be interested in single-wall configurations.

Given the classes of solutions described by the line element (4.10) and their respective coordinate range, we need to find a coordinate patch where we could insert the domain wall by cutting and gluing along a hypersurface. Let us note that (for classes I and II) as $|x| \to 1$, the metric is regular and the surface $|x| = 1$ has vanishing extrinsic curvature. Thus, it is natural to think of x as an angular variable and to identify two mirror images of our geometry across $|x| = 1$. If we then cut each geometry across another constant $x-$surface, $x = x_0$, this will introduce a domain wall into the system, with a tension, μ, given by the Israel equations [116].

A constant $x-$surface, $x = x_0$, which has an induced metric

$$ds^2_{\rm dw} = \gamma_{ab} dx^a dx^b = \frac{1}{\Omega^2}\left(-P(y)d\tau^2 + \frac{dy^2}{P(y)}\right), \tag{4.12}$$

where $a, b = (\tau, y)$ are the coordinates on the domain wall. We glue two copies of the coordinate patch (4.10) mirroring along $x = \pm 1$. The wall is sourced by a localised energy-momentum tensor and we can integrate over the thin wall configuration using Israel equations,

$$8\pi G \int_-^+ T_{ab} = [K_{ab} - \gamma_{ab} K]\,|_-^+ = 8\pi G \mu \gamma_{ab}, \tag{4.13}$$

where K_{ab} is the extrinsic curvature of the hypersurface at $x = x_+$ given by the covariant derivative of the inward-pointing normal to $x = x_0$,

$$\mathbf{n} = \pm \Omega^{-1} Q^{-\frac{1}{2}} dx\,, \tag{4.14}$$

where the plus sign is taken if $x > x_0$ in the interior (i.e. if $x \in [x_0, 1]$ for class I, $x > x_0$ for class II), and vice versa*. The extrinsic curvature $K_{ab} = \nabla_a n_b$ is then easily computed as

$$K_{ab} = \mp A \sqrt{Q} \gamma_{ab}\,. \tag{4.15}$$

*The same principle applies for class III solutions, however, there is now no surface of zero extrinsic curvature, thus we have the choice of having a single cut at $x = x_0$, or a second cut at some other value of x. This is precisely analogous to the Randall-Sundrum models 2 and 1 [117, 118] respectively.

Leading to a domain wall defect with tension

$$\mu = \pm\frac{A}{4\pi}\sqrt{Q(x)}\,. \tag{4.16}$$

This now demonstrates explicitly that taking a mirror image copy of our spacetime and gluing across $|x| = 1$ leads to a continuous and smooth geometry, whereas gluing across $x = x_0$ leads to a defect with positive tension if $x < x_0$, or negative tension if $x > x_0$ lies within our spacetime. For convenience, and to easily distinguish between positive and negative tension defects, we call the positive tension defect a **domain wall**, and the negative tension one a **strut**. When restricting the range of the x coordinate, it may be that the new range of parameters "avoids" one or more of the event horizons that would have been present, or changes the number of horizons that meet the conformal boundary, had the full range of x been considered. As a consequence, (with t timelike) there are eight qualitatively distinct single-wall and seven qualitatively distinct single-strut solutions one can construct through various choices of x_0. We detail the full set of distinct physical solutions in Appendix B. In the following sections, we will focus on describing the different spacetimes configurations that can be constructed by introducing a single wall. We distinguish two different families: particle-like solutions (Class I pushed or pulled by a wall) and accelerating black holes (Class $\mathrm{II}_{\mathrm{left}}$, $\mathrm{II}_{\mathrm{right}}$ and I_{C}). We also comment on Class III, for which a single wall configuration is not possible.

4.3 Accelerating Particles

In three-dimensional gravity, a point particle is represented by a conical deficit, i.e., a δ-function in the Ricci curvature. This means we have to have an "origin" in order to cut out the deficit. A quick look at the metric (4.10) shows that the length of an angular arc, represented by x, becomes zero if $y \to -\infty$ (recall $y < x$). Table 4.2 then shows that only Class I solutions are able to satisfy this requirement while keeping $P \geq 0$.

To construct the accelerating conical defect, we first glue two copies of the Class I geometry (4.10) along $x = \pm 1$, so that we can identify an angular coordinate via $x = \pm\cos\theta$. We then introduce a conical deficit by choosing an $x_+ \in (-1, 1)$ and restricting the range of x to $\pm x \in (x_+, 1]$. The $x = \pm 1$ axis of the newly formed spacetime is regular, but the origin at $y \to -\infty$ has an angular deficit of $2[\pi - \arccos(\pm x_+)]$, with the $x = x_+$ axis marking the position of a wall of tension $\mu = \pm A\sqrt{Q(x_+)}/4\pi$.

Next, we will focus our attention towards the positive tension scenario ($x \in (x_+, 1]$), describing an accelerating particle that is being pulled by a domain wall. Towards the end of this section, we briefly touch upon the negative tension strut, which is calculated using a similar procedure.

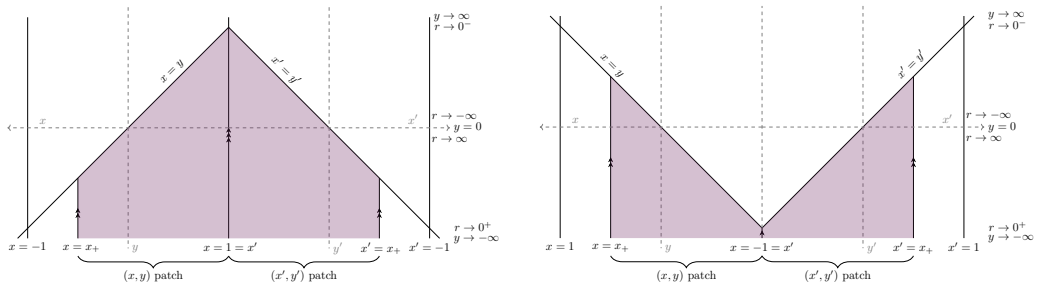

Figure 4.1: The two patches of Class I spacetime used to construct a slowly accelerating conical defect. **Left:** Point particle pulled by a domain wall. **Right:** Point particle pushed by a strut-wall.

4.3.1 Class I: A particle pulled by a domain wall

To take advantage of our intuitive understanding of four-dimensional space, it can be beneficial to express Class I in a more natural form. We introduce dimensionful coordinates $r = -(Ay)^{-1}$ and $t = \alpha A^{-1}\tau$, and identify x with an angular coordinate via $x = \cos(\phi/K)$. The parameter $K \equiv \pi/\arccos(x_+)$ now encodes the range of the x coordinate, fixing the range of ϕ to be $(-\pi, \pi)$. Thus, the metric is

$$ds^2 = \frac{1}{[1 + Ar\cos(\phi/K)]^2}\left[-f(r)\frac{dt^2}{\alpha^2} + \frac{dr^2}{f(r)} + r^2\frac{d\phi^2}{K^2}\right], \tag{4.17}$$

$$f(r) = 1 + (1 - A^2\ell^2)\frac{r^2}{\ell^2}. \tag{4.18}$$

Note that we have introduced the dimensionless parameter α just as in the four–dimensional case. Later, we will identify the value of this parameter by mapping the solution to global coordinates similarly as done in 3.1.0.1. In this form, it is natural to recover global AdS space by taking $A \to 0$. We are also able to identify slow ($A\ell < 1$), saturated ($A\ell = 1$), and rapid ($A\ell > 1$) acceleration readily. For $A\ell < 1$, no horizons are present, and we will see that the accelerating particle is a conical deficit suspended at fixed distance from the centre of AdS, analogous to the four–dimensional slowly accelerating black hole. As A gets larger ($A \geq 1$), a Killing horizon forms at $r = \ell/\sqrt{A^2\ell^2 - 1}$ which we refer to as an *acceleration horizon*. Provided the acceleration is not too large (see below) this horizon is non-compact and masks part of the conformal boundary. The domain wall extends between the particle and the boundary. However, for large acceleration, the domain wall extends from the particle to the horizon, and after identification, the horizon 'wraps around' to mask the entire conformal boundary and the spatial sections become compact. The polar-style coordinate system is helpful in interpreting the accelerating particle spacetimes as the conical deficit sits at $r = 0$ and is easily visualised. Irrespective of acceleration, this is achieved by having $K > 1$ in the metric (4.18). The angular deficit, which one may be inclined to refer to as the

"particle mass" [17], is

$$m_c = \frac{1}{4G}\left(1 - \frac{1}{K}\right), \tag{4.19}$$

while the tension in the domain wall is

$$\mu = \frac{A}{4\pi}\sin\left(\frac{\pi}{K}\right). \tag{4.20}$$

When $K = 1$, both the conical deficit (4.19) and domain wall tension (4.20) vanish, and the geometry becomes global AdS_3 written in an accelerated frame. We have monotonically increasing particle mass as K increases, whereas the domain wall tension first increases, reaching a maximum of $A/4\pi$ at $K = 2$, then decreases further with increasing K. As $K \to \infty$, the "particle mass" asymptotes 1/4, and the domain wall tension tends to zero. In this case, we have excised all of the spacetime, and one can view this as there being nothing to accelerate! As $A \to 0$, the 'mass' of the particle is unaffected and the tension of the domain wall goes to zero.

In the rapid or saturated phases, it is the magnitude of the particle mass relative to the acceleration that determines the horizon structure. For $4\pi\mu\ell < 1$ (or $x_+ < -y_h$), the acceleration horizon is non-compact and the domain wall reaches the boundary. For strongly accelerating particles $A\ell\sin(\pi/K) > 1$, the acceleration horizon compactifies and we have a de Sitter-like state.

To identify that the conical defect is accelerating, we can do the same computation as in 3.1.0.1 to obtain the four-acceleration of a point particle along the worldline traced by the origin. The origin $r = 0$ of the coordinates (4.18) has normalised four-velocity

$$\mathbf{u} = \left.\frac{\alpha\Omega}{\sqrt{f}}\right|_{r\to 0} \partial_t \,. \tag{4.21}$$

The associated four-acceleration is then given by a covariant derivative,

$$\mathbf{a} = \nabla_{\mathbf{u}}\mathbf{u}\,, \tag{4.22}$$

which has magnitude

$$|\mathbf{a}| = \sqrt{-\left(\nabla_{\mathbf{u}}\mathbf{u}\right)^2} = A\,. \tag{4.23}$$

We see that the acceleration parameter gives the locally experienced acceleration of the particle as in the four-dimensional case.

One can also identify the particle's acceleration by considering the temperature of the horizon in the rapid phase. In this phase, demanding regularity of the Euclidean section indicates a horizon temperature of

$$T = \frac{A}{2\pi\alpha}\sqrt{1 - \frac{1}{A^2\ell^2}}\,. \tag{4.24}$$

For accelerations which are large compared to the AdS scale, $A \gg \ell^{-1}$, the particle is close to the acceleration horizon and provides effects which dominate the effect of the background curvature. In this regime, the geometry is approximately flat, and one should expect $\alpha \sim 1$. The horizon is then seen to be Rindler, with temperature $T = (2\pi)^{-1}A$. Similar to what occurs in de Sitter space, there is an associated Gibbons–Hawking entropy [119] which is a quarter of the area of the accelerating horizon

$$S_{\text{Particle}} = \frac{\text{Area}}{4} = -4\ell \operatorname{arctanh}\left[(-A\ell + \sqrt{A^2\ell^2 - 1}\tan\left(\frac{\pi}{2K}\right)\right] . \tag{4.25}$$

An important step into identifying the correct physical quantities is to normalise the generator of time translations ∂_t to that of an observer located at the boundary [120]. That is, we wish to choose α in (4.18) such that t is the same time coordinate as when the geometry is written in global gauge

$$ds^2 = -\left(1 + \frac{R^2}{\ell^2}\right) dt^2_{\text{Global}} + \frac{dR^2}{\left(1 + \frac{R^2}{\ell^2}\right)} + R^2 d\vartheta^2 . \tag{4.26}$$

Note that the function f has the same form as the comparable function in the C-metric in four dimensions, in the limit of vanishing mass parameter [121]. Hence, the transformation between local and global coordinates is already known to be

$$\left(1 + \frac{R^2}{\ell^2}\right) = \frac{f(r)}{\alpha^2 \Omega(r,\phi)^2} , \qquad R\sin\vartheta = \frac{r\sin\left(\phi/K\right)}{\Omega(r,\phi)} . \tag{4.27}$$

This holds only if the temporal rescaling is

$$\alpha = \sqrt{1 - A^2\ell^2} . \tag{4.28}$$

This mapping to the global gauge allows for an intuitive picture of the spacetime to be constructed. By compactifying onto the Poincaré disk, we attain Figure 4.2 for the slowly accelerating conical deficit, which is plotted at some fixed time t. The details of the compactification are given in Appendix C. One must use two (x, y) patches to cover both the eastern and western semicircles, as in Figure 4.1. Note that, since t aligns with the global time coordinate, one may stack an infinite number of identical diagrams to visualise the complete space. We find a conical deficit "pulled" closer to the boundary than the origin of global coordinates by the removal of a distorted wedge.

In fact, although defining the total mass in the rapidly accelerating case is difficult, we can already determine the appropriate Killing vector one should use once a reliable definition becomes available. Consider the portion of AdS_3 described by the metric

$$ds^2 = -\left(-1 + \frac{R^2}{\ell^2}\right) dt^2_{\text{Rindler}} + \frac{dR^2}{\left(-1 + \frac{R^2}{\ell^2}\right)} + R^2 d\vartheta^2 , \tag{4.29}$$

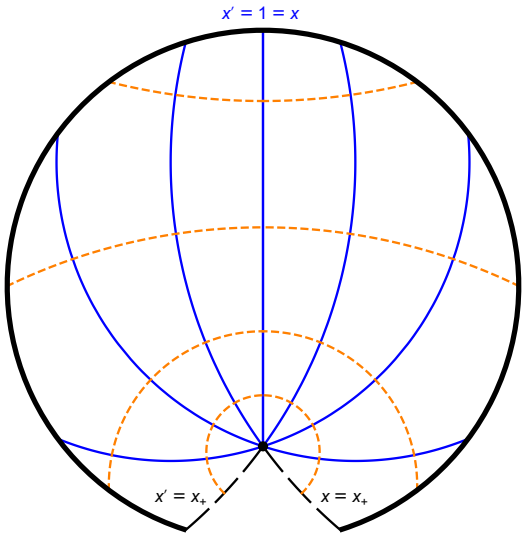

Figure 4.2: The slowly accelerating conical deficit with $A = 0.9\ell$, pulled by a wall, mapped onto the Poincaré disk. The deficit is shown as a black point and accelerates southwards. A "wedge" is removed from the global space, with its edges $x = x_+$ and $x' = x_+$ (long-dashed black) identified to attain a domain wall. Several lines of constant x are shown in blue, with lines of constant y in dashed orange.

with $r > -1$ and $\vartheta \in \mathbb{R}$. This geometry possesses a non-compact bifurcate Killing horizon at $r = -1$, generated by ∂_t, and we will refer to it as either the *planar BTZ geometry* or *Rindler wedge*. Close to the conformal boundary at large r, t is the usual timelike coordinate of the Poincaré patch. This time coordinate provides the zero-mass state for AdS_3 [55]. As such, the appropriate normalisation of t for the rapidly accelerating particle is given by choosing α such that the time coordinate of the solution (4.18) matches that of the Rindler wedge (4.29). This choice of Killing vector closely mirrors the choice made in [122], where — for four-dimensional accelerating black holes without cosmological constant — the generator of the Rindler horizon was shown to provide a mass satisfying a first law. The transformation between the rapid Class I and planar BTZ geometries are given by

$$\left(-1 + \frac{R^2}{\ell^2}\right) = \frac{f(r)}{\alpha^2 \Omega(r,\phi)^2}\,, \qquad R\sinh\vartheta = \frac{r\sin(\phi/K)}{\Omega(r,\phi)}\,, \tag{4.30}$$

where we must take

$$\alpha = \sqrt{A^2\ell^2 - 1}\,. \tag{4.31}$$

Much like the slowly accelerating case, the transformation between local coordinates and the Rindler wedge may be used to understand the rapidly accelerating conical deficit as a subset of AdS_3. For light conical deficits ($m_c \sim 0$), this space is the planar BTZ geometry with a wedge removed. This is shown in Figure 4.3. We must plot two (x, y) patches in order to cover the Rindler wedge. Details of the mapping onto the global space are given in Appendix C. A key feature is that

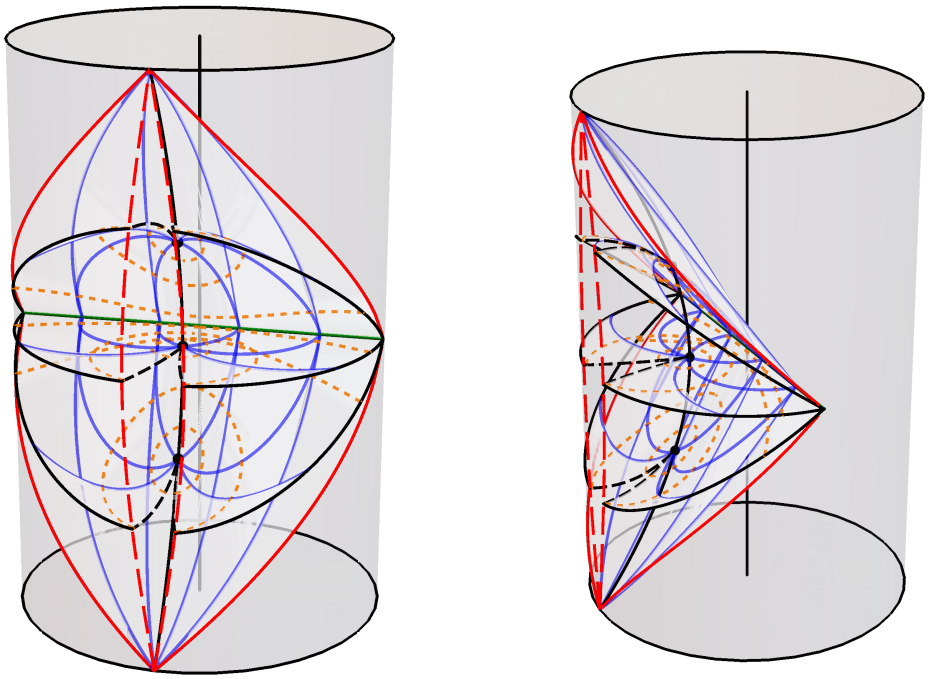

Figure 4.3: The Class $\mathrm{I}_{\mathrm{rapid,A}}$ solution embedded within global AdS_3. The deficit's worldline is shown in solid black. Several surfaces of constant t are plotted. The event horizons are demonstrated by the surfaces at early and late t. The bifurcation surface is shown as a green line. A "wedge" is removed, with its edges $x = x_+$ and $x' = x_+$ identified. These edges are shown in long-dashed black within each time-slice, and in dashed red at the boundary. The boundary of the classically accessible subset of the global boundary is shown in red. Lines of constant x are shown in blue, with lines of constant y in dashed orange. To guide the eye, the axis of the cylinder is also shown in black.

the Rindler time coordinate and the global time do not align. In Figure 4.3, global time runs vertically, aligned with the axis of the cylinder. The conical defect on the other hand is seen to accelerate in from the conformal boundary at early times t, then move back out towards the boundary as $t \to \infty$. Both of these events happen in finite global time, resulting in the particle experiencing an acceleration horizon. It is already known that the planar BTZ geometry describes an acceleration horizon for test particles [21]; our solution describes a particular physical object undergoing acceleration, with the force of acceleration provided by a physical domain wall.

For heavy conical deficits (m_c large enough that $x_+ > -y_h$), the "wedge" removed is so large that includes all of the conformal boundary. This is shown in Figure 4.4. In this phase, the bifurcation surface is compactified to become a circle and the horizon structure is similar to that of de Sitter space.

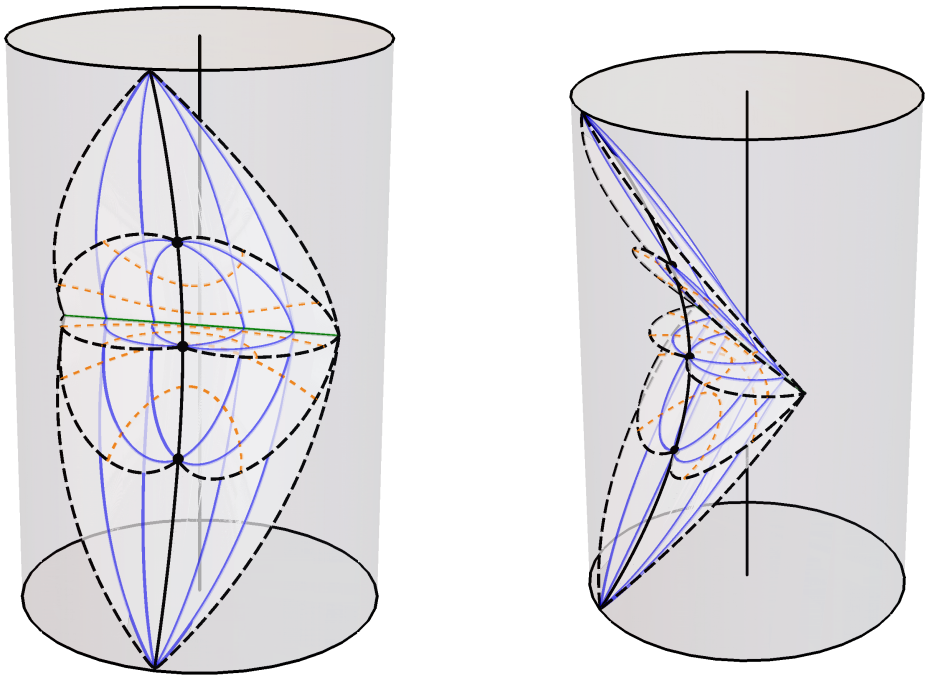

Figure 4.4: The Class $\mathrm{I}_{\mathrm{rapid,B}}$ solution embedded within global AdS_3. The deficit's worldline is shown in solid black. Several surfaces of constant t are plotted. The event horizons are demonstrated by the surfaces at early and late t. The bifurcation surface is shown as a green line. The surfaces $x = x_+$ and $x' = x_+$ identified. Lines of constant t within these surfaces are shown in long-dashed black. None of the conformal boundary is included in the solution. Lines of constant x are shown in blue, with lines of constant y in dashed orange. To guide the eye, the axis of the cylinder is also shown in black.

4.3.2 Class I: A particle pushed by a strut

We now briefly comment on the counterpart solution of a particle being pushed by a strut. In fact, the asymptotically flat version of this construction (which is achieved by taking the $\ell \to \infty$ limit) has been studied by Anber [115]. This solution shares many features in common with the solution of section 4.3.1 so we will discuss it in less detail.

As before, we use the polar representation of the geometry, which is almost in the form of (4.18), but instead set $x = -\cos(\phi/K)$ with the parameter $K = \pi/\arccos(-x_+)$ The metric then takes the form

$$ds^2 = \frac{1}{[1 - Ar\cos(\phi/K)]^2}\left[-f(r)\frac{dt^2}{\alpha^2} + \frac{dr^2}{f(r)} + r^2\frac{d\phi^2}{K^2}\right], \tag{4.32}$$

$$f(r) = 1 + (1 - A^2\ell^2)\frac{r^2}{\ell^2}. \tag{4.33}$$

By similar arguments to those of section 4.3.1, we find that one should take $\alpha = \sqrt{|1 - A^2\ell^2|}$. The local acceleration of the particle is again $|\mathbf{a}| = A$, and the particle

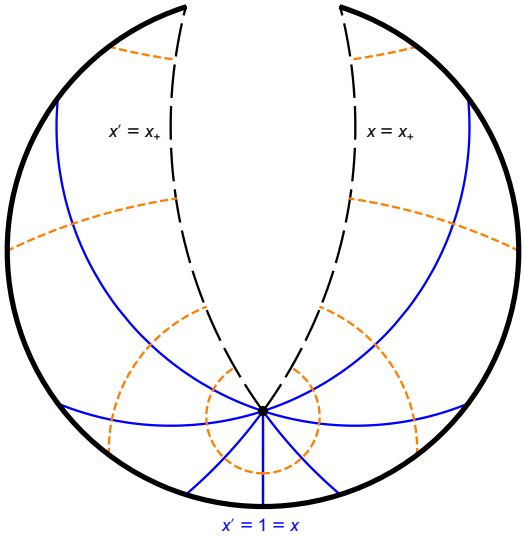

Figure 4.5: The slowly accelerating conical deficit with $A = 0.9\ell$, pushed by a strut, mapped onto the Poincaré disk. The deficit is shown as a black point and accellerates southwards. A "wedge" is removed from the global space, with its edges $x = x_+$ and $x' = x_+$ (long-dashed black) identified to attain a wall. Several lines of constant x are shown in blue, with lines of constant y in dashed orange.

mass and wall tension are, respectively,

$$m_c = \frac{1}{4}\left(1 - \frac{1}{K}\right) \tag{4.34}$$

and

$$\mu = -\frac{A}{4\pi}\sin\left(\frac{\pi}{K}\right) . \tag{4.35}$$

By mapping the solution to a portion of global space, we obtain Figure 4.5 for the slowly accelerating deficit. The details of the mapping are given in Appendix C. The interpretation of this figure is similar to that for the particle accelerated by a wall, (cf. Figure 4.2 and the discussion given in section 4.3.1).

In the rapid and saturated phases, much like with the particle accelerated by a wall, changing the magnitude of the conical deficit can induce a phase transition in the global structure of the spacetime. For light conical deficits, the gluing surface $x = x_+$ connects the conical deficit's worldline to a horizon (in the patch covered by (4.33). One can also view this as removing a "wedge" which includes part of the acceleration horizon from the Rindler wedge. This situation arises for the $\mathrm{I}_{\mathrm{rapid,B}}$ and $\mathrm{I}_{\mathrm{saturated,D}}$ single-strut solutions and the former is shown in Figure 4.6.

On the other hand, for heavier conical deficits, the identified surfaces connect the deficit's worldline to the conformal boundary. This situation arises for the $\mathrm{I}_{\mathrm{rapid,A}}$ and $\mathrm{I}_{\mathrm{saturated,C}}$ single-strut solutions. The portion of space then removed from the Rindler geometry is then so large that it includes the entirety of the horizon, and

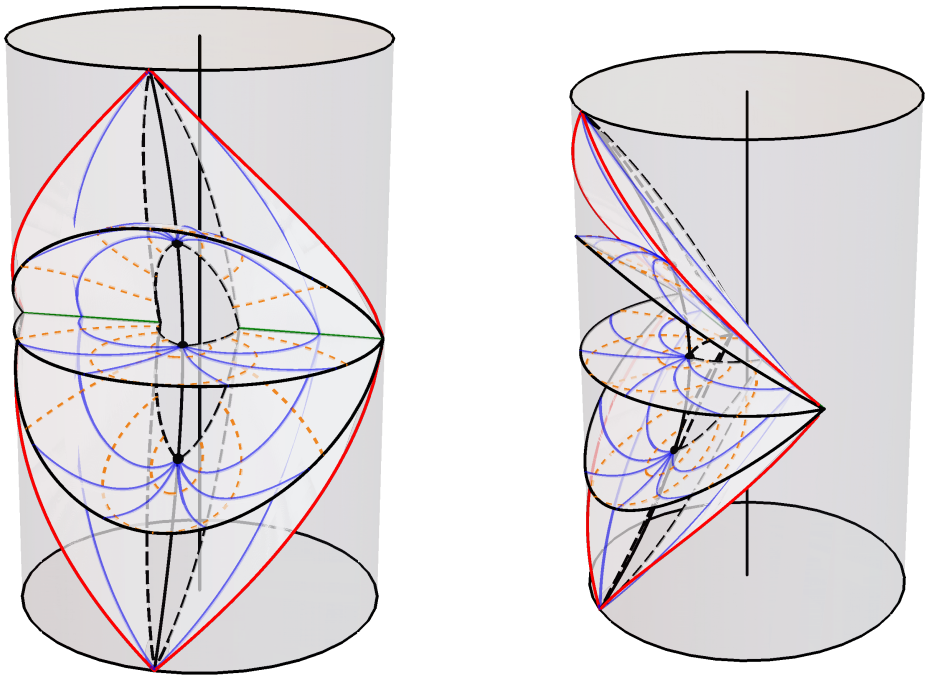

Figure 4.6: The rapidly accelerating light conical deficit with $A > \ell^{-1}$, pushed by a strut, embedded within global AdS_3. The deficit's worldline is shown in solid black. Several surfaces of constant t are plotted. The event horizon is demonstrated by the surfaces at early and late t. The bifurcation surface is shown as a green line. A "wedge" is removed, with its faces $x = x_+$ and $x' = x_+$ identified. These faces are indicated by long-dashed black curves within each time-slice, and in dashed red at the boundary. The boundary of the classically accessible subset of the global boundary is shown in solid red. Lines of constant x are shown in blue, with lines of constant y in dashed orange. To guide the eye, the axis of the cylinder is also shown in black.

we are left with a small segment of spacetime extending from the particle to the boundary as shown in Figure 4.7.

4.4 Accelerating Black Holes

Black holes in three–dimensional gravity are quite different to their four–dimensional counterpart. The biggest difference is that they appear as topological identifications in the spacetime and their "mass" is in fact, sourced by a conical deficit. To obtain them, first, one transforms to a Rindler wedge (or planar BTZ) patch of AdS, then identifies along constant x-lines. In the absence of acceleration (taking the limit $A \to 0$ of (4.10) with judicious coordinate rescalings) these x =const. lines have vanishing extrinsic curvature. Once we have finite A however, the way in which the coordinates slice the Rindler wedge is skewed (see Figures 4.9 & 4.10), so that even though the patch of AdS is the same as for planar BTZ, the new constant x surfaces now have non-vanishing extrinsic curvature. While we have

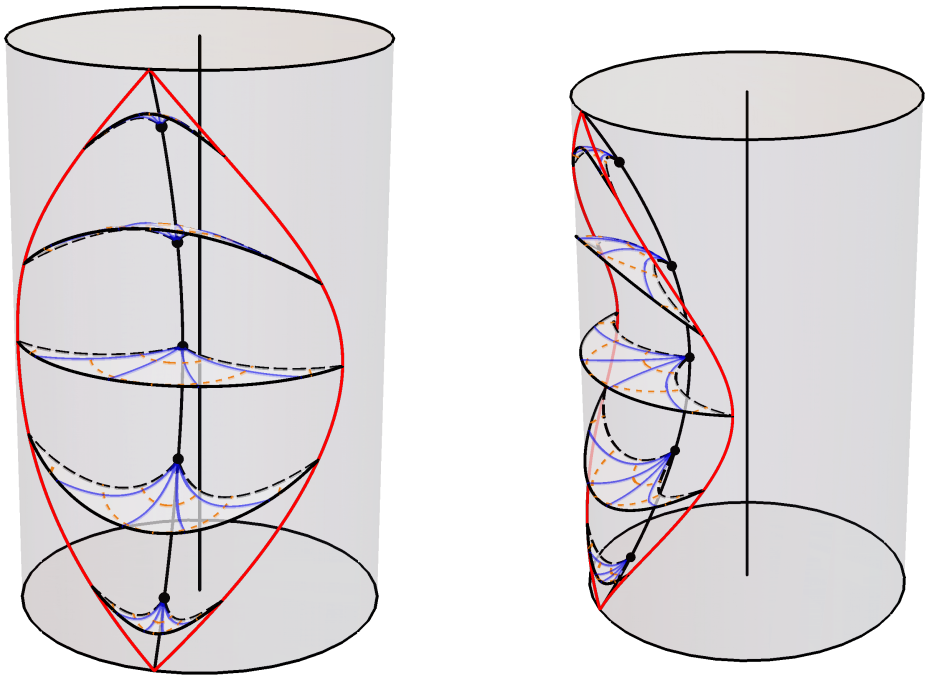

Figure 4.7: The rapidly accelerating heavy conical deficit with $A > \ell^{-1}$, pushed by a strut, embedded within global AdS_3. The deficit's worldline is shown in solid black. Several surfaces of constant t are plotted. The surfaces $x = x_+$ and $x' = x_+$ are identified. Edges of $x = x_+$ are shown in long-dashed black within each time-slice. x_+ is taken positive enough that the entirety of the boundary is removed from the space before identification. The boundary of the classically accessible subset of the global boundary is shown in red. Lines of constant x are shown in blue, with lines of constant y in dashed orange. To guide the eye, the axis of the cylinder is also shown in black.

long been aware that AdS can be sliced in many ways, this new phenomenon has not been noticed in the literature to our knowledge.

This procedure is natural in Class II which describes accelerating black holes that can be considered as a one parameter extension of the BTZ black hole [20, 21]. This means that by taking the parameter $A \to 0$, we recover the standard form of the static three-dimensional black hole.

There are two possible scenarios for Class II, depending on the sign of x. As seen in 4.2, we can either have $x > 1$ or $x < 1$. When $x > 1$ (Class II_{right}), the domain wall has negative tension and by gluing along $x = 1$, induces a conical deficit $K = \pi/\operatorname{arcosh}(x_+)$. On the other hand, when $x < -1$ (Class II_{left}), the domain wall has positive tension and by gluing along $x = -1$, we get a conical deficit $K = \pi/\operatorname{arcosh}(-x_+)$. These two cases are referred as accelerating BTZ pushed by a strut (negative tension) and pulled by a wall (positive tension). Next, we will describe both solutions and their properties.

Nevertheless, these are not the only black hole solutions that we can construct.

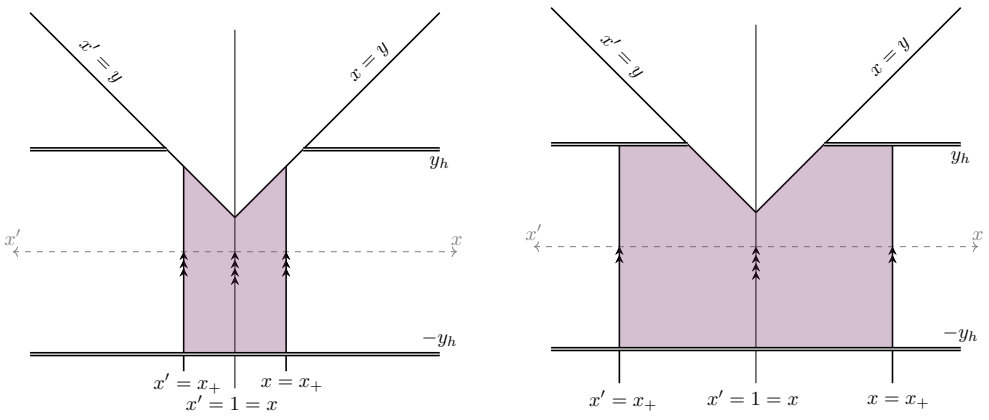

Figure 4.8: **Left:** $\mathrm{II}_{\mathrm{right,slow}}$. The two patches of type II spacetime – with $x > 1$ – and the identifications used to construct a black hole accelerated by a pushing strut when $x_+ < y_h$. **Right:** $\mathrm{II}_{\mathrm{right,rapid}}$. The two patches of type II spacetime – with $x > 1$ – and the identifications used to construct a black hole accelerated by a pushing strut when $x_+ > y_h$.

Hidden within Class I, there is an accelerating black hole – which we refer to as Class $\mathrm{I_C}$ – that does not have the BTZ black hole as a non-accelerating limit. In fact, this solution exists within a particular range of parameters where the acceleration and mass are bounded.

We will expand on this discussion later.

4.4.1 Class $\mathrm{II}_{\mathrm{right}}$: A BTZ black hole pushed by a strut

Let us choose some value $x_+ > 1$ and define a patch with $x \in [1, x_+)$. We glue two copies of this patch, mirroring along both $x = 1$ and $x = x_+$. The identifications are shown in Figure 4.8. The $x = 1$ axis of the newly formed spacetime is regular, while $x = x_+$ marks the position of a domain wall of negative tension $\mu = -A(4\pi)^{-1}\sqrt{Q(x_+)}$. The resulting spacetime describes the exterior of a black hole with horizon located at $-y_h = -\sqrt{1 + A^{-2}\ell^{-2}}$. If x_+ is larger than y_h, there is also a "droplet" horizon [108] present at $y = y_h$ for $x > y_h$. The slow accelerating phase was first described by Astorino in [123] while the rapid phase is a novel feature. The existence of such a phase strengthens the analogy with the four-dimensional accelerating black hole.

To cast the metric in more intuitive coordinates, take $x = \cosh(\psi/K)$ where $K = \pi/\operatorname{arcosh}(x_+)$. Defining dimensionful coordinates $\rho = -(Ay)^{-1}$ and $t = \alpha A^{-1}\tau$, the metric becomes

$$\begin{aligned} ds^2 &= \frac{1}{\left(1 + A\rho\cosh\left(\frac{\psi}{K}\right)\right)^2}\left(-f(\rho)\frac{dt^2}{\alpha^2} + \frac{d\rho^2}{f(\rho)} + \rho^2\frac{d\psi^2}{K^2}\right), \\ f(r) &= -1 + (1 + A^2\ell^2)\rho^2/\ell^2\,, \end{aligned} \tag{4.36}$$

where again we leave room for the possibility that t should be scaled by some dimensionless quantity α. The parameter K has been chosen such that the range of ψ is $(-\pi, \pi)$. We require both $K > 0$ and $\pi/K < \text{arcosh}(y_h)$. This patch does not cover the entire region between the black hole horizon and the boundary (and the acceleration horizon). The region immediately exterior to the black hole has $r > 0$. Proceeding from the black hole along a line of constant ψ in the direction of increasing r, one encounters a coordinate singularity as $r \to \infty$, which is a geometrically uninteresting locus. One must take a second patch with $r < 0$ to cover the region bounded by the conformal boundary (for small ψ) and possibly also the acceleration horizon (for large ψ). This is exactly analogous to the slowly accelerating black hole in 4D. The conformal boundary is then approached as $r \to -\left[A \cosh\left(\psi/K\right)\right]^{-1}$. There is a regular semi-axis at $\psi = 0$, while along $\psi = \pm\pi$ lies a domain wall of (negative) tension

$$\mu = -\frac{A}{4\pi} \sinh\left(\frac{\pi}{K}\right) . \tag{4.37}$$

These Class II_{right} solutions form a one parameter extension of the well-known family of static BTZ black holes. To highlight the relationship, take the metric (4.36) and make the parameter redefinitions $K = m^{-1}$ and $A = m\mathcal{A}$. Also, make the coordinate rescalings $r = m\rho$ and $\tilde{t} = m^{-1}t$. The metric becomes

$$\begin{aligned} ds^2 &= \frac{1}{\Omega(r,\psi)^2}\left[-F(r)\frac{d\tilde{t}^2}{\alpha^2} + \frac{dr^2}{F(r)} + r^2 d\psi^2\right] , \\ F(r) &= -m^2(1 - \mathcal{A}^2 r^2) + \frac{r^2}{\ell^2} , \\ \Omega(r,\psi) &= 1 + \mathcal{A} r \cosh(m\psi) . \end{aligned} \tag{4.38}$$

We require that both $m > 0$ and the slow acceleration condition, which is now $m \sinh\left(m\pi\right) < \left(\mathcal{A}\ell\right)^{-1}$, hold. A chart with $r > 0$ covers the region immediately exterior to the black hole horizon, which lies at $r_h = m\ell(1+m^2\mathcal{A}^2\ell^2)^{-1/2}$. A second chart with $r < 0$ covers the region bordered by the conformal boundary, which lies at $r \to -\left[\mathcal{A}\cosh(m\psi)\right]^{-1}$. Considering now the Euclidean version of the solution, the black hole has Hawking temperature and entropy given by

$$\begin{aligned} T &= \frac{|f'(r_h)|}{4\pi\alpha} = \frac{m\sqrt{1 + m^2\mathcal{A}^2\ell^2}}{2\pi\ell\alpha} , \\ S &= \frac{\ell}{G} \text{arctanh}\left[\left(\sqrt{1 + m^2\mathcal{A}^2\ell^2} - m\mathcal{A}\ell\right) \tanh\left(\frac{m\pi}{2}\right)\right] , \end{aligned} \tag{4.39}$$

where once again, the entropy has been obtained as a quarter of the area of the black hole horizon.

To understand the solution, we can again perform a mapping to global AdS_3, the details of which are given in Appendix C. A solution in the slow phase $x_+ < y_h$ is shown in Figure 4.9, while one in the rapid phase $x_+ > y_h$ is shown in Figure

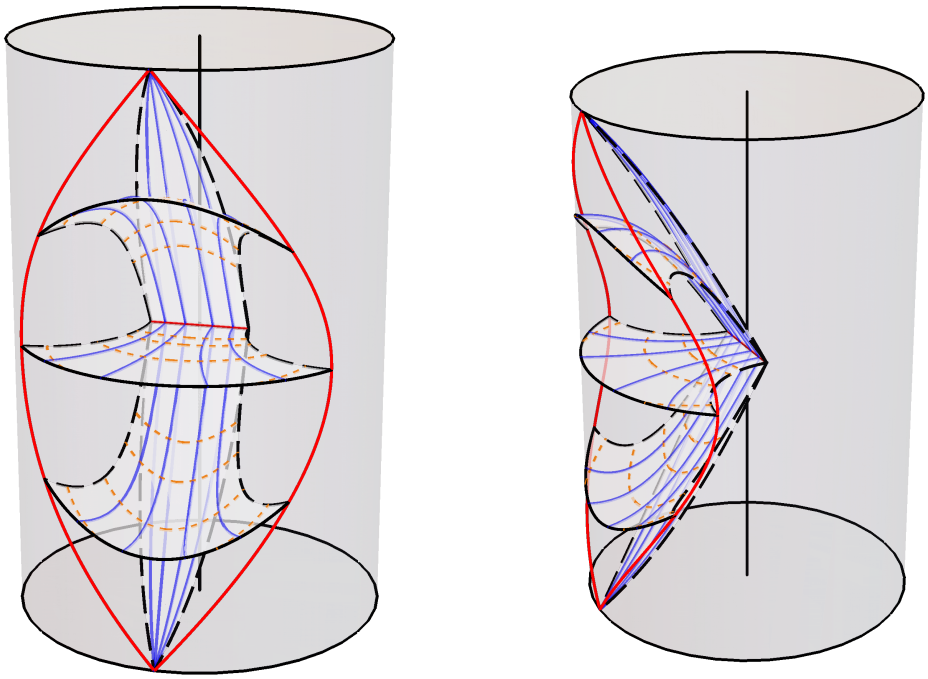

Figure 4.9: The Class $\mathrm{II}_{\mathrm{right,\ slow}}$ black hole. Several surfaces of constant t are shown. The lines $x = x_+ < y_h$ are shown in dashed black, and are identified with their partner within the same time slice, wrapping the bifurcation surface (shown as a horizontal red line) into a circle. The early and late time-slices demonstrate the event horizon. Lines of constant y are shown in dashed orange. Lines of constant x are shown in blue. The classically accessible region of the boundary is delimited in red.

4.10. In the slow phase, there is a single bifurcate Killing horizon generated by ∂_t. Upon making the appropriate identification, the bifurcation surface of this horizon acquires the topology of a circle. All of the lines of constant x (and t) connect the bifurcation surface of this horizon to the conformal boundary (consider the blue lines in Figure 4.9). This construction mirrors that of the usual, static BTZ black hole (cf. Figure C.1). Of course, when constructing the Class $\mathrm{II}_{\mathrm{right,slow}}$ black hole, surfaces of constant x are glued resulting in a strut. In the usual BTZ construction the surfaces to identify are specifically chosen by quotienting (the universal covering space of) AdS_3 by the group of integers to maintain regularity. In the rapid phase, ∂_t generates two disjoint bifurcate horizons. There exist lines of constant $x > y_h$ (and t) which connect the black hole bifurcation surface to a second, disjoint bifurcation surface with topology $\mathbb{R}$. While the slow phase is qualitatively similar to the traditional, static BTZ solution, albeit with induced tension in the identified surface, the rapid phase hitherto absent from the literature is qualitively distinct.

As done for Class I solutions, we wish to identify the value of α such that the generator of time translations is that of an asymptotic observer. For that, let us

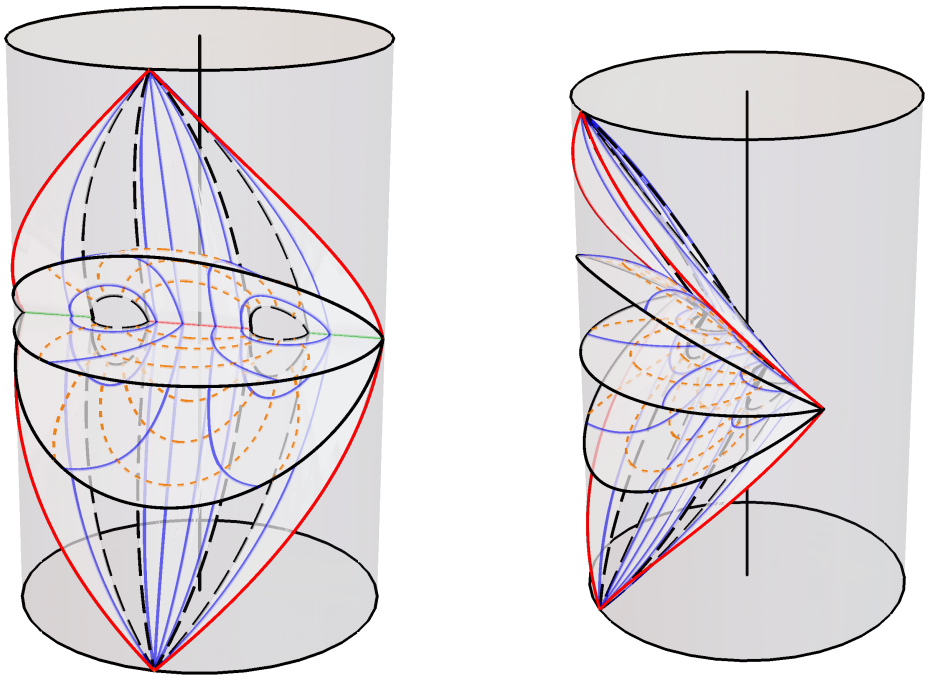

Figure 4.10: The Class $\text{II}_{\text{right,rapid}}$ black hole. Several surfaces of constant t are shown. The lines $x = x_+ < y_h$ are shown in dashed black, and are identified with their partner within the same time slice. The early and late time-slices show the event horizons. The black hole event horizon has a compact bifurcation surface with topology S^1, shown in red, while the green line denotes the "acceleration horizon" or droplet's bifurcation line with topology $\mathbb{R}$. Lines of constant y are shown in dashed orange. Lines of constant x are shown in blue. The classically accessible region of the boundary is delimited in red.

focus on the case where the parameter A is small enough that

$$\pi/K < \operatorname{arcosh}\left(\sqrt{1 + A^{-2}\ell^{-2}}\right) . \tag{4.40}$$

Before proceeding with the calculation, a comment is warranted on the choice of Killing vector from which to calculate the conserved charge. To identify α, one might try to again posit that ∂_t is the appropriate Killing vector with which to calculate the mass when it coincides with the time coordinate of the Rindler wedge. In fact, a slight modification of this procedure is required: one should scale the time coordinate by a factor of m in order to reproduce the zero-mass of AdS_3 as the black hole horizon size is taken to zero [20]. The mapping between the Class II geometry and the Rindler geometry is

$$\left(-1 + \frac{R^2}{\ell^2}\right) = \frac{F(r)}{m^2\alpha^2\Omega(r,\psi)^2} , \qquad R\sinh\vartheta = \frac{r\sinh(m\psi)}{m\Omega(r,\psi)} , \tag{4.41}$$

where we must also scale the time coordinate

$$\tilde{t} = \frac{t_{\text{Rindler}}}{m} \tag{4.42}$$

and set

$$\alpha = \sqrt{1 + m^2 \mathcal{A}^2 \ell^2}\,. \tag{4.43}$$

Note that, as m is taken to zero, the metric (4.38) becomes

$$ds^2 = \frac{1}{(1+\mathcal{A}r)^2}\left(-\frac{r^2}{\ell^2}d\tilde{t}^2 + \frac{\ell^2}{r^2}dr^2 + r^2 d\psi^2\right)\,. \tag{4.44}$$

The transformation

$$R = \frac{r}{1+\mathcal{A}r} \tag{4.45}$$

reveals the parameter $\mathcal{A}$ to then be a gauge artifact; the geometry is nothing else than Poincaré AdS_3:

$$ds^2 = \frac{\ell^2}{R^2}dR^2 + \frac{R^2}{\ell^2}\left(-d\tilde{t}^2 + \ell^2 d\psi^2\right)\,. \tag{4.46}$$

This conclusion is solidified by noticing that the tension

$$\mu = -\frac{m\mathcal{A}}{4\pi}\sinh(m\pi) \tag{4.47}$$

inducing the domain wall also vanishes in this limit. Poincaré AdS_3 sets the zero-point energy of three-dimensional gravity holographically [55]. As such, it is natural that the mass of the Class II solutions should be calculated with respect to $\tilde{t}$, using equation (4.42). We will comeback to this point later.

4.4.2 Class $\mathbf{II_{left}}$: A BTZ black hole pulled by a wall

It is also possible to construct another one parameter extension to the family of static BTZ black holes, where the defect emerging from the horizon has a positive energy density. As such, this solution is arguably more physical than the solution of section 4.4.1.

Starting from a patch of Class II spacetime (4.10) with $x < -1$, as presented in table 4.2, choose some value $x_+ \in (-y_h, -1)$, where $y_h = \sqrt{1 + A^{-2}\ell^{-2}}$, and define a patch with $x \in (x_+, -1]$. Glue two copies of this patch, mirroring along both $x = x_+$ and $x = -1$. The identifications are shown in Figure 4.11. The $x = -1$ axis of the newly formed spacetime is regular. Along $x = x_+$, one finds a domain wall of positive tension $\mu = A(4\pi)^{-1}\sqrt{Q(x_+)}$. In contrast to the soluton with a strut, here there is always one—and only one—compact horizon present at $y = -y_h$, regardless of the values of A and x_+. As $|x_+| \to y_h$, instead of the system forming a non-compact horizon. the black hole horizon merges with the conformal boundary,

To cast the metric in more familiar coordinates, take $x = -\cosh(\psi/K)$, where $K = \pi/\operatorname{arcosh}(-x_+)$. Defining dimensionful coordinates $\rho = -(Ay)^{-1}$ and $t = \alpha A^{-1}\tau$,

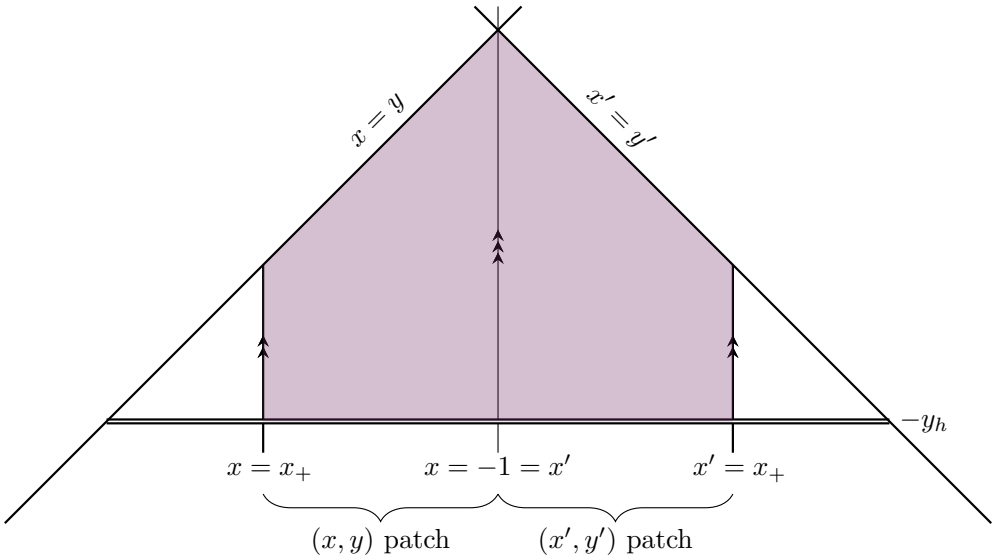

Figure 4.11: The two patches of type II spacetime used to construct a black hole with a pulling wall.

the metric becomes

$$ds^2 = \frac{1}{[1 - A\rho\cos(\psi/K)]^2}\left[-f(\rho)\frac{dt^2}{\alpha^2} + \frac{d\rho^2}{f(\rho)} + \rho^2\frac{d\psi^2}{K^2}\right], \qquad (4.48)$$
$$f(\rho) = -1 + (1 + A^2\ell^2)\rho^2/\ell^2 .$$

Yet again, we anticipate a rescaling of t by α. The range of ψ is $(-\pi, \pi)$. This (ρ, ψ) patch covers both (x, y) coordinate patches; it covers the entire region region between the black hole horizon and the conformal boundary (the region shaded purple in Figure 4.11). The coordinate ρ is everywhere positive in this domain. As long as the acceleration parameter A is sufficiently small, it is possible to set the magnitude of x_+ as large as one wishes. We thus have two conditions on K for this solution: $K > 0$ and $\pi/K < \text{arcosh}(y_h)$.

The semiaxis $\psi = 0$ is regular, while the domain wall, which now lies along $\psi = \pm\pi$, has tension

$$\mu = \frac{A}{4\pi}\sinh\left(\frac{\pi}{K}\right). \qquad (4.49)$$

Much like the solutions with a strut considered in Section 4.4.1, the solutions we have constructed in this section comprise a one parameter extension to the family of static BTZ black holes. One may demonstrate this in a similar way. Take the metric (4.48) and again make the parameter redefinitions $K = m^{-1}$ and $A = m\mathcal{A}$.

Also, make the coordinate rescalings $r = m\rho$ and $\tilde{t} = m^{-1}t$. The metric becomes

$$\begin{aligned} ds^2 &= \frac{1}{\Omega(r,\psi)^2}\left[-F(r)\frac{d\tilde{t}^2}{\alpha^2} + \frac{dr^2}{F(r)} + r^2 d\psi^2\right], \\ F(r) &= -m^2(1-\mathcal{A}^2 r^2) + \frac{r^2}{\ell^2}, \\ \Omega(r,\psi) &= 1 - \mathcal{A} r\cosh(m\psi). \end{aligned} \tag{4.50}$$

We now have the conditions $0 \leq m\sinh(m\pi) < (\mathcal{A}\ell)^{-1}$. Note that, much as for the solution with a strut, the point $m = 0$ in parameter space was inaccessible using the parameterisation (4.48). The black hole horizon lies at $r_h = m\ell(1 + m^2\mathcal{A}^2\ell^2)^{-1/2}$ with temperature and entropy as given in (4.39). The tension in the domain wall is an increasing function of m:

$$\mu = \frac{m\mathcal{A}}{4\pi}\sinh(m\pi). \tag{4.51}$$

It is interesting to note that the bounds on m translate into bounds on the induced defect stress

$$0 \leq \mu < \frac{1}{4\pi\ell}. \tag{4.52}$$

To understand the geometry, we map onto a subset of global AdS_3 and plot the geometry by compactifying the spatial section. This process is described in Appendix C, with the result being Figure 4.12. One finds a spacetime qualitatively similar to the BTZ black hole (cf. Figure C.1), but with non-zero tensile force present in the identification surface. The bifurcate Killing horizon generated by ∂_t has a compact bifurcation surface, with the topology of a circle.

The biggest difference with respect to Class II_{right} is that this solution never forms an acceleration horizon. This means that we are free of constraints over K to compute thermodynamic quantities. The transformations as written in (4.41) hold in the present case (though of course one must use the appropriate Ω), leading to the same value of $\tilde{t}$ and α (4.43) .

4.4.3 Class I_C: A (non) BTZ black hole pulled by a wall

We now return to the Class I solutions to explore a novel BTZ accelerating black hole that has only a limited allowed parameter range and is disconnected from the non-accelerating BTZ black hole.

Consider a Class I geometry in the rapid (or saturated) phase, so that $A^2\ell^2 \geq 1$. For positive y, there is a Killing horizon at $y_h = \sqrt{1 - A^{-2}\ell^{-2}}$. Now choose $x_+ \in (y_h, 1)$, so that the y coordinate lies in the range (y_h, x) for $x \in (x_+, 1)$. As usual, we glue two copies of this chart along both $x = x_+$ and $x = 1$. Diagrammatically, we are joining two copies of the upper right corner most heavily shaded region

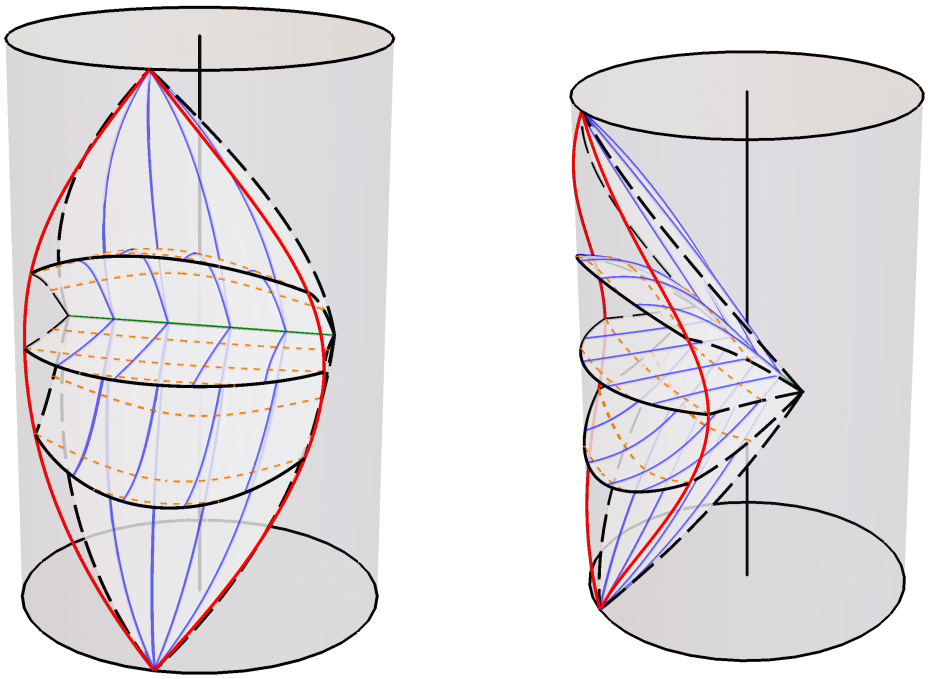

Figure 4.12: The Class II_{left} black hole. Several surfaces of constant t are shown; those of large positive and negative t outline the event horizon. The surface $x = x_+$ – shown in dashed black – is identified with its partner within each time-slice. The bifurcation surface of the Killing horizon is shown in green and has topology S^1. Lines of constant x and y are shown in solid blue and dashed orange respectively. The classically accessible region of the conformal boundary is delimited in red.

in Figure B.1(Left) where the relevant value of x_+ is denoted by C. There is no tension along the gluing surface $x = 1$ as usual, and along $x = x_+$, there is a domain wall with positive tension

$$\mu = \frac{A}{4\pi}\sqrt{1 - x_+^2}\,. \tag{4.53}$$

This positive tension domain wall extends out from the (now) compact horizon to the conformal boundary at $y = x$.

As before, we transform to the more intuitive coordinate system

$$\tau = \frac{At}{\alpha}\,, \qquad y = \frac{1}{A\rho}\,, \qquad x = \cos\left(\phi/K\right)\,, \tag{4.54}$$

where $K = \pi/\arccos\left(x_+\right)$. Since for these solutions $x_+ \in (y_h, 1)$ and $y_h \geq 0$, we have that $K > \pi/\arccos\left(y_h\right) > 2$. K can only approach its minimal value of 2 as the solution becomes close to saturated. The metric takes the form

$$\begin{aligned} ds^2 &= \frac{1}{\left[A\rho\cos\left(\frac{\phi}{K}\right) - 1\right]^2}\left(-f(\rho)\frac{dt^2}{\alpha^2} + \frac{d\rho^2}{f(\rho)} + \rho^2\frac{d\phi^2}{K^2}\right)\,, \\ f(\rho) &= 1 - (A^2\ell^2 - 1)\rho^2/\ell^2\,. \end{aligned} \tag{4.55}$$

The range of ϕ is $(-\pi, \pi)$, covering both (x, y) patches. The horizon lies at $\rho_h = (Ay_h)^{-1}$, with the conformal boundary $\rho_{\text{conf.}} = (A\cos(\phi/K))^{-1}$ satisfying $0 < \rho_{\text{conf.}} < \rho < \rho_h$. With this parameterisation, the domain wall lies on the line $\phi = \pm\pi$ and has tension

$$\mu = \frac{A}{4\pi} \sin\left(\frac{\pi}{K}\right) . \tag{4.56}$$

The tension is bounded above by

$$\mu_{\max} = \frac{A}{4\pi} , \tag{4.57}$$

which is only approachable for saturated or (nearly saturated) solutions with values of K very close to 2. It is monotonically decreasing with K and bounded below by zero.

An alternative parameterisation of the solution is available via the substitutions

$$m = \frac{1}{K} , \qquad \mathcal{A} = \frac{A}{m} ; \qquad \tilde{t} = \frac{t}{m} , \qquad r = m\rho . \tag{4.58}$$

The metric becomes

$$\begin{aligned} ds^2 &= \frac{1}{\Omega(r,\phi)^2} \left(-F(r)\frac{d\tilde{t}^2}{\alpha^2} + \frac{dr^2}{F(r)} + r^2 d\phi^2 \right) , \\ F(r) &= -m^2(\mathcal{A}^2 r^2 - 1) + \frac{r^2}{\ell^2} , \\ \Omega(r,\phi) &= \mathcal{A} r \cos(m\phi) - 1 . \end{aligned} \tag{4.59}$$

The bounds on K translate into bounds on m:

$$0 < m < \frac{1}{\pi} \arccos(y_h) < \frac{1}{2} . \tag{4.60}$$

Since m is bounded above by one half, no geometries of this type are possible with $\mathcal{A}\ell < 2$. Thus, this corner of solution space, while representing an accelerating BTZ black hole, is not connected to the canonical BTZ solution as $A \to 0$ is not allowed for these solutions. In fact, after the reparameterization, y_h now depends on m. This makes the second inequality in (4.60) slightly tricky; it is more easily expressed as a bound on $\mathcal{A}\ell$:

$$\frac{1}{m} \leq \mathcal{A}\ell < \frac{1}{m \sin(m\pi)} . \tag{4.61}$$

This effective upper bound on m combines with the lower bound provided by the rapid acceleration condition to form an allowed range of m values for a given $\mathcal{A}\ell$, shown in Figure 4.13.

The conformal boundary lies at $r_{\text{conf.}} = (\mathcal{A}\cos(m\phi))^{-1} \geq \mathcal{A}^{-1}$. The minimal value of $\mathcal{A}^{-1}$ is achieved only at a single point: the point on the boundary for which $\phi = 0$. For a rapid ($m\mathcal{A}\ell > 1$) solution, the horizon lies at

$$r_h = \frac{m\ell}{\sqrt{m^2\mathcal{A}^2\ell^2 - 1}} \tag{4.62}$$

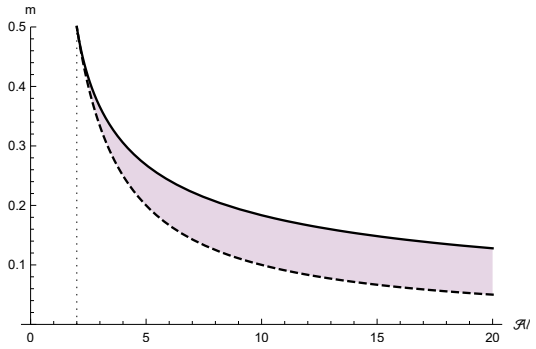

Figure 4.13: The parameter space of the $\mathrm{I}_{\mathrm{rapid,C}}$ solution (shaded purple).

and satisfies $r_h > \mathcal{A}^{-1}$. As the solution becomes saturated ($m\mathcal{A}\ell = 1$), the horizon moves out to infinity and these coordinates become less useful.

By regularity of the Euclidean section, the horizon temperature is

$$T = \frac{|f'(r_h)|}{4\pi\alpha} = \frac{1}{2\pi\ell\alpha}\sqrt{m^2\mathcal{A}^2\ell^2 - 1}\,. \tag{4.63}$$

It is interesting to note that either of the possible normalisations ∂_t and $\partial_{\tilde{t}}$ yield a temperature independent of the acceleration parameter $\mathcal{A}$. At the saturation point $m\mathcal{A}\ell = 1$, where the solution is massless, the system approaches absolute zero.

One might be concerned that r is decreasing as one nears the conformal boundary. The length of a closed ring of constant r is

$$\int_{-\pi}^{\pi} \frac{r}{\mathcal{A}r\cos(m\phi) - 1} d\phi = \frac{r}{m\sqrt{\mathcal{A}^2r^2 - 1}} \operatorname{arctanh}\left[\sqrt{\frac{\mathcal{A}r+1}{\mathcal{A}r-1}} \tan\left(\frac{m\pi}{2}\right)\right]. \tag{4.64}$$

This function is monotonically decreasing with r, as shown in Figure 4.15. A ring close to the horizon is smaller than a ring close to the boundary; the system is behaving in an intuitive fashion, despite the unintuitive metric. Calculating the minimal value of (4.64), we obtain the horizon entropy

$$S_{I_{\mathrm{C}}} = \ell \operatorname{arctanh}\left[m\mathcal{A}\ell\,(1+y_h)\tan\left(\frac{m\pi}{2}\right)\right]. \tag{4.65}$$

The entropy is monotonically increasing in m, with the massless solution $M = m\mathcal{A}\ell \to 0$ attaining the minimal entropy

$$S_{M=0} = \ell \operatorname{arctanh}\left[\tan\left(\frac{\pi}{2\mathcal{A}\ell}\right)\right]. \tag{4.66}$$

The entropy is plotted against m, for various values of $\mathcal{A}\ell$, in Figure 4.14. In the figure, the entropy of the massless solution is marked by a shape. The entropy is monotonically increasing with the mass and diverges as m approaches its supremum.

To better understand the solution, we can map it to a subset of global AdS_3 and plot it by compactifying the spatial section. This process is described in Appendix C,

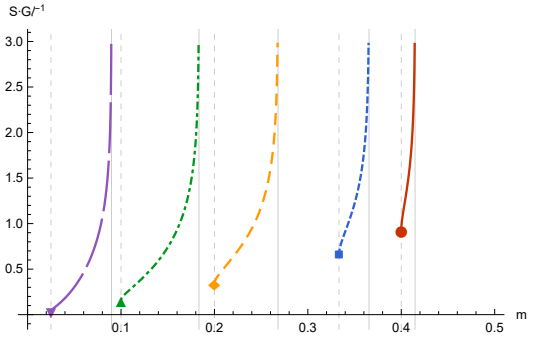

Figure 4.14: The entropy $\ell^{-1}S$ of the $\mathrm{I}_{\mathrm{rapid,C}}$ solution at various values of $\mathcal{A}\ell$: $\mathcal{A}\ell = 2.5$ (solid red), $\mathcal{A}\ell = 3.0$ (dotted blue), $\mathcal{A}\ell = 5.0$ (dashed orange), $\mathcal{A}\ell = 10$ (dot-dashed green), $\mathcal{A}\ell = 40$ (long-dashed purple). A solid grey vertical line denotes an asymptote where the divergence $\mathcal{A}\ell = (m\sin(m\pi))^{-1}$ is met. A dashed grey line dentotes the value of m for a massless solution; the entropy at this point is marked with a shape.

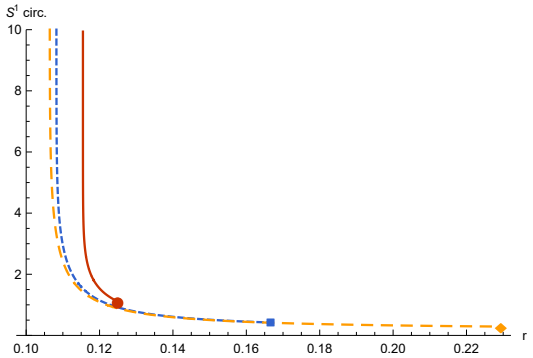

Figure 4.15: The "circumference" of loops of constant r. ℓ is set to unity with $\mathcal{A} = 10$. Three values of m (6^{-1}, 8^{-1}, and 9^{-1}) are shown (in solid red, dotted blue, and dashed orange respectively). The value at the horizon radius $r = r_h$ is marked by a shape.

with the result being Figure 4.16. One finds a result qualitatively similar to the BTZ black hole, (see Figure C.1), but with non-zero stress present in the identification surface. This is the key to understanding the $\mathrm{I}_{\mathrm{rapid,C}}$ and $\mathrm{I}_{\mathrm{saturated,E},y>0}$ solutions. The static BTZ black hole is constructed by taking the AdS_3 Rindler wedge (4.29) and identifying complete orbits of the Killing vector generating rotations, (see Appendix C.0.2 for a short review). The Class I_{C} black hole is constructed similarly, though one is identifying instead surfaces of constant x.

The explicit mapping of the Class I_{C} geometry to the planar BTZ geometry (4.29) is given by

$$\left(-1+\frac{R^2}{\ell^2}\right) = \frac{F(r)}{m^2\alpha^2\Omega(r,\phi)^2}\,, \qquad R\sinh\vartheta = \frac{r\sin(m\phi)}{m\Omega(r,\phi)}\,, \tag{4.67}$$

where the time coordinates are related by

$$\tilde{t} = \frac{t_{\mathrm{Rindler}}}{m}\,. \tag{4.68}$$

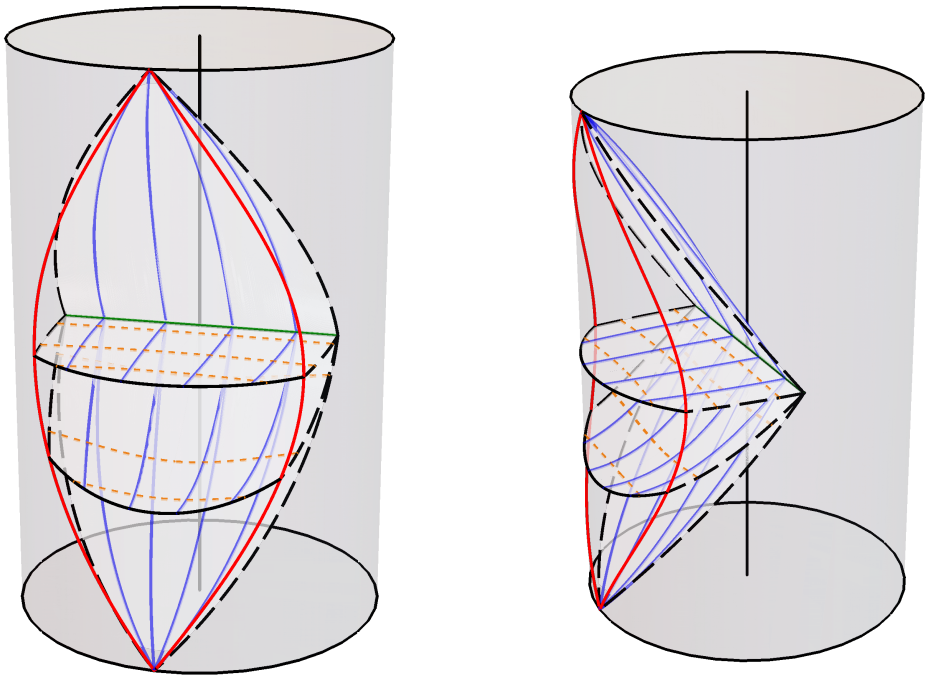

Figure 4.16: The Class $\mathrm{I}_{\mathrm{rapid,C}}$ solution, as a portion of global AdS_3. Several surfaces of constant t are shown. The horizon is shown by the surfaces at early and late times, with the bifuration surface shown in green. The lines $x = x_+$ and $x' = x_+$ within each time-slice (shown in long-dashed black) are identified, which imbues the birfurcation surface with the topology of a circle. Lines of constant x are shown in blue, with lines of constant y shown in dashed orange. The classically accessible subset of the global boundary is delimited in red. To guide the eye, the locus of the cylinder is shown in solid black.

The above transformation necessitates

$$\alpha = \sqrt{m^2\mathcal{A}^2\ell^2 - 1}\,. \tag{4.69}$$

There are then two obvious candidates, ∂_t and $\partial_{\bar{t}}$, for the Killing vector from which to compute physical quantities such as the mass and temperature. It is not clear which, if either, of these is the correct choice, as the solution is not smoothly connected to any familiar ones.

4.5 Class III solutions

As stated in section 4.1, if $A^2\ell^2 \geq 1$ then P is everywhere non-positive. We thus restrict to the case where $A^2\ell^2 < 1$. There are then two disconnected, non-compact horizons in the spacetime at $y = \pm y_h$, where $y_h \equiv \sqrt{A^{-2}\ell^{-2} - 1}$. Solutions of Class III have no roots for $Q(x)$ and so the acceptable range of x is $x > y > -y_h$. The (x, y) parameter space is shown in Figure 4.17. Since there are no roots of Q at which to form a regular semi-axis, it is not possible to form a single-wall solution

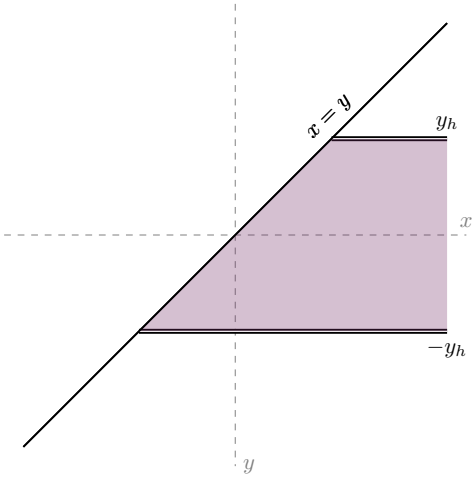

Figure 4.17: Coordinate ranges for the Class III solution.

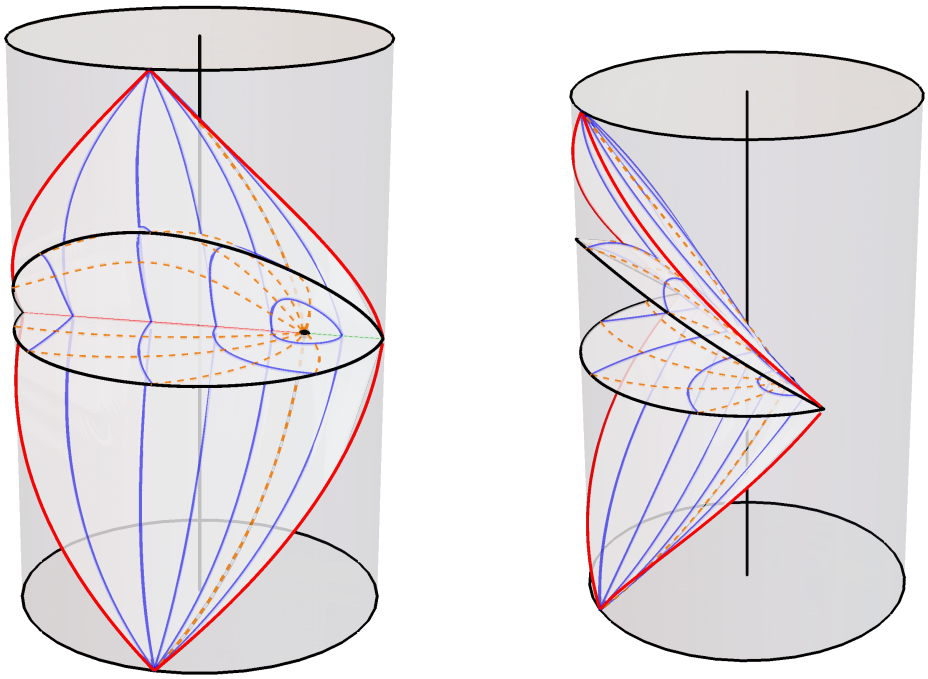

Figure 4.18: The Class III solution. Several surfaces of constant τ are shown, with those at very early and very late times outlining the two disjoint bifurcate Killing horizons. The red bifurcation surface is $y = -y_h$, while the green bifurcation surface is $y = +y_h$. The black dot denotes the point $x \to \infty$. Lines of constant finite x are shown in solid blue, with lines of constant y shown in dashed orange.

with the interpretation of x as an angular coordinate. While it is possible to form a black hole solution with two domain walls, we do not do so here.

Although it is not possible to make a single-wall solution with a periodic x coordinate, One could — if one desired — cut the patch denoted in Figure 4.18 along some line $x = x_+$ which connects the $y = -y_h$ horizon to either the conformal

boundary (for $x_+ < y_h$) or the $y = -y_h$ horizon (for $x_+ > y_h$). Identifying two copies for the remaining space along the cut still gives a solution, although x is not periodic. Four such solutions are possible, depending on a choice of signs for $x_+ - y_h$ and $x - x_+$. This solution is a stark departure from the ones we have considered in previous sections. In particular, the resulting space is some subset of *two* copies of the anti-de Sitter covering space, $\mathrm{AdS}_3 \times \mathrm{AdS}_3$; the solution is no-longer guaranteed to be embeddable within a single copy of AdS_3. This is a "braneworld solution", with the brane at $x = x_+$ dividing the two copies of global space. We will not comment on the detailed properties of these solutions here, but it is worth acknowledging as a curiosity.

Chapter 5

Holography of Accelerating Black Holes in 2+1-dimensions

At the classical level, accelerating black hole solutions are well-understood, but the asymptotic structure of these solutions presents a notable challenge in determining the physical quantities that characterise them. In recent years, there have been significant efforts to elucidate the thermodynamic behaviour of accelerating black hole [85, 101, 105, 106, 111, 122, 124]. One key approach that has proven particularly fruitful involves integrating the effects of acceleration and tension of the cosmic string, which serves as a key ingredient in achieving full cohomogeneity in the first law.

Another interesting challenge, but probably less explored so far, is the effect of acceleration from the holographic point of view. The holographic dual of an accelerating black hole is not yet fully understood and remains an active area of research. Some of the holographic properties have been reviewed in Section 3.3 where we saw that the dual theory may correspond to a strongly correlated system living in a black hole background [101, 108].

A huge step towards a formal holographic description has been done through the discovery of supersymmetric accelerating black holes and their embedding into supergravity/M–theory [84, 85, 125–127] providing a promising avenue for studying these solutions by means of AdS/CFT correspondence. Moreover, this approach also seems to suggest the existence of higher–dimensional accelerating solutions which have not been explored yet.

An alternative approach would be to consider a simpler toy model. In this regard, three–dimensional gravity seems to be the perfect candidate to test the boundary properties of accelerating black holes as properties of two–dimensional field theories are well understood.

Through this chapter, we will explore some boundary and thermodynamic aspects

of the different classes of geometries associated with the three-dimensional C-metric with particular emphasis on accelerating BTZ black holes. As done for the four-dimensional case, we consider accelerating black holes in the slow accelerating phase where the second accelerating horizon is not present. This simplification puts the black hole in thermal equilibrium for which the standard holographic and thermodynamic techniques are still valid. At the same time, solutions where an accelerating horizon can be present, such as Class $\mathrm{II}_{\mathrm{right}}$, impose extra constraints on the parameter space.

In order to describe the boundary of the spacetime, we have two options: either the Fefferman-Graham gauge or ADM coordinates. We sketch both procedures as done in Section 3.3 noting that the ADM frame provides a better framework to have a complete description of the boundary. Moving forward, we compute the Euclidean action and show that the standard renormalised action for AdS_3 contains an additional divergence originating from the domain wall extending from the black hole to the boundary. We add the Nambu–Goto action to account for the domain wall and ensure that the new Euclidean action satisfies the correct quantum statistical relation.

Furthermore, we compute the associated entanglement entropy by utilising the relationship between these solutions and Rindler–AdS, finding that the total entanglement decreases with the acceleration. We finish by commenting on the first law of thermodynamics for these black holes.

5.1 Holographic stress tensor via FG

Following the recipe shown in Section 3.3.1 one expands the metric in the Fefferman-Graham frame

$$ds^2 = \frac{\ell^2}{z^2}dz^2 + \frac{\ell^2}{z^2}(g_{(0)ij} + \cdots + z^d(g_{(d)ij} + h_{(d)ij}\log(z)) + \cdots)dx^i dx^j \ , \qquad (5.1)$$

that in three-dimensions terminates exactly at order z^2 [55, 58, 59] . We do not consider the logarithmic contribution explicitly. The holographic stress tensor $\langle T\rangle$ is completely determined by $g_{(0)}$ and $g_{(2)}$:

$$\langle T\rangle = -\frac{\ell}{8\pi}\left(g_{(2)} - g_{(0)}\,\mathrm{Tr}[g_{(0)}^{-1}g_{(2)}]\right) . \qquad (5.2)$$

Therefore, the problem reduces to finding $g_{(0)}$ and $g_{(2)}$. We transform the metric (4.10) to Fefferman-Graham gauge near the boundary using

$$y = \xi + \sum_{m=1}^{\infty} F_m(\xi)\left(\frac{z}{\ell}\right)^m , \qquad x = \xi + \sum_{m=1}^{\infty} G_m(\xi)\left(\frac{z}{\ell}\right)^m . \qquad (5.3)$$

In fact, it is straightforward to determine each of the functions F and G by solving Einstein's equations order by order. To determine G_1 we expand the resulting

metric to order z^{-2}, and impose the lack of a cross term $g_{z\xi} = 0$. We then expand to order z^{-1}, then z^{-2}, and so on, sequentially fixing the F_m's and G_m's to acquire Fefferman-Graham form. In this process, F_1 remains unfixed, appearing as a conformal factor in the boundary metric $g_{(0)}$ as in the four-dimensional case. Also, the metric expansion explicitly terminates at $\mathcal{O}(z^2)$: once one gauge fixes $g_{zz} = \ell^2 z^{-2}$ and $g_{z\xi} = 0$ at order $m = 7$, the other metric components at the same order vanish identically. This property persists at orders $m > 7$; one is always able to add terms to the coordinate expansions (5.3) such that the $g_{(n)}$ with $i \geq 5$ are identically zero to arbitrary order. As we are primarily interested in describing the accelerating BTZ black holes, we will particularise the procedure for Class II solutions although applying the procedure to Class I is trivial. Moreover, we restrict the case where the solutions only possess a compact horizon. In the case of the accelerating BTZ pushed by a strut, the parameter A must be small enough to satisfy

$$\pi/K < \operatorname{arcosh}\left(\sqrt{1 + A^{-2}\ell^{-2}}\right) . \tag{5.4}$$

Let us introduce a redefinition of the conformal factor in terms of a new (non-zero) function ω,

$$F_1(\xi) = \frac{\Upsilon^{3/2}}{A\ell\omega(\xi)} , \tag{5.5}$$

where we have also introduced a dimensionless function

$$\Upsilon = 1 - A^2\ell^2(\xi^2 - 1) , \tag{5.6}$$

The boundary metric is then

$$ds^2_{(0)} = \omega(\xi)^2 \left[-\frac{dt^2}{\alpha^2} + \frac{\ell^2 d\xi^2}{(\xi^2 - 1)\,\Upsilon^2} \right] . \tag{5.7}$$

Note that $g_{(0)}$ has the correct dimensions of length squared. The leading correction in the Fefferman-Graham expansion $g_{(2)}$ is dimensionless and contains higher derivatives of ω. Raising and lowering indices with $g_{(0)}$, the non-zero components of the stress tensor are

$$\begin{aligned} 16\pi G\ell\omega(\xi)^4\langle T^\tau_\tau\rangle = \Bigg[m^2 \Bigg(& 3\left(\xi^2-1\right)\omega'(\xi)^2\Upsilon^2 + 2\omega(\xi)\Upsilon\Bigg(-\left(\xi^2-1\right)\omega''(\xi)\Upsilon + \\ & \xi\omega'(\xi)\left(3\mathcal{A}^2m^2\left(\xi^2-1\right)\ell^2 - 1\right)\Bigg) - \omega(\xi)^2\left(\mathcal{A}^2m^2\ell^2+1\right)\Bigg)\Bigg] , \end{aligned} \tag{5.8}$$

and

$$16\pi G\ell\omega(\xi)^4\langle T^\xi_\xi\rangle = m^2\left(\omega(\xi)^2\left(\mathcal{A}^2m^2\ell^2+1\right) - \left(\xi^2-1\right)\omega'(\xi)^2\Upsilon^2\right) . \tag{5.9}$$

where we have used $A = m\mathcal{A}$. As expected for a two-dimensional boundary theory [51, 58], tracing this stress tensor reproduces the usual Weyl anomaly

$$\langle \mathrm{Tr}[g^{-1}_{(0)}T]\rangle = \frac{c_{\mathrm{Virasoro}}}{24\pi} R(g_{(0)}) , \tag{5.10}$$

where $R(g_{(0)})$ is the Ricci scalar of the boundary metric $g_{(0)}$

$$R(g_{(0)}) = \frac{2m^2\Upsilon}{\ell^2\omega(\xi)^4}\Bigg[\omega(\xi)\Bigg(\left(\xi^2-1\right)\omega''(\xi)\Upsilon - \xi\omega'(\xi)\left(3\mathcal{A}^2m^2\left(\xi^2-1\right)\ell^2-1\right)\Bigg) - \left(\xi^2-1\right)\omega'(\xi)^2\Upsilon\Bigg], \quad (5.11)$$

The central charge is calculated to be $c_{\text{Virasoro}} = 3\ell/2$, suggesting the existence of a local Virasoro asymptotic symmetry group. The stress tensor is covariantly conserved: $\nabla_\mu T^\mu{}_\nu = 0$. Additionally, it is worth noting that the stress tensor can be expressed in the form of a perfect fluid

$$\langle T_{ij}\rangle = (p(\xi)+\rho)\,u_iu_j + p(\xi)g_{(0)ij}\ , \quad (5.12)$$

on a curved background $g_{(0)}$ with timelike velocity u^i given by

$$u_i = \omega(\xi)\delta_i^t\ . \quad (5.13)$$

pressure

$$p = \frac{(1+m^2\mathcal{A}^2\ell^2)\omega^2 + (\xi^2-1)\Upsilon^2\omega'^2}{16\pi G\ell\alpha^2\omega^4}\ , \quad (5.14)$$

and energy density

$$\rho = -\frac{m}{16\pi\alpha G\sqrt{\xi^2-1}\Upsilon\omega(\xi)^2}\Bigg(2\Upsilon\omega(\xi)\Bigg(-\xi\omega'(\xi)\left(3\mathcal{A}^2m^2\left(\xi^2-1\right)\ell^2-1\right) + \left(\xi^2-1\right)\Upsilon\omega''(\xi)\Bigg) + \omega(\xi)^2\left(\mathcal{A}^2m^2\ell^2+1\right) - 3\left(\xi^2-1\right)\Upsilon^2\omega'(\xi)^2\Bigg) \quad (5.15)$$

Although we have been able to construct the boundary stress tensor, integrating the $tt-$component to obtain the holographic mass is not a simple task. In fact, contrary to the four-dimensional case, the integrand of the holographic mass (3.35) depends on the conformal representative ω. Choosing a particular ω is analogous to choosing the ground state of the boundary CFT. In [1], ω was chosen in such a way that the boundary metric renders to a cylinder that is nothing else than using Brown–Henneaux boundary conditions for AdS_3. Despite the fact that the conformal freedom permits one to make that decision, the CFT described by $\omega = 1$ might not correspond to the dual of the accelerating black hole. We will come back to this discussion later as we present the computation using the ADM formulation.

5.2 Holographic stress tensor via ADM decomposition

Again, we follow the prescription given in [85, 108] and define

$$\tilde{z} = x - y, \quad (5.16)$$

that leaves the boundary at $\tilde{z} = 0$. The canonical metric (4.10) renders

$$ds^2 = \frac{1}{\Omega^2}\Big[- P d\tau^2 + \frac{(dx^2 + d\tilde{z}^2 - 2dxd\tilde{z})}{P} + \frac{dx^2}{Q}\Big] ,$$
$$\Omega = A\tilde{z} . \tag{5.17}$$

From here, we can cast the metric in an ADM-like form near the boundary where the spacetime coordinates are $x^\mu = (z, \tau, x)$ and induced coordinates on the hypersurfaces are $x^i = (\tau, x)$, viz.

$$\begin{aligned} ds^2 &= N^2 d\tilde{z}^2 + h_{ij}(dx^i + N^i d\tilde{z})(dx^j + N^j d\tilde{z}) \\ &= \left[N^2 + h_{xx}\left(N^x\right)^2\right] d\tilde{z}^2 + 2N_x dx d\tilde{z} + h_{ij}dx^i dx^j , \end{aligned} \tag{5.18}$$

with h_{ij} the induced metric, N lapse function and N^i shift vector. We read the form of these quantities by comparing (5.17) and (5.18),

$$N^2 = \Omega^{-2}(P+Q)^{-1} , \tag{5.19}$$
$$N^i = \frac{Q}{P+Q}\delta^i_x , \tag{5.20}$$
$$h_{ij} = \mathrm{diag}\left(-\frac{P}{\Omega^2}, \frac{Q+P}{\Omega^2 PQ}\right) . \tag{5.21}$$

We can see that this metric is singular as we approach to the conformal boundary. Instead, we are going to introduce a small regulator $\delta \geq 0$ such that near the boundary $\tilde{z} = \delta$. The boundary metric is then defined by

$$\begin{aligned} ds^2_{\mathrm{bdy}} &= \lim_{\delta\to 0} \delta^2 h_{ij}|_{\tilde{z}=\delta} dx^i dx^j = g_{(0)ij} dx^i dx^j \\ &= \frac{1}{A^2}\begin{pmatrix} -P & 0 \\ 0 & \frac{P+Q}{PQ} \end{pmatrix} . \end{aligned} \tag{5.22}$$

So far, we have not specified the particular class under consideration. In fact, this method allows to obtain the boundary metric for any of the values of P and Q in (4.1) in a compact form and free of the conformal ambiguity. Let us remind the definition of the outward-pointing unit vector normal to the hypersurfaces of constant z is given by

$$n = \frac{1}{N}\left(N^i\partial_i - \partial_{\tilde{z}}\right) , \tag{5.23}$$

and the extrinsic curvature

$$K_{ij} = -\frac{1}{2}\mathcal{L}_n g_{ij} = \frac{1}{2N}\left(\partial_{\tilde{z}} - \nabla_i N_j - \nabla_j N_i\right) , \tag{5.24}$$

with ∇_i the covariant derivative respect to h_{ij} , with trace $K = h^{ij}K_{ij}$. With all these ingredients we can easily evaluate the quasilocal stress tensor *à la* Balasubramanian–Kraus for any of the three-dimensional solutions.

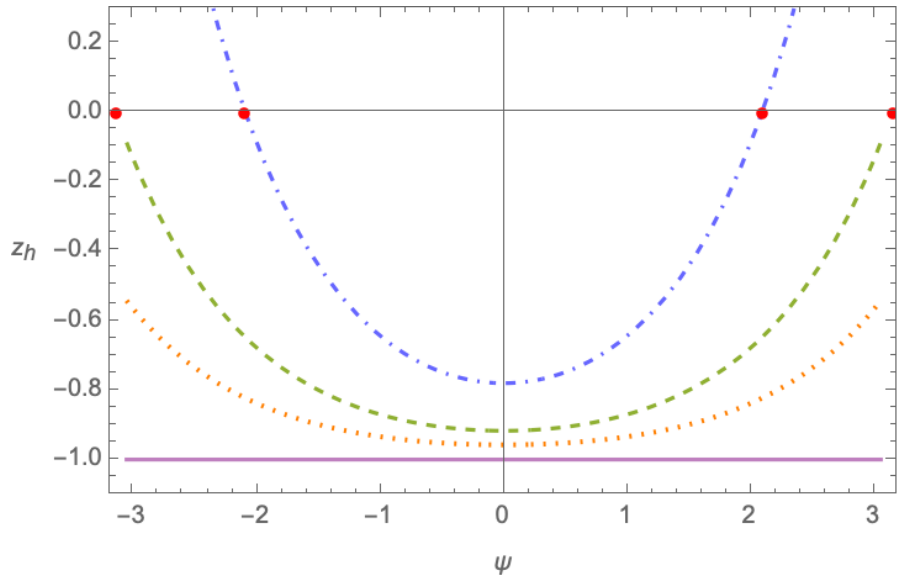

Figure 5.1: Accelerated horizon radius as a function of the azimuthal coordinate ψ, for different values of the parameter $\mathcal{A}$ that characterises the acceleration of the black hole. The solid purple line corresponds to the case $\mathcal{A} = 0$, where the horizon remains constant and never touches the conformal boundary. The green dashed curve corresponds to the critical value $\mathcal{A} = (\ell m \sinh m\pi)^{-1}$, where the horizon touches the conformal boundary exactly at the endpoints $\psi = \pm\pi$. The blue dot-dashed curve corresponds to $\mathcal{A} = 3(\ell m \sinh m\pi)^{-1}$, which is below the critical bound and the red dots indicate the points where the horizon touches the conformal boundary. The orange dotted curve corresponds to $\mathcal{A} = (2\ell m \sinh m\pi)^{-1}$, which is an acceptable value where the horizon remains smooth throughout.

We can particularise the calculation to the case of the accelerating BTZ pushed by a strut to obtain explicitly the holographic stress tensor. It is convenient to use the polar coordinates r, ψ in which the metric takes the form (4.38). We also use

$$\frac{1}{r} \equiv z - \mathcal{A}\cosh(m\psi) \ . \tag{5.25}$$

It is important to note that in this coordinate system, the horizon is described by a function $z_h = z_h(z, \psi)$. The accelerated horizon is plotted in Figure 5.1, and considering both horizons the considered region can be seen in Figure 5.2. The slow acceleration condition

$$m\mathcal{A}\ell \sinh(m\pi) < 1 \ , \tag{5.26}$$

ensures that the horizon does not touch the conformal boundary $z_{\rm cb}$.

Then, the boundary metric can be written as

$$\begin{aligned} ds^2_{(0)} &= g_{(0)ij}dx^i dx^j = \lim_{\delta\to 0} \delta^2 h_{ij} dx^i dx^j \\ &= G(\xi)\left(-d\tilde{\tau}^2 + d\xi^2\right) \ , \end{aligned} \tag{5.27}$$

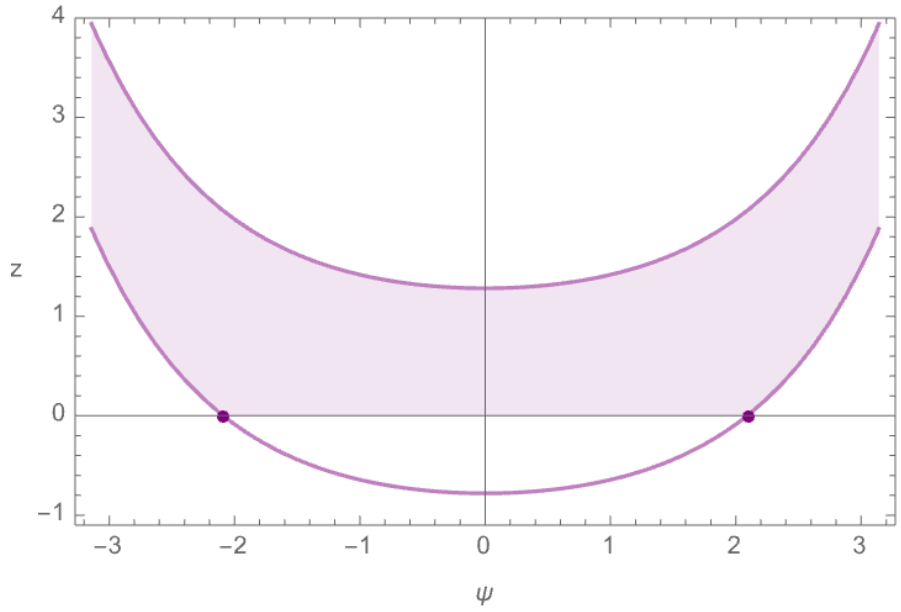

Figure 5.2: Domain of the z coordinate in terms of the coordinate ψ in the presence of the two horizons. The upper thick curve corresponds to the black hole horizon and the bottom one corresponds to the accelerating horizon touching the conformal boundary at the two dark dots. The shaded region corresponds to the region where spacetime is defined.

where

$$\tau = \alpha\ell\tilde{\tau} \ , \quad \xi = \frac{\operatorname{arctanh}\left(\alpha \tanh(m\psi)\right)}{m\alpha} \ , \tag{5.28}$$

and the conformal factor

$$G(\xi) = \frac{2\alpha^2}{2 + \alpha^2\left(1 + \cosh(2m\xi\alpha)\right)} \ . \tag{5.29}$$

is fully determined in terms of the auxiliary coordinate ξ. Evaluating the holographic stress tensor gives

$$\begin{aligned} \langle T^{\tau}{}_{\tau}\rangle &= -\frac{m^2\ell}{32\pi G}\left(2 + m^2\mathcal{A}^2\ell^2 - 3m^2\mathcal{A}^2\ell^2\cosh(2m\psi)\right) \ , \\ \langle T^{\phi}{}_{\phi}\rangle &= \frac{m^2\ell}{32\pi G}\left(2 + m^2\mathcal{A}^2\ell^2 + m^2\mathcal{A}^2\ell^2\cosh(2m\psi)\right) \ , \end{aligned} \tag{5.30}$$

which is, indeed, covariantly conserved with respect to the boundary metric $g_{(0)}$, viz, $\nabla^{(0)}_i T^{ij} = 0$. We can check that it reproduces the trace anomaly as expected

$$\langle T^{i}{}_{i}\rangle = \frac{c}{24\pi}\mathcal{R}[g_{(0)}] \ , \tag{5.31}$$

where $c = 3\ell/2G$ matches the Brown–Henneaux central charge [51], and $\mathcal{R}[g_{(0)}] = 2m^4\mathcal{A}^2\ell^2\cosh(2m\psi)$ is the curvature of the boundary metric. Once again, we can express the stress tensor in the form of a perfect fluid (5.12) on a curved background

$g_{(0)}$ with timelike velocity u^i given by

$$u^i = \frac{1}{\sqrt{-g_{(0)tt}}} \left(\frac{\partial}{\partial t}\right)^i \ , \quad u_i u_j g^{ij}_{(0)} = -1 \ , \tag{5.32}$$

where the energy density ρ and pressure $p(x)$ are defined as

$$\begin{aligned} \rho &= \frac{m^2 \ell}{32\pi G} \left[2 + m^2 \mathcal{A}^2 \ell^2 - 3m^2 \mathcal{A}^2 \ell^2 \cosh(2m\psi)\right] \ , \\ p(x) &= \frac{m^2 \ell}{32\pi G} \left\{2 + m^2 \mathcal{A}^2 \ell^2 \left[1 + \cosh(2m\psi)\right]\right\} \ . \end{aligned} \tag{5.33}$$

Moreover, we observe that the energy density ρ generates the energy flow of the fluid since $u_i T^{ij} = -\rho u^j$.

It is worth pausing to analyse these results and compare them with their four-dimensional counterpart. The fluid interpretation is relatively similar in the sense that the CFT is still lying on a curve background given by $g_{(0)}$ (5.27). When $A \to 0$, the background becomes flat and the stress tensor has constant components. In 3+1 dimensions, the stress tensor cannot be expressed in the form of a perfect fluid, and corrections associated with the acceleration parameter cause the boundary metric to be non-conformally flat, leading to non-trivial stress tensor components [101, 111]. That is not the case in 2+1 dimensions. As there is no shear nor viscosity in 1+1 dimensional fluids [128, 129], the accelerating black hole describes a perfect fluid with non-constant pressure. This can be seen as a "dissipative" effect due to the acceleration as the $\mathcal{A} \to 0$ limit gives a constant pressure as seen for the BTZ black hole. The second important point is the conformal representative. In the previous section we saw that using Fefferman-Graham expansion, all the boundary data is determined up to a conformal factor. In the ADM formulation, this is not the case as we are able to obtain the boundary metric with a specific conformal representative (5.29). As we can see, this conformal factor is crucial in order to obtain the correct behaviour of the dual CFT. The fact that this CFT lies on a curved background is due to the acceleration as can be seen from the zero acceleration limit of (5.27). In that regime, $G(\xi)$ becomes a constant, and therefore the background of the CFT is flat. This indicates that starting from the Fefferman–Graham gauge, we are only allowed to choose ω in which the background metric remains curved to capture the effect of the acceleration.

5.2.1 Holographic energy

Class I: For this class of solutions, it is convenient to preserve the canonical coordinates x, y as the physical interpretation is simpler and does not require extra physical parameters. We use the above method to obtain the boundary metric, evaluate the stress tensor and then integrate it to obtain the mass.

The components of the holographic stress tensor

$$\begin{aligned}\langle T^{\tau}{}_{\tau}\rangle &= \frac{A\ell + A^3(-2+3x^2)\ell^3}{16\pi G}, \\ \langle T^{x}{}_{x}\rangle &= \frac{A\ell}{16\pi G}\left(-1 + A^2\ell^2x^2\right) ,\end{aligned} \tag{5.34}$$

The holographic energy is obtained by integrating the $\tau\tau$-component leading to

$$\begin{aligned}M_{\rm I} &= \int_{-1}^{1} dx\sqrt{-g_{(0)}}\langle T^{\tau}{}_{\tau}\rangle \\ &= \frac{A^2\ell^2 - 2}{16\alpha G},\end{aligned} \tag{5.35}$$

whose zero-accelerating limit gives

$$\lim_{A\to 0} M_{\rm I} = -\frac{1}{8G} , \tag{5.36}$$

which corresponds to the vacuum energy of AdS_3 space [55]. Note that $A\ell < 1$ for slow acceleration. This means that the energy for accelerating particles is always in the negative spectrum $-\frac{1}{8G} < M_{\rm I} < 0$ as expected from the structure of AdS_3 space.

Class II: We can make use of the computations done in Section 5.2, and integrate the $\tau\tau$-component of the stress tensor (5.30), leading to

$$\begin{aligned}M_{\rm II} &= \int_{-\pi}^{\pi} d\phi\sqrt{-g_{(0)}}\langle T^{\tau}{}_{\tau}\rangle \\ &= -\frac{m^2\left[3m^2\mathcal{A}^2\ell^2\sinh(2m\pi) - 2\pi(2+m^2\mathcal{A}^2\ell^2)\right]}{32\pi G\alpha} .\end{aligned} \tag{5.37}$$

We can check again the zero-accelerating limit

$$\lim_{\mathcal{A}\to 0} M_{\rm II} = \frac{m^2}{8G} , \tag{5.38}$$

that leads to the BTZ mass normalised such that the pure vacuum energy corresponds to $m^2 \to -1$ as for Class I . The behaviour of the mass can be seen in Figure5.3 and Figure 5.4.

Class $\mathbf{I_C}$: Again, the results presented in Section 5.2 are fully applicable to Class I, i.e., the holographic stress tensor can be obtained in a closed form, it is covariantly conserved respect to the CFT metric and can be written as the one of a perfect fluid (5.12). After integration, we get the holographic mass for the Class $\rm I_C$ black hole

$$M_{\rm I_C} = \frac{m^2\left[4\pi - 2\pi m^2\mathcal{A}^2\ell^2 + 3m\mathcal{A}^2\ell^2\sin(2\pi m)\right]}{32\pi G\alpha} , \tag{5.39}$$

which does not have a well-defined zero-acceleration limit (α becomes purely imaginary). This is expected as this solution is not connected to the BTZ black hole, $\mathcal{A}\to 0$ is not in the range of parameters allowed 4.60.

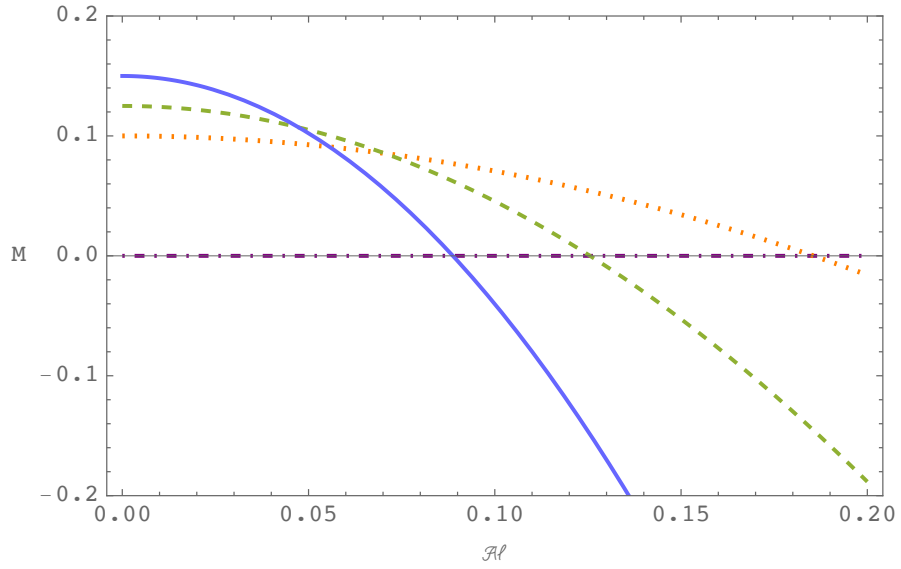

Figure 5.3: Holographic mass of the accelerated BTZ pushed by a strut as a function of $\mathcal{A}\ell$ with $m = 0, 0.8, 1, 1.2$ for the dot-dashed purple, dotted orange, dashed green, and solid blue curves, respectively.

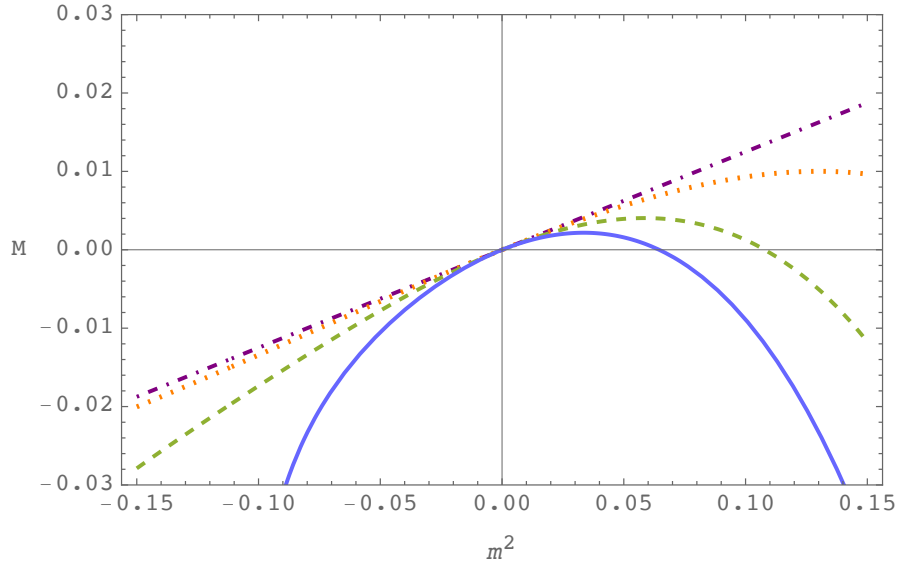

Figure 5.4: Holographic mass of the accelerated BTZ pushed by a strut as a function of m^2 with $\mathcal{A}\ell = 0, 1, 2, 3$ for the dot-dashed purple, dotted orange, dashed green, and solid blue curves, respectively.

5.3 Euclidean Action: Counterterms and domain wall.

Holographic quantities are known to suffer from UV divergences, which are mapped to IR divergences appearing in the gravitational sector of theories on asymptotically anti-de Sitter spaces. Consequently, defining observables requires having a well-defined renormalised action. This has been achieved consistently in [55, 58, 59,

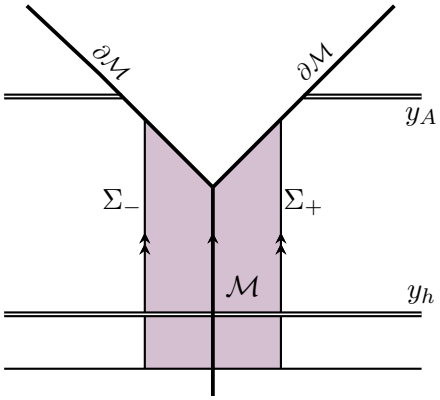

Figure 5.5: Regions of Class II spacetime with no accelerating horizon. The upper diagonal denotes the conformal boundary $\partial\mathcal{M}$, and the lateral lines are the two internal boundaries Σ_- and Σ_+ that are identified in order to obtain a compact horizon. The resulting spacetime corresponds to the accelerated BTZ solution with a domain wall extending from the black hole horizon to the conformal boundary.

79] by adding counterterms that depend only on intrinsic quantities of the boundary as we saw in Chapter 2. For AdS_3 gravity, the renormalised Euclidean action consists of the Einstein–Hilbert action supplemented with the Gibbons–Hawking–York term, which ensures a well-posed variational principle. Moreover, a counterterm is included to regulate the IR divergences of the bulk, viz.

$$I_{\text{ren}} = \frac{1}{16\pi G}\int_{\mathcal{M}} d^3x\sqrt{g}\,(R-2\Lambda) + \frac{1}{8\pi G}\int_{\partial\mathcal{M}} d^2x\sqrt{h}\left(K-\frac{1}{\ell}\right)\,, \tag{5.40}$$

where $\Lambda = -\ell^{-2}$ is the cosmological constant, $\mathcal{A}M$ corresponds to the bulk geometry restricted to some short IR regulator δ while $\partial\mathcal{M}$ is its boundary which is endowed with a metric h_{ij} evaluated at $z = \delta$. The regulator is used to regulate the IR divergences of the bulk. At the end of the computation, the limit $\delta \to 0$ is taken, which recovers the original manifold with a finite on-shell action. We are interested in evaluating (5.40) for the accelerating BTZ black hole. For simplicity, we focus again on the case pushed by a strut and use the boundary metric derived using ADM decomposition (5.19). Naively, if we evaluate the Euclidean version of (5.40), we find an extra divergence of order $\mathcal{O}(\delta^{-1})$. This contribution indicates that the counterterm proposed in Section 2.3.1 may not be sufficient to regularise three-dimensional accelerating black holes as expected initially. In fact, we need to be more careful with the geometric construction that we have done in Chapter 4. The slow accelerating BTZ black hole contains different regions illustrated in Figure 5.5 that must be considered in order to have a well-defined variational principle. This includes taking into account the internal boundaries Σ_- and Σ_+ located at $x = -x_+$ and $x = x_+$ respectively. At each of these lines of constant x, we need to insert a Gibbons–Hawking–York term such that the variation with respect to the induce metric γ leads to the Israel equations (4.13). We denote these

contributions as

$$I_{\text{internal}} = -\frac{1}{8\pi G}\left[\int_{\Sigma_+} d^2x\sqrt{\gamma}\mathcal{K}_+ + \int_{\Sigma_-} d^2x\sqrt{\gamma}\mathcal{K}_-\right] = -\frac{1}{8\pi G}\int_{\Sigma} d^2x\sqrt{\gamma}\,[\mathcal{K}]\,|_-^+\,, \tag{5.41}$$

where we have made use of $\mathbb{Z}_2$ symmetry identifying the dynamics between Σ_- and Σ_+ into a single surface Σ, denoting $[\mathcal{K}]\,|_-^+$ as the jump of the extrinsic curvature along the domain wall. From the trace of (4.13), we see that these two terms combine into a single piece

$$I_{\text{internal}} = -\frac{1}{8\pi G}\int_{\Sigma} d^2y\sqrt{\gamma}\,[\mathcal{K}]\,|_-^+ = \int_{\Sigma} d^2y\sqrt{\gamma}\;\mu\; = I_{\text{dw}}\;, \tag{5.42}$$

where μ is the tension of the domain wall (4.16) and I_{dw} denotes the Nambu–Goto action of the domain wall [130]. Thus, the total action reads

$$I = I_{\text{ren}} + I_{\text{dw}}\;, \tag{5.43}$$

Performing a Wick rotation in the time coordinate $t = i\tau$ with τ a compact coordinate with period $\beta = 1/T$ where T is the temperature of the black hole, we evaluate these terms on-shell having in mind that, when integrating z at the conformal boundary, $z \to \delta$. Finally, the limit $\delta \to 0$ is taken recovering the original manifold with a finite on-shell action. The on-shell Euclidean action contributions are

$$-I_{\text{ren}} = \beta M - S - \frac{\beta\mathcal{A}m\sinh(\pi m)}{4\pi\alpha G}\left(\frac{1}{r_h} - \frac{1}{\delta}\right)\;, \tag{5.44}$$

from the Einstein–Hilbert action and Balasubramanian–Kraus counterterm, whereas the domain wall gives

$$-I_{\text{dw}} = \frac{\beta\mathcal{A}m\sinh(\pi m)}{4\pi\alpha G}\left(\frac{1}{r_h} - \frac{1}{\delta}\right)\;, \tag{5.45}$$

such that the total Euclidean action (5.43) yields the standard quantum statistical relation

$$I_{\text{E}} = -I_{\text{ren}} - I_{\text{dw}} = \beta M - S\;, \tag{5.46}$$

where M is the black hole energy found in (5.37), β and S are the inverse of the temperature and the entropy found in (4.39), respectively. Note that if one considers only the Balasubramanian-Kraus counterterm on top of the Einstein–Hilbert and GHY terms, the resulting Euclidean action is divergent and the horizon contribution does not gives the black hole entropy (4.39). As the domain wall extends from the interior (black hole horizon) to the conformal boundary contributing with a divergent term exactly as the one coming from the AdS_3 renormalised action but with an opposite sign, making the on-shell action well-defined and reproducing on-shell the quantum statistical relation between the gravitational Euclidean action and the Gibbs thermodynamic free energy.

5.4 Entanglement entropy

A powerful tool to obtain valuable information of the dual field theory is the holographic entanglement entropy [29, 131]. It measures the degree of correlation between two subsystems on the CFT using the nature of the spacetime. The celebrated Ryu—Takayanagi (RT) formula states that the holographic entanglement entropy can be obtained by minimising the area of a co-dimension two spatial* hypersurface Γ (referred as the RT surface) whose boundary is anchored at the AdS conformal boundary, namely

$$S_{\mathrm{E}} = \frac{A_\Gamma}{4G} \ . \tag{5.47}$$

The RT surface divides the boundary into two subsystems A and A^c and (5.47) indicates the number of states on A whose measures are consistent with the ones of A^c . In general, the Euler–Lagrange problem is not easy to solve, and the profile of the RT surface is usually not obtained analytically as the existence of conservation laws is not guaranteed. An interesting observation made by Johnson [132] is that in global AdS coordinates, the complexity of the problem reduces significantly. In Chapter 4, we saw that, locally, it is possible to map the solutions to Rindler-AdS which allows to treat the problem in a simplified manner. Let us first consider a slice bounded by a line of latitude ϕ_0 and treat ϕ as time in the minimisation problem. To obtain the RT surface for the accelerating BTZ, we use the coordinate transformation given in Section 4.41, which allows to find the extremal surface for the Rindler observer. The minimal surface is then parametrised by

$$R_{\mathrm{e}}(\vartheta) = \ell \left(\frac{1 - \cosh^2 \vartheta}{\cosh^2 \vartheta_0} \right)^{-\frac{1}{2}} \ , \tag{5.48}$$

where ϑ_0 satisfies that the radial coordinates go to infinity at the endpoints. This is mapped to the boundary condition $r(\psi_0) = -(\mathcal{A}\cosh(m\psi_0))^{-1}$, such that the surface is anchored to the conformal boundary. Now we can map the surface to the coordinates used in Section 4.4.1; for the sake of notation we define $\mathcal{B} \equiv \cosh(m\psi_0)$ and $\psi_0 = m^{-1}\vartheta_0$, resulting in

$$r_{\mathrm{e}}(\psi) = \frac{m\ell \left(\alpha \mathcal{A} m \ell \cosh(m\phi) + \mathcal{B}\sqrt{\mathcal{B}^2 - \alpha^2 \sinh^2(m\psi) - 1} \right)}{\alpha \left(-\mathcal{B}^2 + \mathcal{A}^2 m^2 \ell^2 \cosh^2(m\psi) + \sinh^2(m\psi) + 1 \right)} \ , \tag{5.49}$$

whose expansion for small acceleration

$$r_{\mathrm{e}}(\psi) = \frac{m\ell}{\sqrt{1 - \frac{\cosh^2(m\psi)}{\cosh^2(m\psi_0)}}} - \frac{m^2 \mathcal{A} \ell \cosh(m\psi)}{\cosh^2(m\psi_0) - \cosh^2(m\psi)} + \mathcal{O}(\mathcal{A}^2) \ . \tag{5.50}$$

*See [30] for the covariant generalisation.

Replacing the parametrisation into the area functional, one obtains the value of the minimal area that is proportional to the holographic entanglement entropy. Despite the simplicity of the last expression, obtaining the area is quite involved. It is divergent at $\phi = \phi_0$, and therefore, a short distance cutoff ϵ must be introduced. Then, following [29], we consider the integration from ϵ to $\phi_0 - \epsilon$ and expanding again for small acceleration, we get that the entanglement entropy (5.47) becomes

$$S_{\rm E} = \frac{c}{3}\log\left[\frac{\beta}{\pi\epsilon}\sinh\left(\frac{\pi L}{\beta}\right)\right] - 2\ell^2\mathcal{A}\left(\frac{2\pi\ell}{\beta\epsilon}\sinh\left(\frac{\pi L}{\beta}\right)\right)^{\frac{1}{2}}\tanh\left(\frac{\pi L}{2\beta}\right) - \frac{\mathcal{A}^2\ell^4\pi}{\beta\epsilon}\sinh\left(\frac{\pi L}{\beta}\right) + \dots \,, \tag{5.51}$$

where we used $L \equiv 4\ell\psi_0$ which relates the expression with the size of the entangling region. Note that, as the temperature is independent of the acceleration when mapping to Rindler spacetime, the leading order corresponds to the usual result for the pure BTZ black hole [29]. However, the next to leading order gives subleading divergences which decrease the amount of entanglement with the acceleration growth. In fact, from the perspective of the black hole solution, as the acceleration – or in other words, the conical deficit – increases, the size of the boundary accessible for an asymptotic observer decreases. This can be interpreted as an indication of some information loss in the dual theory due to the acceleration.

5.5 First law for accelerating black holes in 2+1 dimensions

Although so far we have been able to obtain similar results between accelerating black holes in 2+1 and 3+1 dimensions, the thermodynamic relations in the three-dimensional case are still inconclusive. In particular, obtaining the first law is not an easy task. Let us, again, consider the accelerating BTZ black hole pushed by a strut. The thermodynamic quantities are

$$\begin{aligned} T &= \frac{m\sqrt{1+m^2\mathcal{A}^2\ell^2}}{2\pi\ell\alpha}\,, \\ S &= \frac{\ell}{G}\,\mathrm{arctanh}\left[\left(\sqrt{1+m^2\mathcal{A}^2\ell^2} - m\mathcal{A}\ell\right)\tanh\left(\frac{m\pi}{2}\right)\right] \\ M &= -\frac{m^2\left[3m^2\mathcal{A}^2\ell^2\sinh(2m\pi) - 2\pi(2+m^2\mathcal{A}^2\ell^2)\right]}{32\pi G\alpha}\,. \end{aligned} \tag{5.52}$$

In its purest form, the first law of black hole thermodynamics states

$$\delta M = T\delta S\,, \tag{5.53}$$

which is evidently not satisfied by the above quantities (5.52). One could then consider generalisations of the first law including pressure terms or new chemical

potentials [50, 105, 106, 124] that could possibly combine into a consistent thermodynamic relation. Interestingly, satisfying the first law in this setup requires more than including new thermodynamic contributions. Recall that the energy has been computed from the boundary metric (5.27) defined for a particular conformal representative $G(\xi)$. In principle, the choice of the representative is arbitrary and should not affect the temperature T or entropy S which are defined with respect to the black hole horizon. However, the energy depends explicitly on the choice of the conformal representative [133] as seen from the computation in Fefferman–Graham coordinates. The same happens with the on-shell Euclidean action which from the quantum statistical relation, we can see that a variation with respect to an arbitrary conformal representative ω gives

$$\delta_\omega I = \beta \delta_\omega M \,. \tag{5.54}$$

The left-hand side is in fact the conformal anomaly [58]

$$\delta_\omega I = -\int_{\partial\mathcal{M}} d^2x \sqrt{g_{(0)}} \mathcal{A} \delta\omega \tag{5.55}$$

whereas the right-hand side

$$\delta_\omega M = \int dx \sqrt{-g_{(0)}} \left(-2\langle T^\tau{}_\tau \rangle \delta\omega + \delta_\omega \langle T^\tau{}_\tau \rangle\right) , \tag{5.56}$$

with $\delta_\omega \langle T^\tau{}_\tau \rangle$ containing derivatives of ω associated to the Schwarzian derivative. This implies that the variations of the mass will always be present for a theory with conformal anomaly. In fact, Papadimitriou and Skenderis proposed that the modified first law must include, at the right-hand side, variations of the energy with respect to the conformal representative, namely

$$\delta M = T\delta_\omega I + T\delta S = \delta_\omega M + T\delta S \,. \tag{5.57}$$

Identifying how this relation is realised in the case of the accelerating BTZ black hole remains an open question. We hope to address this problem in the future.

Chapter 6

Conclusions

In this thesis, our aim was to describe accelerating solutions in 2+1 dimensions resembling properties of the four-dimensional C-metric.

We started by introducing some key elements and necessary concepts used in this thesis to quickly move to the description of the C-metric in 3+1 dimensions in Chapter 3. We analysed the different coordinate systems and their physical properties. In the massless limit, we saw that the interpretation of the acceleration parameter becomes evident: the black hole is pulled towards the boundary of AdS as the acceleration increases. This effect is in fact driven by a cosmic string that is inserted along the polar axis of the black hole generating antipodal defects. At both ends, the black hole experiences a different tension, being this imbalance the responsible for the acceleration. One is always allowed to choose the parameters in such a way that the cosmic string only deforms one of the poles of the black hole. We also reviewed some of the holographic and thermodynamic properties of the solution. In particular, we focused in two ways in which we can obtain the boundary data: Fefferman-Graham gauge and ADM foliation. We compared these two schemes showing that they produce similar results in 3+1 dimensions.

Moving forward, in Chapter 4 we studied the C-metric in 2+1 dimensions and the three classes of solutions obtained after removing all gauge freedom from the metric functions. To mimic the effect of the cosmic string in three-dimensions, we introduced a codimension one defect – a domain wall – by cutting and gluing the spacetime along a $x = \text{const}$ surface. Using Israel junction conditions we found the tension of the domain wall which gives rise to the "acceleration". With the allowed range of coordinates in mind for each class, we proceed to analyse them distinguishing between particle-like solutions coming from Class I, and accelerating BTZ black holes coming from Class II. Additionally in Class I, we find a novel black hole that is not continuously connected with the BTZ black hole which we refer to as "Class $\mathrm{I_C}$".

We described two particle-like solutions either pulled by the domain wall or pushed

by a strut. These exhibit similar slow accelerating phase as the accelerating black hole in 3+1 dimensions. Nevertheless, there are novel phases which are not shared with their four-dimensional cousin. A clear example is to look at the Class $\mathrm{I}_{\mathrm{rapid,\ A}}$ which describes a rapidly accelerating particle pulled by the wall. For light conical deficit, the structure is analogous to the small four-dimensional accelerating black hole. As the mass increases a phase transition occurs to Class $\mathrm{I}_{\mathrm{rapid,\ B}}$. In this limit the solution is compact and the only accessible region of the conformal boundary is at the two points in the far future and past of the Rindler worldline. A similar compactification occurs for rapidly accelerating particles pulled by a strut solutions although in this case the accessible region of the conformal boundary is still two-dimensional. The interpretation of these novel phases is still not clear.

Accelerating BTZ black holes are obtained from Class II. Once again, depending on the sign of the tension, we have two subfamilies exhibiting different phases. We refer to the accelerating BTZ pushed by a strut (domain wall with negative energy density) as Class $\mathrm{II}_{\mathrm{right}}$ and accelerating BTZ pulled by a wall (domain wall with positive energy density) as Class $\mathrm{II}_{\mathrm{left}}$, both being one parameter extensions of the BTZ black hole. We showed how these solutions may be constructed from identifications of the Rindler wedge of AdS_3, just as the BTZ black hole [20, 21]. Identifying on a surface of constant tension induces the domain wall and therefore, the "acceleration". Instead, choosing an identification surface with zero tension produces the static BTZ solution. Apart from the presence of a wall-like defect, the Class $\mathrm{II}_{\mathrm{left}}$ solution is qualitatively similar to the usual BTZ black hole without a domain wall. It does not form a second horizon for any value of the acceleration parameter. However, this is not true for the Class $\mathrm{II}_{\mathrm{right}}$ solution. Here, both "rapid" and "slow" phases exist. The rapid phase attained for large acceleration parameter is qualitatively distinct from the usual BTZ black hole, possessing a non-compact horizon reminiscent of the acceleration horizon which can be present in the four-dimensional AdS C-metric geometry. In some sense the solution is a hybrid between the BTZ black hole and the four-dimensional AdS C-metric.

However, one should be careful not to carry this analogy too far. While the conical deficit solutions of Section 4.3 may uncontroversially be called accelerating objects, the Class II BTZ black holes are more subtle. For the particle in three dimensions, as with the black hole in four dimensions, we can take the mass of the particle / black hole to zero *at fixed* A, and obtain a Rindler spacetime – either a Rindler wedge for rapid acceleration, or a slow acceleration Rindler coordinatisation of global AdS_3. For these Class II solutions however, taking $m \to 0$ at fixed A is not a meaningful limit – we cannot remove the black hole without removing the entire spacetime. For either of the Class II black holes, shrinking the horizon size to zero requires $m \to 0$, which in turn requires $K \to \infty$ or $x_+ \to 1$, i.e., removing the spacetime. Physically, there is then no object which to "accelerate". Mathemat-

ically, in $2+1$ dimensions, Einstein gravity corresponds to a topological theory. While the four-dimensional solution is a "true" black hole, the three dimensional black hole is constructed by imposing identifications on the acceleration horizon of a fictitious observer [21]. There is then no meaningful sense hitherto established in which one may talk of the acceleration of this extended object. For the Class $\mathrm{II}_{\mathrm{right}}$ black hole in its rapid phase, the temperature of the non-compact "acceleration" horizon also suggests that the black hole is inertial. By regularity of the Euclidean section, the temperature, with the correct normalisation of Killing vector (4.43), is found to be $T = m(2\pi\ell)^{-1}$, which is independent of $\mathcal{A}$. If the parameter $\mathcal{A}$ did in some way parametrise an acceleration of the black hole, the Unruh effect would be violated.

In Chapter 5, we discussed the boundary structure of the 2+1 C-metric. Since the conformal boundary is defined by a surface $\Omega = 0$, determining the boundary metric becomes a non-trivial task. To address this, we followed the same paths as for the four-dimensional accelerating black hole. We saw that it is possible to write the spacetime in the Fefferman-Graham gauge allowing us to compute the boundary data in the "traditional" manner. The boundary metric is determined up to a conformal representative which in three-dimensions prevents us to obtain the holographic mass explicitly. Due to the conformal anomaly, we are required to choose a representative to have a well-defined variational principle which breaks part of bulk diffeomorphism [113].

It is possible to obtain a particular representative by posing the boundary using an alternative gauge. Building in the work of Hubeny et al [108] and Cassani et al [85], we consider an alternative coordinate system which incorporates a new "holographic coordinate", z, that is normal to the boundary. In this framework, the metric can be expressed in terms of a radial ADM foliation, revealing crossed terms that are typically suppressed when writing the C-metric in the FG fashion [101, 111]. In fact, as noticed in [108], beyond the leading order in z, the ADM gauge differs from the FG one. Moreover, the first order of the expansion fully determines the variational principle as the conformal representative is fixed and therefore, the structure of the boundary stress tensor. We make the explicit computation for the case of the accelerating black hole pushed by a strut. Additionally, we formulated the holographic stress tensor using the fluid/gravity correspondence, wherein the dual CFT is interpreted as a perfect fluid with non-constant pressure on a curved background. This is in contrast to the four-dimensional case, which incorporates shears and corrections arising from the non-conformal flatness of the boundary metric.

Extending these results, we obtained the holographic mass for each class by integrating the energy density of the stress tensor. The zero acceleration limit leads to either the Casimir energy of global AdS_3 in the case of particle-like solutions or

the BTZ mass for the accelerating BTZ black holes.

Next, we computed the renormalised action by employing the standard counterterm prescription in AdS/CFT, as developed in [58, 59, 80]. We observed that the standard renormalised AdS_3 action contains an extra divergence. This is in fact an indication that the variational principle is not satisfied. Instead, it is necessary to include Gibbons–Hawking–York for each internal boundary produced when cutting the spacetime. After identifying the dynamics of each internal boundary, we re-expressed the boundary terms into a single contribution which corresponds to the Nambu–Goto action of the domain wall. Therefore, the total on-shell Euclidean action, including both the standard renormalised AdS_3 action and Nambu–Goto term, gives the correct quantum statistical relation. Geometrically, the domain wall extends from the black hole horizon to the boundary of the spacetime generating a divergence exactly at $z = 0$. Not only that, it provides an extra contribution at the black hole horizon which combined with the bulk action gives the black hole entropy. In a similar spirit to [134–136], the higher-codimension defect induces extra contributions into the partition function modifying the thermodynamics of the system under consideration.

We close this chapter by obtaining the holographic entanglement entropy of the system. Noting the relation between accelerating BTZ black holes and Rindler-AdS patch, we obtain the Ryu–Takayanagui surface in a simple manner and compute the holographic entanglement entropy on the dual CFT. We found that the well-known logarithmic divergence of the entanglement entropy in a conformal field theory holds in this context. However, we also discovered new subleading divergences that are proportional to the acceleration and possess a negative sign. In Chapter 4, we saw that the boundary of the spacetime is altered by the tension of the domain wall. A simple example is to consider the accelerating particle pulled by a domain wall shown in Figure 4.2 where it is clear that the access to the boundary depends on the size of the conical deficit. In fact, the behaviour of the entanglement is consistent with this interplay between acceleration and boundary for all classes of solutions: as the acceleration increases, a bigger portion of the AdS boundary is cut out and therefore, there is some information that is lost in the dual field theory as suggested by (5.51). This procedure is specific to three dimensions, as only massless four-dimensional accelerating solutions can be mapped to the Rindler patch highlighting that three dimensions offer a unique yet comprehensive setting for exploring holographic two-dimensional CFTs in the presence of acceleration.

In the future, an obvious step in understanding the three-dimensional C-metric is to establish a consistent thermodynamic description of the system. This entails studying the first law, Smarr relation, isoperimetric inequality [137] and the whole machinery of black hole thermodynamics. Given that we have obtained the quantum statistical relation, it seems very plausible to have a full Euclidean thermody-

namic prescription for accelerating black holes in 2+1 dimensions as it has been done for the four–dimensional counterpart in [101]. Additionally, it would be intriguing to investigate the role of acceleration in the dual theory using the extended first law developed in [106, 122]. This modified first law incorporates new chemical potentials that are conjugate to the cosmic string tension, potentially providing insights into the physical properties of these additional terms. Furthermore, recent work [138–140] has shown that the extended first law of black hole thermodynamics introduces a new chemical potential responsible for the change in the central charge of the dual CFT. However, the analysis in [140] assumes a conformally flat background, which is not satisfied by the four-dimensional C-metric. Thus, further investigations in this direction are necessary to explore the implications of the modified first law in the context of accelerating black holes and non-conformally flat backgrounds. Realising these topological solutions as truncations of supergravity solutions is also an open problem.

Another interesting direction that would shed light on the role of acceleration from the dual CFT perspective is to explore the hydrodynamic behaviour of the holographic stress tensor for four-dimensional accelerating black holes. While the stress tensor has been expressed within the framework of fluid/gravity correspondence [101], it remains unclear whether it possesses a valid hydrodynamic description that allows for the identification of associated transport coefficients. It would be interesting to see whether the acceleration plays a significant role in determining the transport coefficients and if they can be utilised to describe more realistic field theories. Additionally, an expansion regarding the fluid velocity and acceleration of the dual fluid stress tensor is still an open question. The three-dimensional case studied in this paper serves as a good starting point, as the solution is relatively simple yet rich enough to generate a stress tensor that exhibits non-constant pressure. This enriches the opportunities for studying more realistic systems through the scope of fluid/gravity correspondence.

Appendix **A**

Chern-Simons formulation of three-dimensional AdS gravity

Three-dimensional gravity can be formulated as a Chern-Simons gauge theory. To do so, we will consider the fundamental fields in the first-order formalism. We introduce the vielbein $e^a = e^a_\mu dx^\mu$ [†] defined by

$$g_{\mu\nu}(x) = e^a_\mu(x)\eta_{ab}e^b_\nu(x). \tag{A.1}$$

On the other hand, the spin connection is given as

$$\omega^a = \frac{1}{2}\epsilon^{abc}\omega_{\mu bc}dx^\mu. \tag{A.2}$$

The Lie group $\mathrm{SO}(2,2)$ is isomorphic to two copies of $\mathrm{SL}(2,\mathbb{R})$, i.e., $\mathrm{SO}(2,2) \simeq \mathrm{SL}(2,\mathbb{R})\oplus\mathrm{SL}(2,\mathbb{R})$. We introduce two gauge connections for each copy of $\mathrm{SL}(2,\mathbb{R})$, namely

$$A^a = \omega^a + \frac{1}{\ell}e^a, \quad \bar{A}^a = \omega^a - \frac{1}{\ell}e^a. \tag{A.3}$$

We also introduce the CS action for an arbitrary field A of a Lie group $\mathcal{G}$,

$$S_{CS} = \frac{k}{4\pi}\int_{\mathcal{M}} \langle A\wedge dA + \frac{2}{3}A\wedge A\wedge A\rangle \tag{A.4}$$

where $\langle\rangle$ stands for trace defined on the Lie group and k is the Chern-Simons level. It can be shown that the Einstein-Hilbert action (2.1) can be written as a sum of CS terms for each gauge field (A.3),

$$S_{EH} = S_{CS}(A) + S_{CS}(\bar{A}), \tag{A.5}$$

where the CS coupling k is identified to be proportional to the Newton's constant $k = \ell/4G$. The field equations shows that the connections $A^{(\pm)}$ are in fact flat, i.e.,

$$F = dA + A\wedge A = 0, \quad \bar{F} = d\bar{A} + \bar{A}\wedge\bar{A} = 0. \tag{A.6}$$

[†] $a, b = 0, 1, 2$ are indices in the tangent space.

which is consistent with the constant curvature condition 2.4. The CS formulation of gravity in 2+1 dimensions has several advantages due to its manifest gauge invariance* as this seems to play a crucial role in the understanding of physically renormalisable theories. Also, the possibility of including supersymmetry has been explored [141, 142].

*CS action (A.4) is invariant under a gauge transformation $A \to A + d\lambda$ up to a boundary term.

Appendix B

Classification of Solutions

Figure B.1 shows all of the possible distinct single-wall solutions constructable from Class I geometries. Figure B.1a shows the rapidly accelerating subclass $\mathrm{I}_{\mathrm{rapid}}$, with three possible single-wall solutions: A denotes a choice of $x_+ \in (-1, -y_h)$ with $y < 0$, for which there are no horizons. B denotes a choice of $x_+ \in (-y_h, 1)$ with $y < 0$, for which there is a single horizon. C denotes a choice of $x_+ \in (-y_h, 1)$ with $y > 0$. There are three similar solutions for $\mathrm{I}_{\mathrm{saturated}}$, shown in figure B.1b. D denotes a solution with $x_+ < 0$ and E one with $x_+ > 0$. Having chosen $x_+ > 0$, one may then construct single-wall solutions with either $y > 0$ or $y < 0$. Figure B.3a shows the unique single-wall solution which can be derived from Class II. Table B.4 gives a representation of all the possible single-wall solutions with $t > 0$.

Similarly, figures B.2 and B.3b show all of the possible qualitatively distinct single-strut solutions constructable from Class I and II geometries respectively. The letters A, B, C, and D in figures B.2a and B.2b denote choices of x_+ that determine whether the constructed solution has (for B and D), or does not have (for A and C), a horizon. Table B.5 gives a representation of all the possible single-strut solutions with $t > 0$.

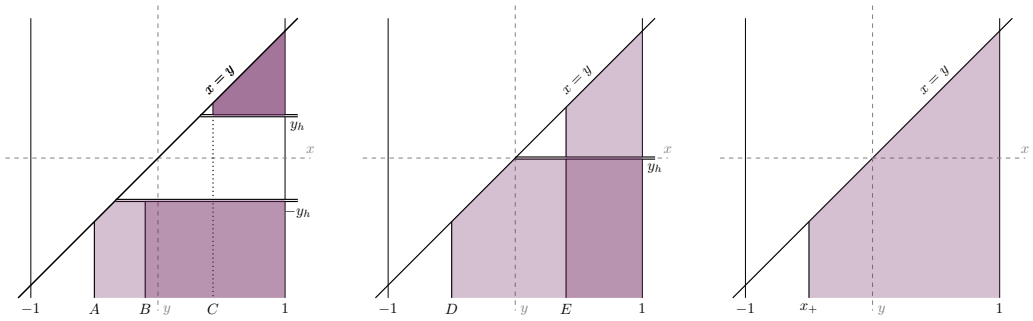

Figure B.1: Coordinate ranges for single-wall solutions constructed from metrics of Class I (with t timelike). Left: three qualitatively distinct solutions are shown for class $\mathrm{I}_{\mathrm{rapid}}$, Centre: three for class $\mathrm{I}_{\mathrm{saturated}}$, and Right: one for class $\mathrm{I}_{\mathrm{slow}}$.

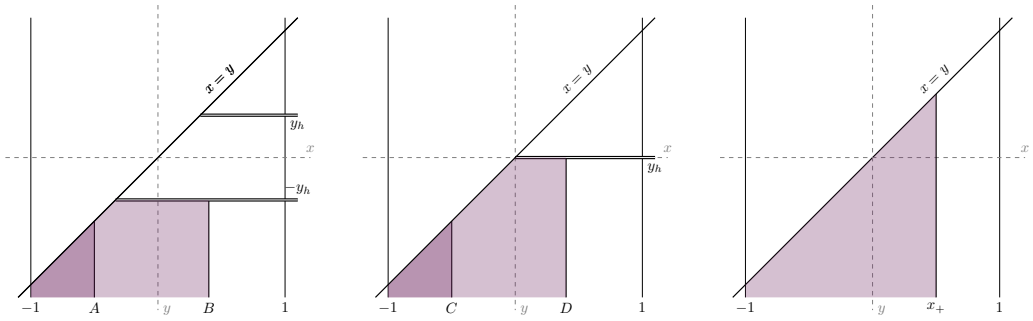

Figure B.2: Coordinate ranges for single-strut solutions constructed from metrics of Class I (with t timelike). Left: two qualitatively distinct solutions are shown for class $\mathrm{I}_{\mathrm{rapid}}$, Centre: two for class $\mathrm{I}_{\mathrm{saturated}}$, and Right: one for class $\mathrm{I}_{\mathrm{slow}}$.

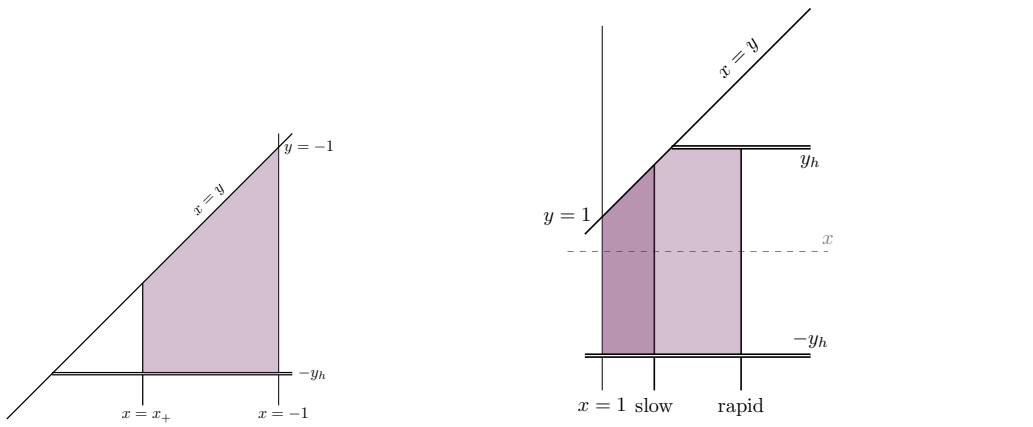

Figure B.3: Coordinate ranges for single-defect solutions constructed from metrics of Class II. Left: A wall solution for class $\mathrm{II}_{\mathrm{left}}$, and RIght: two qualitatively distinct strut solutions for class $\mathrm{II}_{\mathrm{right}}$.

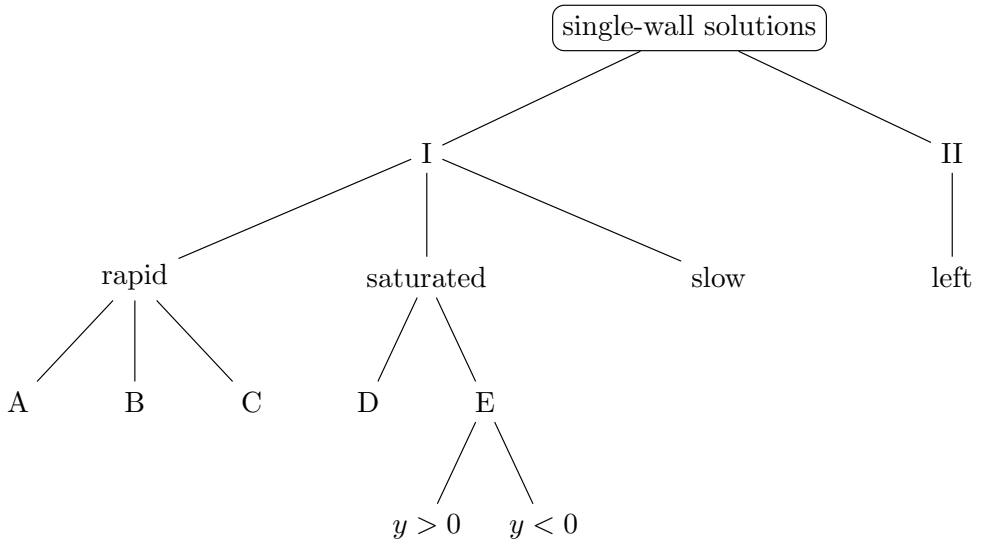

Figure B.4: Classification of distinct single-wall solutions with t timelike. Each leaf node represents a qualitatively-distinct solution.

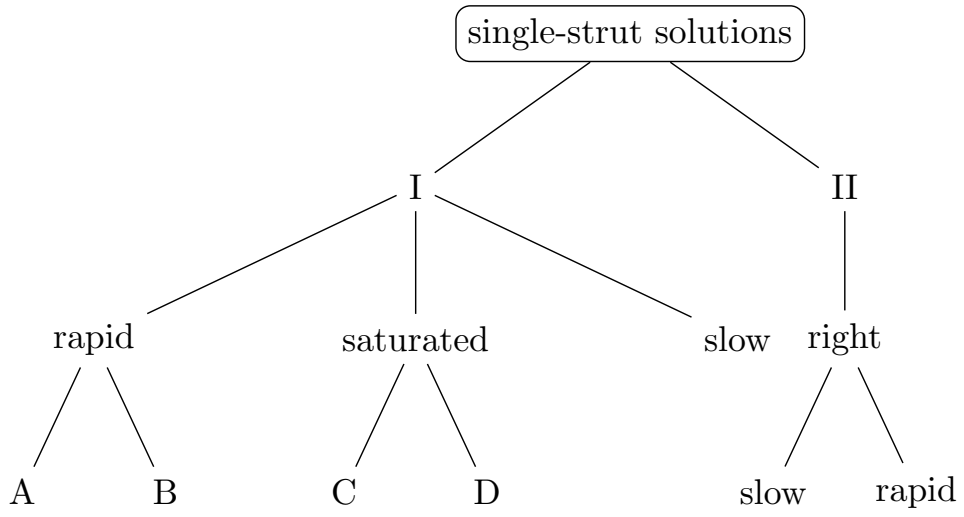

Figure B.5: Classification of distinct single-strut solutions with t timelike. Each leaf node represents a qualitatively-distinct solution.

Appendix C

Embedding coordinates to Global AdS_3

In this appendix, we collate mappings from the three-dimensional C-metric geometries to subsets of global AdS_3. These mappings were used to create the 3D embedding diagrams in the main text.

C.0.1 Global AdS_3

First, we define global AdS_3 by its embedding as a hyperboloid in $\mathbb{R}^{2,2}$. The embedding is

$$\begin{aligned} X_0 &= \ell\sqrt{1+\frac{R^2}{\ell^2}}\sin\left(\frac{T}{\ell}\right), \quad X_1 = R\sin\Theta\,, \\ X_3 &= \ell\sqrt{1+\frac{R^2}{\ell^2}}\cos\left(\frac{T}{\ell}\right), \quad X_2 = R\cos\Theta\,. \end{aligned} \tag{C.1}$$

The hyperboloid is

$$\sum_{i=0}^{3}\eta_{ii}X_i^2 = -\ell^2\,, \tag{C.2}$$

with induced metric

$$\sum_{i=0}^{3}\eta_{ii}dX_i^2 = -\left(1+\frac{R^2}{\ell^2}\right)dT^2 + \frac{dR^2}{\left(1+\frac{R^2}{\ell^2}\right)} + R^2d\Theta^2\,. \tag{C.3}$$

Note in the above two sums that η has the signature $(-++-)$. The coordinates lie in the ranges $R\in(0,\infty)$, $\Theta\in(-\pi,\pi)$, and T can be taken in the full range of $\mathbb{R}$, with a primary domain of $T\in[-\pi\ell/2, 3\pi\ell/2]$ (chosen for later convenience).

Conversely, the global coordinates are defined from the embedding coordinates by

$$\begin{aligned} T_G &= \arctan\left(\frac{X_0}{X_3}\right), \quad R_G = \sqrt{X_1^2+X_2^2}\,, \\ X_G &= X_1\,, \qquad\qquad Y_G = X_2\,. \end{aligned} \tag{C.4}$$

We may then compactify the spatial two-section to attain the Poincaré disk:

$$\hat{X} = \frac{X_G}{\ell + \sqrt{\ell^2 + X_G^2 + Y_G^2}}\,, \qquad \hat{Y} = \frac{Y_G}{\ell + \sqrt{\ell^2 + X_G^2 + Y_G^2}}\,. \tag{C.5}$$

The global space then appears as a cylinder in $(T_G, \hat{X}, \hat{Y})$ coordinates. This cylinder is defined by $|T_G| < \pi/2$, $\hat{X}^2 + \hat{Y}^2 < 1$. Note that this covers only half of the embedding hyperboloid, as for $T \in [-\pi\ell/2, \pi\ell/2]$ we have $X_3 > 0$.

Given some metric ds_3^2, by finding a set of embedding coordinates X_i such that

$$\sum_{i=0}^{3} \eta_{ii} X_i^2 = -\ell^2\,, \tag{C.6}$$

and

$$\sum_{i=0}^{3} \eta_{ii} dX_i^2 = ds_3^2\,, \tag{C.7}$$

one may plot the geometry as a subset of the global cylinder by applying the transformations (C.4) and (C.5).

C.0.2 The Rindler wedge and the static BTZ black hole

For the non-rotating BTZ geometry,

$$ds_3^2 = -\left(-m^2 + \frac{r^2}{\ell^2}\right) dt^2 + \frac{dr^2}{\left(-m^2 + \frac{r^2}{\ell^2}\right)} + r^2 d\phi^2\,, \tag{C.8}$$

the embedding is well known [21]:

$$\begin{aligned} X_0 &= \mathcal{B}(r) \sinh\left(\frac{r_h t}{\ell^2}\right)\,, \quad X_1 = \mathcal{A}(r) \sinh\left(\frac{r_h \phi}{\ell}\right)\,, \\ X_3 &= \mathcal{A}(r) \cosh\left(\frac{r_h \phi}{\ell}\right)\,, \quad X_2 = \mathcal{B}(r) \cosh\left(\frac{r_h t}{\ell^2}\right)\,, \end{aligned} \tag{C.9}$$

where

$$\mathcal{A}(r) = \ell \frac{r}{r_h}\,, \qquad \mathcal{B}(r) = \ell \sqrt{\left(\frac{r}{r_h}\right)^2 - 1}\,, \tag{C.10}$$

with

$$r_h = m\ell\,. \tag{C.11}$$

If ϕ is taken to be non-compact, then we have a portion of AdS_3 bounded by a bifurcate acceleration horizon and the conformal boundary [21]. This geometry is the *planar BTZ geometry* or *Rindler wedge*. In this case m is a gauge parameter which may be set to unity by a rescaling of both r and ϕ. Alternatively, one may identify $\phi \to \phi + 2\pi$ to attain the static BTZ black hole [20]. We plot both geometries as subsets of global AdS_3 using the technique described above in figure C.1.

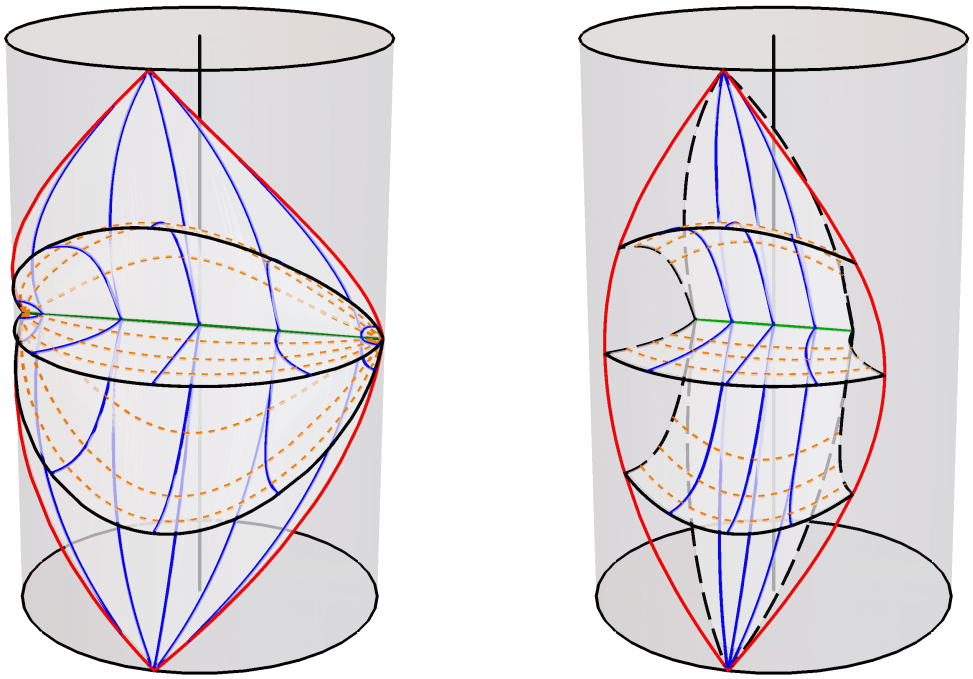

Figure C.1: The planar and compact (static) BTZ black holes. Lines of constant ϕ are shown in blue, with lines of constant r in dashed orange. Several surfaces of constant time t are shown. The classically accessible subset of the boundary is bounded in red. To guide the eye, the locus of the cylinder is shown in solid black. (a): $\phi \in \mathbb{R}$, giving the planar BTZ geometry or "Rindler wedge". The bifurcation surface (green) has topology $\mathbb{R}$. (b): ϕ identified with period 2π, giving the BTZ black hole. Lines of constant t and $\phi = \pm\pi$ are plotted in long-dashed black, pairs of which are identified across the same time-slice. The bifurcation surface (green) has topology S^1.

C.0.3 Class I solutions

The Class I geometry is given by

$$ds_3^2 = \frac{1}{\Omega^2}\left[-P d\tau^2 + \frac{dy^2}{P} + \frac{dx^2}{Q}\right], \tag{C.12}$$

where

$$Q = 1 - x^2\,, \qquad \Omega = A(x-y)\,. \tag{C.13}$$

In the slowly accelerating phase, $A^2\ell^2 < 1$ and the lapse function is given by

$$P = y^2 + S^2\,, \qquad S = \sqrt{\frac{1}{A^2\ell^2} - 1}\,. \tag{C.14}$$

The embedding is then

$$\begin{aligned} X_0 &= \frac{\sqrt{P}}{S\Omega}\sin S\tau\,, \quad X_1 = \frac{\sqrt{Q}}{\Omega}\,, \\ X_3 &= \frac{\sqrt{P}}{S\Omega}\cos S\tau\,, \quad X_2 = \frac{A\ell}{\Omega}\left(Sx + \frac{y}{S}\right). \end{aligned} \tag{C.15}$$

In the rapid phase, $A^2\ell^2 > 1$, so the lapse function now has roots:

$$P = y^2 - y_h^2\,, \qquad y_h = \sqrt{1 - \frac{1}{A^2\ell^2}}\,. \tag{C.16}$$

We thus require the alternative embedding

$$\begin{aligned} X_0 &= \frac{\sqrt{P}}{y_h\Omega}\sinh y_h\tau\,, \qquad X_1 = \frac{\sqrt{Q}}{\Omega}\,, \\ X_3 &= \frac{A\ell}{\Omega}\left|y_h x - \frac{y}{y_h}\right|\,, \quad X_2 = \frac{\sqrt{P}}{y_h\Omega}\cosh y_h\tau\,. \end{aligned} \tag{C.17}$$

C.0.4 Class II solutions

The Class II geometry is given by

$$ds_3^2 = \frac{1}{\Omega^2}\left[-Pd\tau^2 + \frac{dy^2}{P} + \frac{dx^2}{Q}\right]\,, \tag{C.18}$$

with metric functions

$$P = -y^2 + y_h^2\,, \qquad Q = x^2 - 1\,, \qquad \Omega = A(x-y)\,, \tag{C.19}$$

where

$$y_h = \sqrt{1 + \frac{1}{A^2\ell^2}}\,. \tag{C.20}$$

The embedding in the region where P is positive is then

$$\begin{aligned} X_0 &= \frac{\sqrt{P}}{y_h\Omega}\sinh y_h\tau\,, \qquad X_1 = \frac{\sqrt{Q}}{\Omega}\,, \\ X_3 &= \frac{A\ell}{\Omega}\left(y_h x - \frac{y}{y_h}\right)\,, \quad X_2 = \frac{\sqrt{P}}{y_h\Omega}\cosh y_h\tau\,. \end{aligned} \tag{C.21}$$

C.0.5 Class III solutions

For the Class III solution of section 4.5, the line element is

$$ds_3^2 = \frac{1}{\Omega^2}\left[-Pd\tau^2 + \frac{dy^2}{P} + \frac{dx^2}{Q}\right]\,. \tag{C.22}$$

The metric functions are

$$P = -y^2 + y_h^2\,, \qquad Q = 1 + x^2\,, \qquad \Omega = A(x-y)\,, \tag{C.23}$$

where

$$y_h = \sqrt{\frac{1}{A^2\ell^2} - 1}\,. \tag{C.24}$$

The embedding for $|y| < y_h$ is then

$$\begin{aligned} X_0 &= \frac{\sqrt{P}}{y_h\Omega}\sinh y_h\tau\,, \quad X_1 = \frac{A\ell}{\Omega}\left(y_h x + \frac{y}{y_h}\right)\,, \\ X_3 &= \frac{\sqrt{Q}}{\Omega}\,, \qquad\qquad\quad X_2 = \frac{\sqrt{P}}{y_h\Omega}\cosh y_h\tau\,. \end{aligned} \tag{C.25}$$

Bibliography

[1] Gabriel Arenas-Henriquez, Ruth Gregory, and Andrew Scoins. "On acceleration in three dimensions". In: *JHEP* 05 (2022), p. 063. arXiv: 2202.08823 [hep-th].

[2] Gabriel Arenas-Henriquez, Adolfo Cisterna, Felipe Diaz, and Ruth Gregory. "Accelerating Black Holes in $2+1$ dimensions: Holography revisited". In: (2023). arXiv: 2308.00613 [hep-th].

[3] Gabriel Arenas-Henriquez, Felipe Diaz, and Per Sundell. "Logarithmic corrections, entanglement entropy, and UV cutoffs in de Sitter spacetime". In: *JHEP* 08 (2022), p. 261. arXiv: 2206.10427 [hep-th].

[4] Gabriel Arenas-Henriquez, Felipe Diaz, and Yerko Novoa. "Thermal fluctuations of black holes with non-linear electrodynamics and charged Renyi entropy". In: *JHEP* 05 (2023), p. 072. arXiv: 2211.06355 [hep-th].

[5] Jacob D. Bekenstein. "Black holes and entropy". In: *Phys. Rev. D* 7 (1973), pp. 2333–2346.

[6] James M. Bardeen, B. Carter, and S.W. Hawking. "The Four laws of black hole mechanics". In: *Commun. Math. Phys.* 31 (1973), pp. 161–170.

[7] S.W. Hawking. "Particle Creation by Black Holes". In: *Commun. Math. Phys.* 43 (1975). Ed. by G.W. Gibbons and S.W. Hawking. [Erratum: Commun.Math.Phys. 46, 206 (1976)], pp. 199–220.

[8] S.W. Hawking. "Black Holes and Thermodynamics". In: *Phys. Rev. D* 13 (1976), pp. 191–197.

[9] G. W. Gibbons and S. W. Hawking. "Action integrals and partition functions in quantum gravity". In: *Phys. Rev. D* 15 (10 May 1977), pp. 2752–2756.

[10] S.W. Hawking and Don N. Page. "Thermodynamics of Black Holes in anti-De Sitter Space". In: *Commun. Math. Phys.* 87 (1983), p. 577.

[11] Andrew Strominger and Cumrun Vafa. "Microscopic origin of the Bekenstein-Hawking entropy". In: *Phys. Lett. B* 379 (1996), pp. 99–104. arXiv: `hep-th/9601029`.

[12] Gerard 't Hooft. "Dimensional reduction in quantum gravity". In: *Conf. Proc. C* 930308 (1993), pp. 284–296. arXiv: `gr-qc/9310026`.

[13] Leonard Susskind. "The World as a hologram". In: *J. Math. Phys.* 36 (1995), pp. 6377–6396. arXiv: `hep-th/9409089`.

[14] Juan Martin Maldacena. "The Large N limit of superconformal field theories and supergravity". In: *Int. J. Theor. Phys.* 38 (1999), pp. 1113–1133. arXiv: `hep-th/9711200`.

[15] Edward Witten. "Anti-de Sitter space and holography". In: *Adv. Theor. Math. Phys.* 2 (1998), pp. 253–291. arXiv: `hep-th/9802150`.

[16] Edward Witten. "(2+1)-Dimensional Gravity as an Exactly Soluble System". In: *Nucl. Phys. B* 311 (1988), p. 46.

[17] Stanley Deser, R. Jackiw, and Gerard 't Hooft. "Three-Dimensional Einstein Gravity: Dynamics of Flat Space". In: *Annals Phys.* 152 (1984), p. 220.

[18] Stanley Deser and R. Jackiw. "Three-Dimensional Cosmological Gravity: Dynamics of Constant Curvature". In: *Annals Phys.* 153 (1984), pp. 405–416.

[19] R. Jackiw. "Lower Dimensional Gravity". In: *Nucl. Phys. B* 252 (1985). Ed. by R. Baier and H. Satz, pp. 343–356.

[20] Maximo Banados, Claudio Teitelboim, and Jorge Zanelli. "The Black hole in three-dimensional space-time". In: *Phys. Rev. Lett.* 69 (1992), pp. 1849–1851. arXiv: `hep-th/9204099`.

[21] Maximo Banados, Marc Henneaux, Claudio Teitelboim, and Jorge Zanelli. "Geometry of the (2+1) black hole". In: *Phys. Rev. D* 48 (1993). [Erratum: Phys.Rev.D 88, 069902 (2013)], pp. 1506–1525. arXiv: `gr-qc/9302012`.

[22] Steven Carlip. "The Statistical mechanics of the (2+1)-dimensional black hole". In: *Phys. Rev. D* 51 (1995), pp. 632–637. arXiv: `gr-qc/9409052`.

[23] Steven Carlip. "The (2+1)-Dimensional black hole". In: *Class. Quant. Grav.* 12 (1995), pp. 2853–2880. arXiv: `gr-qc/9506079`.

[24] Ofer Aharony, Steven S. Gubser, Juan Martin Maldacena, Hirosi Ooguri, and Yaron Oz. "Large N field theories, string theory and gravity". In: *Phys. Rept.* 323 (2000), pp. 183–386. arXiv: `hep-th/9905111`.

[25] G. Policastro, Dan T. Son, and Andrei O. Starinets. "The Shear viscosity of strongly coupled N=4 supersymmetric Yang-Mills plasma". In: *Phys. Rev. Lett.* 87 (2001), p. 081601. arXiv: `hep-th/0104066`.

[26] Andreas Karch and Emanuel Katz. "Adding flavor to AdS / CFT". In: *JHEP* 06 (2002), p. 043. arXiv: hep-th/0205236.

[27] Tadakatsu Sakai and Shigeki Sugimoto. "Low energy hadron physics in holographic QCD". In: *Prog. Theor. Phys.* 113 (2005), pp. 843–882. arXiv: hep-th/0412141.

[28] P. Kovtun, Dan T. Son, and Andrei O. Starinets. "Viscosity in strongly interacting quantum field theories from black hole physics". In: *Phys. Rev. Lett.* 94 (2005), p. 111601. arXiv: hep-th/0405231.

[29] Shinsei Ryu and Tadashi Takayanagi. "Holographic derivation of entanglement entropy from AdS/CFT". In: *Phys. Rev. Lett.* 96 (2006), p. 181602. arXiv: hep-th/0603001.

[30] Veronika E. Hubeny, Mukund Rangamani, and Tadashi Takayanagi. "A Covariant holographic entanglement entropy proposal". In: *JHEP* 07 (2007), p. 062. arXiv: 0705.0016 [hep-th].

[31] Steven S. Gubser. "Breaking an Abelian gauge symmetry near a black hole horizon". In: *Phys. Rev. D* 78 (2008), p. 065034. arXiv: 0801.2977 [hep-th].

[32] Sean A. Hartnoll, Christopher P. Herzog, and Gary T. Horowitz. "Building a Holographic Superconductor". In: *Phys. Rev. Lett.* 101 (2008), p. 031601. arXiv: 0803.3295 [hep-th].

[33] Jerome P. Gauntlett, Julian Sonner, and Toby Wiseman. "Holographic superconductivity in M-Theory". In: *Phys. Rev. Lett.* 103 (2009), p. 151601. arXiv: 0907.3796 [hep-th].

[34] Christos Charmousis, Blaise Gouteraux, Bom Soo Kim, Elias Kiritsis, and Rene Meyer. "Effective Holographic Theories for low-temperature condensed matter systems". In: *JHEP* 11 (2010), p. 151. arXiv: 1005.4690 [hep-th].

[35] Horacio Casini, Marina Huerta, and Robert C. Myers. "Towards a derivation of holographic entanglement entropy". In: *JHEP* 05 (2011), p. 036. arXiv: 1102.0440 [hep-th].

[36] Stephen H. Shenker and Douglas Stanford. "Black holes and the butterfly effect". In: *JHEP* 03 (2014), p. 067. arXiv: 1306.0622 [hep-th].

[37] Aristomenis Donos and Jerome P. Gauntlett. "Thermoelectric DC conductivities from black hole horizons". In: *JHEP* 11 (2014), p. 081. arXiv: 1406.4742 [hep-th].

[38] Juan Maldacena and Douglas Stanford. "Remarks on the Sachdev-Ye-Kitaev model". In: *Phys. Rev. D* 94.10 (2016), p. 106002. arXiv: 1604.07818 [hep-th].

[39] Geoff Penington, Stephen H. Shenker, Douglas Stanford, and Zhenbin Yang. "Replica wormholes and the black hole interior". In: *JHEP* 03 (2022), p. 205. arXiv: 1911.11977 [hep-th].

[40] Ahmed Almheiri, Thomas Hartman, Juan Maldacena, Edgar Shaghoulian, and Amirhossein Tajdini. "Replica Wormholes and the Entropy of Hawking Radiation". In: *JHEP* 05 (2020), p. 013. arXiv: 1911.12333 [hep-th].

[41] A Ashtekar and A Magnon. "Asymptotically anti-de Sitter space-times". In: *Classical and Quantum Gravity* 1.4 (July 1984), pp. L39–L44.

[42] M. Henneaux and C. Teitelboim. "The Cosmological Constant as a Canonical Variable". In: *Phys. Lett. B* 143 (1984), pp. 415–420.

[43] M. Henneaux and C. Teitelboim. "Asymptotically anti-De Sitter Spaces". In: *Commun. Math. Phys.* 98 (1985), pp. 391–424.

[44] A. Achucarro and P.K. Townsend. "A Chern-Simons Action for Three-Dimensional anti-De Sitter Supergravity Theories". In: *Phys. Lett. B* 180 (1986). Ed. by A. Salam and E. Sezgin, p. 89.

[45] Edward Witten. "Three-Dimensional Gravity Revisited". In: (June 2007). arXiv: 0706.3359 [hep-th].

[46] J.David Brown, J. Creighton, and Robert B. Mann. "Temperature, energy and heat capacity of asymptotically anti-de Sitter black holes". In: *Phys. Rev. D* 50 (1994), pp. 6394–6403. arXiv: gr-qc/9405007.

[47] Maximo Banados. "Global charges in Chern-Simons field theory and the (2+1) black hole". In: *Phys. Rev. D* 52 (1996), pp. 5816–5825. arXiv: hep-th/9405171.

[48] David Kastor, Sourya Ray, and Jennie Traschen. "Enthalpy and the Mechanics of AdS Black Holes". In: *Class. Quant. Grav.* 26 (2009), p. 195011. arXiv: 0904.2765 [hep-th].

[49] David Kubiznak and Robert B. Mann. "Black hole chemistry". In: *Can. J. Phys.* 93.9 (2015). Ed. by Arundhati Dasgupta, pp. 999–1002. arXiv: 1404.2126 [gr-qc].

[50] David Kubiznak, Robert B. Mann, and Mae Teo. "Black hole chemistry: thermodynamics with Lambda". In: *Class. Quant. Grav.* 34.6 (2017), p. 063001. arXiv: 1608.06147 [hep-th].

[51] J.David Brown and M. Henneaux. "Central Charges in the Canonical Realization of Asymptotic Symmetries: An Example from Three-Dimensional Gravity". In: *Commun. Math. Phys.* 104 (1986), pp. 207–226.

[52] Maximo Banados. "Three-dimensional quantum geometry and black holes". In: *AIP Conf. Proc.* 484.1 (1999). Ed. by H. Falomir, R.E. Gamboa Saravi, and F.A. Schaposnik, pp. 147–169. arXiv: hep-th/9901148.

[53] D. Cangemi, M. Leblanc, and Robert B. Mann. "Gauge formulation of the spinning black hole in (2+1)-dimensional anti-De Sitter space". In: *Phys. Rev. D* 48 (1993), pp. 3606–3610. arXiv: gr-qc/9211013.

[54] Seungjoon Hyun, Won Tae Kim, and Julian Lee. "Statistical entropy and AdS / CFT correspondence in BTZ black holes". In: *Phys. Rev. D* 59 (1999), p. 084020. arXiv: hep-th/9811005.

[55] Vijay Balasubramanian and Per Kraus. "A Stress tensor for Anti-de Sitter gravity". In: *Commun. Math. Phys.* 208 (1999), pp. 413–428. arXiv: hep-th/9902121.

[56] Gerard 't Hooft. "A Planar Diagram Theory for Strong Interactions". In: *Nucl. Phys. B* 72 (1974). Ed. by J. C. Taylor, p. 461.

[57] S.S. Gubser, Igor R. Klebanov, and Alexander M. Polyakov. "Gauge theory correlators from noncritical string theory". In: *Phys. Lett. B* 428 (1998), pp. 105–114. arXiv: hep-th/9802109.

[58] M. Henningson and K. Skenderis. "The Holographic Weyl anomaly". In: *JHEP* 07 (1998), p. 023. arXiv: hep-th/9806087.

[59] Sebastian de Haro, Sergey N. Solodukhin, and Kostas Skenderis. "Holographic reconstruction of space-time and renormalization in the AdS / CFT correspondence". In: *Commun. Math. Phys.* 217 (2001), pp. 595–622. arXiv: hep-th/0002230.

[60] Kostas Skenderis. "Asymptotically Anti-de Sitter space-times and their stress energy tensor". In: *Int. J. Mod. Phys. A* 16 (2001). Ed. by A. Semikhatov, M. Vasilev, and V. Zaikin, pp. 740–749. arXiv: hep-th/0010138.

[61] Massimo Bianchi, Daniel Z. Freedman, and Kostas Skenderis. "Holographic renormalization". In: *Nucl. Phys. B* 631 (2002), pp. 159–194. arXiv: hep-th/0112119.

[62] James W. York. "Role of Conformal Three-Geometry in the Dynamics of Gravitation". In: *Phys. Rev. Lett.* 28 (16 Apr. 1972), pp. 1082–1085.

[63] G. W. Gibbons and S. W. Hawking. "Action Integrals and Partition Functions in Quantum Gravity". In: *Phys. Rev. D* 15 (1977), pp. 2752–2756.

[64] Charles Fefferman and C. Robin Graham. *The ambient metric*. 2008. arXiv: 0710.0919 [math.DG].

[65] J.David Brown and Jr. York James W. "Quasilocal energy and conserved charges derived from the gravitational action". In: *Phys. Rev. D* 47 (1993), pp. 1407–1419. arXiv: gr-qc/9209012.

[66] T. Levi-Civita. "ds^2 einsteiniani in campi newtoniani. I". In: *Rend. Accad. Lincei* 27 (6 1918), pp. 220–229.

[67] H. Weyl. "Bemerkung über die statischen kugelsymmetrischen Lösungen von Einsteins "kosmologischen" Gravitationsgleichungen". In: *Phys. Z.* 20 (1919), pp. 31–34.

[68] William Kinnersley and Martin Walker. "Uniformly Accelerating Charged Mass in General Relativity". In: *Phys. Rev. D* 2 (8 Oct. 1970), pp. 1359–1370.

[69] William B. Bonnor. "The sources of the vacuum C-metric". In: *General Relativity and Gravitation* 15 (1983), pp. 535–551.

[70] J. F. Plebanski and M. Demianski. "Rotating, charged, and uniformly accelerating mass in general relativity". In: *Annals Phys.* 98 (1976), pp. 98–127.

[71] Patricio S. Letelier and Samuel R. Oliveira. "On uniformly accelerated black holes". In: *Phys. Rev. D* 64 (2001), p. 064005. arXiv: `gr-qc/9809089`.

[72] J. Bicak and Vojtech Pravda. "Spinning C metric: Radiative space-time with accelerating, rotating black holes". In: *Phys. Rev. D* 60 (1999), p. 044004. arXiv: `gr-qc/9902075`.

[73] Jiri Podolsky and J. B. Griffiths. "Null limits of the C metric". In: *Gen. Rel. Grav.* 33 (2001), pp. 59–64. arXiv: `gr-qc/0006093`.

[74] Vojtech Pravda and A. Pravdova. "Coaccelerated particles in the C metric". In: *Class. Quant. Grav.* 18 (2001), pp. 1205–1216. arXiv: `gr-qc/0010051`.

[75] Oscar J.C. Dias and Jose P.S. Lemos. "Pair of accelerated black holes in anti-de Sitter background: AdS C metric". In: *Phys. Rev. D* 67 (2003), p. 064001. arXiv: `hep-th/0210065`.

[76] J.B. Griffiths and J. Podolsky. "A New look at the Plebanski-Demianski family of solutions". In: *Int. J. Mod. Phys. D* 15 (2006), pp. 335–370. arXiv: `gr-qc/0511091`.

[77] Pavel Krtous. "Accelerated black holes in an anti-de Sitter universe". In: *Phys. Rev. D* 72 (2005), p. 124019. arXiv: `gr-qc/0510101`.

[78] Fay Dowker, Jerome P. Gauntlett, David A. Kastor, and Jennie H. Traschen. "Pair creation of dilaton black holes". In: *Phys. Rev. D* 49 (1994), pp. 2909–2917. arXiv: `hep-th/9309075`.

[79] Roberto Emparan, Gary T. Horowitz, and Robert C. Myers. "Exact description of black holes on branes". In: *JHEP* 01 (2000), p. 007. arXiv: `hep-th/9911043`.

[80] Roberto Emparan, Gary T. Horowitz, and Robert C. Myers. "Exact description of black holes on branes. 2. Comparison with BTZ black holes and black strings". In: *JHEP* 01 (2000), p. 021. arXiv: `hep-th/9912135`.

[81] Roberto Emparan, Ruth Gregory, and Caroline Santos. "Black holes on thick branes". In: *Phys. Rev. D* 63 (2001), p. 104022. arXiv: `hep-th/0012100`.

[82] Ruth Gregory, Simon F. Ross, and Robin Zegers. "Classical and quantum gravity of brane black holes". In: *JHEP* 09 (2008), p. 029. arXiv: `0802.2037 [hep-th]`.

[83] H. Lü and Justin F. Vázquez-Poritz. "C-metrics in Gauged STU Supergravity and Beyond". In: *JHEP* 12 (2014), p. 057. arXiv: `1408.6531 [hep-th]`.

[84] Pietro Ferrero, Jerome P. Gauntlett, Juan Manuel Pérez Ipiña, Dario Martelli, and James Sparks. "Accelerating black holes and spinning spindles". In: *Phys. Rev. D* 104.4 (2021), p. 046007. arXiv: `2012.08530 [hep-th]`.

[85] Davide Cassani, Jerome P. Gauntlett, Dario Martelli, and James Sparks. "Thermodynamics of accelerating and supersymmetric AdS4 black holes". In: *Phys. Rev. D* 104.8 (2021), p. 086005. arXiv: `2106.05571 [hep-th]`.

[86] Pietro Ferrero, Matteo Inglese, Dario Martelli, and James Sparks. "Multicharge accelerating black holes and spinning spindles". In: *Phys. Rev. D* 105.12 (2022), p. 126001. arXiv: `2109.14625 [hep-th]`.

[87] Jiri Podolsky. "Accelerating black holes in anti-de Sitter universe". In: *Czech. J. Phys.* 52 (2002), pp. 1–10. arXiv: `gr-qc/0202033`.

[88] Don N. Page. "Taub - Nut Instanton With an Horizon". In: *Phys. Lett. B* 78 (1978), pp. 249–251.

[89] S. W. Hawking, C. J. Hunter, and Don N. Page. "Nut charge, anti-de Sitter space and entropy". In: *Phys. Rev. D* 59 (1999), p. 044033. arXiv: `hep-th/9809035`.

[90] Robert B. Mann. "Misner string entropy". In: *Phys. Rev. D* 60 (1999), p. 104047. arXiv: `hep-th/9903229`.

[91] Kenneth Hong and Edward Teo. "A New form of the C metric". In: *Class. Quant. Grav.* 20 (2003), pp. 3269–3277. arXiv: `gr-qc/0305089`.

[92] J. Bicak and B. Schmidt. "Asymptotically flat radiative space-times with boost-rotation symmetry: The general structure". In: *Phys. Rev. D* 40 (6 Sept. 1989), pp. 1827–1853.

[93] Mukunda Aryal, L. H. Ford, and Alexander Vilenkin. "Cosmic strings and black holes". In: *Phys. Rev. D* 34 (8 Oct. 1986), pp. 2263–2266.

[94] Ruth Gregory and Mark Hindmarsh. "Smooth metrics for snapping strings". In: *Phys. Rev. D* 52 (1995), pp. 5598–5605. arXiv: `gr-qc/9506054`.

[95] Richard L. Arnowitt, Stanley Deser, and Charles W. Misner. "Dynamical Structure and Definition of Energy in General Relativity". In: *Phys. Rev.* 116 (1959), pp. 1322–1330.

[96] Vivek Iyer and Robert M. Wald. "Some properties of Noether charge and a proposal for dynamical black hole entropy". In: *Phys. Rev. D* 50 (1994), pp. 846–864. arXiv: gr-qc/9403028.

[97] Stefan Hollands, Akihiro Ishibashi, and Donald Marolf. "Comparison between various notions of conserved charges in asymptotically AdS-spacetimes". In: *Class. Quant. Grav.* 22 (2005), pp. 2881–2920. arXiv: hep-th/0503045.

[98] Abhay Ashtekar and Saurya Das. "Asymptotically Anti-de Sitter spacetimes: Conserved quantities". In: *Class. Quant. Grav.* 17 (2000), pp. L17–L30. arXiv: hep-th/9911230.

[99] Dileep P. Jatkar, Georgios Kofinas, Olivera Miskovic, and Rodrigo Olea. "Conformal Mass in AdS gravity". In: *Phys. Rev. D* 89.12 (2014), p. 124010. arXiv: 1404.1411 [hep-th].

[100] Gabriel Arenas-Henriquez, Olivera Miskovic, and Rodrigo Olea. "Vacuum Degeneracy and Conformal Mass in Lovelock AdS Gravity". In: *JHEP* 11 (2017), p. 128. arXiv: 1710.08512 [hep-th].

[101] Andrés Anabalón et al. "Holographic Thermodynamics of Accelerating Black Holes". In: *Phys. Rev.* D98.10 (2018), p. 104038. arXiv: 1805.02687 [hep-th].

[102] Glenn Barnich and Friedemann Brandt. "Covariant theory of asymptotic symmetries, conservation laws and central charges". In: *Nucl. Phys. B* 633 (2002), pp. 3–82. arXiv: hep-th/0111246.

[103] P. Mora, R. Olea, R. Troncoso, and J. Zanelli. "Finite action principle for Chern-Simons AdS gravity". In: *JHEP* 06 (2004), p. 036. arXiv: hep-th/0405267.

[104] Olivera Miskovic and Rodrigo Olea. "On boundary conditions in three-dimensional AdS gravity". In: *Phys. Lett. B* 640 (2006), pp. 101–107. arXiv: hep-th/0603092.

[105] Michael Appels, Ruth Gregory, and David Kubiznak. "Thermodynamics of Accelerating Black Holes". In: *Phys. Rev. Lett.* 117.13 (2016), p. 131303. arXiv: 1604.08812 [hep-th].

[106] Michael Appels, Ruth Gregory, and David Kubiznak. "Black Hole Thermodynamics with Conical Defects". In: *JHEP* 05 (2017), p. 116. arXiv: 1702.00490 [hep-th].

[107] Ruth Gregory. "Accelerating Black Holes". In: *J. Phys. Conf. Ser.* 942.1 (2017), p. 012002. arXiv: 1712.04992 [hep-th].

[108] Veronika E. Hubeny, Donald Marolf, and Mukund Rangamani. "Black funnels and droplets from the AdS C-metrics". In: *Class. Quant. Grav.* 27 (2010), p. 025001. arXiv: 0909.0005 [hep-th].

[109] Giorgos Anastasiou, Ignacio J. Araya, and Rodrigo Olea. "Energy functionals from Conformal Gravity". In: *JHEP* 10 (2022), p. 123. arXiv: 2209.02006 [hep-th].

[110] Giorgos Anastasiou, Ignacio J. Araya, Mairym Busnego-Barrientos, Cristobal Corral, and Nelson Merino. "Conformal renormalization of scalar-tensor theories". In: (Dec. 2022). arXiv: 2212.04364 [hep-th].

[111] Andrés Anabalón, Finnian Gray, Ruth Gregory, David Kubizňák, and Robert B. Mann. "Thermodynamics of Charged, Rotating, and Accelerating Black Holes". In: *JHEP* 04 (2019), p. 096. arXiv: 1811.04936 [hep-th].

[112] Mukund Rangamani. "Gravity and Hydrodynamics: Lectures on the fluid-gravity correspondence". In: *Class. Quant. Grav.* 26 (2009). Ed. by A. M. Uranga, p. 224003. arXiv: 0905.4352 [hep-th].

[113] Ioannis Papadimitriou and Kostas Skenderis. "AdS / CFT correspondence and geometry". In: *IRMA Lect. Math. Theor. Phys.* 8 (2005). Ed. by O. Biquard, pp. 73–101. arXiv: hep-th/0404176.

[114] Alexander Maloney and Edward Witten. "Quantum Gravity Partition Functions in Three Dimensions". In: *JHEP* 02 (2010), p. 029. arXiv: 0712.0155 [hep-th].

[115] Mohamed M. Anber. "AdS(4) / CFT(3) + Gravity for Accelerating Conical Singularities". In: *JHEP* 11 (2008), p. 026. arXiv: 0809.2789 [hep-th].

[116] W. Israel. "Singular hypersurfaces and thin shells in general relativity". In: *Nuovo Cim. B* 44S10 (1966). [Erratum: Nuovo Cim.B 48, 463 (1967)], p. 1.

[117] Lisa Randall and Raman Sundrum. "A Large mass hierarchy from a small extra dimension". In: *Phys. Rev. Lett.* 83 (1999), pp. 3370–3373. arXiv: hep-ph/9905221.

[118] Lisa Randall and Raman Sundrum. "An Alternative to compactification". In: *Phys. Rev. Lett.* 83 (1999), pp. 4690–4693. arXiv: hep-th/9906064.

[119] G. W. Gibbons and S. W. Hawking. "Cosmological event horizons, thermodynamics, and particle creation". In: *Phys. Rev. D* 15 (10 May 1977), pp. 2738–2751.

[120] Marco M. Caldarelli, Guido Cognola, and Dietmar Klemm. "Thermodynamics of Kerr-Newman-AdS black holes and conformal field theories". In: *Class. Quant. Grav.* 17 (2000), pp. 399–420. arXiv: hep-th/9908022.

[121] J. B. Griffiths, P. Krtous, and J. Podolsky. "Interpreting the C-metric". In: *Class. Quant. Grav.* 23 (2006), pp. 6745–6766. arXiv: gr-qc/0609056.

[122] Ruth Gregory, Zheng Liang Lim, and Andrew Scoins. "Thermodynamics of Many Black Holes". In: *Front. in Phys.* 9 (2021), p. 187. arXiv: 2012.15561 [gr-qc].

[123] Marco Astorino. "Accelerating black hole in 2+1 dimensions and 3+1 black (st)ring". In: *JHEP* 01 (2011), p. 114. arXiv: 1101.2616 [gr-qc].

[124] Ruth Gregory and Andrew Scoins. "Accelerating Black Hole Chemistry". In: *Phys. Lett.* B796 (2019), pp. 191–195. arXiv: 1904.09660 [hep-th].

[125] Pietro Ferrero, Jerome P. Gauntlett, Juan Manuel Pérez Ipiña, Dario Martelli, and James Sparks. "D3-Branes Wrapped on a Spindle". In: *Phys. Rev. Lett.* 126.11 (2021), p. 111601. arXiv: 2011.10579 [hep-th].

[126] Pietro Ferrero, Jerome P. Gauntlett, and James Sparks. "Supersymmetric spindles". In: *JHEP* 01 (2022), p. 102. arXiv: 2112.01543 [hep-th].

[127] Andrea Boido, Jerome P. Gauntlett, Dario Martelli, and James Sparks. "Entropy Functions For Accelerating Black Holes". In: *Phys. Rev. Lett.* 130.9 (2023), p. 091603. arXiv: 2210.16069 [hep-th].

[128] Michael Haack and Amos Yarom. "Nonlinear viscous hydrodynamics in various dimensions using AdS/CFT". In: *JHEP* 10 (2008), p. 063. arXiv: 0806.4602 [hep-th].

[129] Luca Ciambelli, Charles Marteau, P. Marios Petropoulos, and Romain Ruzziconi. "Gauges in Three-Dimensional Gravity and Holographic Fluids". In: *JHEP* 11 (2020), p. 092. arXiv: 2006.10082 [hep-th].

[130] Alexander Vilenkin. "Cosmic Strings and Domain Walls". In: *Phys. Rept.* 121 (1985), pp. 263–315.

[131] Shinsei Ryu and Tadashi Takayanagi. "Aspects of Holographic Entanglement Entropy". In: *JHEP* 08 (2006), p. 045. arXiv: hep-th/0605073.

[132] Clifford V. Johnson. "Large N Phase Transitions, Finite Volume, and Entanglement Entropy". In: *JHEP* 03 (2014), p. 047. arXiv: 1306.4955 [hep-th].

[133] Ioannis Papadimitriou and Kostas Skenderis. "Thermodynamics of asymptotically locally AdS spacetimes". In: *JHEP* 08 (2005), p. 004. arXiv: hep-th/0505190.

[134] Erik A. Martinez and James W. York Jr. "Thermodynamics of black holes and cosmic strings". In: *Phys. Rev. D* 42 (1990), pp. 3580–3583.

[135] Myungseok Eune, Wontae Kim, and Sang-Heon Yi. "Hawking-Page phase transition in BTZ black hole revisited". In: *JHEP* 03 (2013), p. 020. arXiv: 1301.0395 [gr-qc].

[136] Cesar Arias, Felipe Diaz, Rodrigo Olea, and Per Sundell. "Liouville description of conical defects in dS_4, Gibbons-Hawking entropy as modular entropy, and dS_3 holography". In: *JHEP* 04 (2020), p. 124. arXiv: 1906.05310 [hep-th].

[137] M. Cvetic, G. W. Gibbons, D. Kubiznak, and C. N. Pope. "Black Hole Enthalpy and an Entropy Inequality for the Thermodynamic Volume". In: *Phys. Rev. D* 84 (2011), p. 024037. arXiv: 1012.2888 [hep-th].

[138] Manus R. Visser. "Holographic thermodynamics requires a chemical potential for color". In: *Phys. Rev. D* 105.10 (2022), p. 106014. arXiv: 2101.04145 [hep-th].

[139] Wan Cong, David Kubiznak, and Robert B. Mann. "Thermodynamics of AdS Black Holes: Critical Behavior of the Central Charge". In: *Phys. Rev. Lett.* 127.9 (2021), p. 091301. arXiv: 2105.02223 [hep-th].

[140] Moaathe Belhaj Ahmed, Wan Cong, David Kubizňák, Robert B. Mann, and Manus R. Visser. "Holographic Dual of Extended Black Hole Thermodynamics". In: *Phys. Rev. Lett.* 130.18 (2023), p. 181401. arXiv: 2302.08163 [hep-th].

[141] Maximo Banados, Ricardo Troncoso, and Jorge Zanelli. "Higher dimensional Chern-Simons supergravity". In: *Phys. Rev. D* 54 (1996), pp. 2605–2611. arXiv: gr-qc/9601003.

[142] Jorge Zanelli. "Lecture notes on Chern-Simons (super-)gravities. Second edition (February 2008)". In: *7th Mexican Workshop on Particles and Fields*. Feb. 2005. arXiv: hep-th/0502193.